Study of the Effect of Polyethylene Resin Particle Size on the Degree of Fluidized Bed Reactor Electrification and Wall Fouling

uOttawa

by

Ye Tian

Thesis submitted to the
Faculty of Graduate and Postdoctoral Studies
In partial fulfillment of the requirements
For the degree of M.A.S.C in Chemical Engineering

Department of Chemical and Biological Engineering
Faculty of Engineering
University of Ottawa

ABSTRACT

In gas-solid fluidized bed reactors, such as those employed for polyethylene production, the generation of electrostatic charge is almost unavoidable. Electrostatic charges are generated due to the continuous contacts between particles and particles and the reactor wall. In such processes, accumulation of electrostatic charge causes a layer of particles to adhere to the reactor wall, a problem known as "sheeting" in polyolefin industry. Sheeting results in frequent reactor shutdowns for clean-up and in turn significant economic loss. The overall focus of this research is to better understand the underlying mechanisms of charge generation in gas-solid fluidized beds to ultimately be able to find means to reduce or eliminate this problem. The specific objective of this thesis is to determine the effect of fluidizing particle size on the degree of bed electrification and reactor wall coating. The experimental program involved the fluidization of polyethylene resins received directly from commercial reactors (i.e., having a wide size distribution of 20-1500 micron), as well as mono-sized large particles (600-710 micron) and binary mixture of small particles (200-300 micron and 300-425 micron with fractions up to 20 wt%) and large particles (600-710 micron). Experiments were carried out under atmospheric conditions in 3D fluidization columns housing two Faraday Cups for electrostatic charge measurement. For all conditions, the charge, mass and size distribution of particles fouled on the reactor wall as well as the layer thickness were measured and compared. Fluidization of the resins as received resulted in a certain size of particles (400 μm and smaller) to adhere to the column wall. For binary mixtures, the particles layer formed on the reactor wall mainly consisted of the smaller particles. Although the extent of wall coating declined as the amount of the smaller particles increased, but the smaller particles had a much higher net specific charge and thus replaced the large particles within the wall coating. Such high charge of small particles accumulated on the column wall in turn prevented the wall coating growth due to repelling the oppositely charged particles to the bulk of the bed. Regardless of the charge polarity of the bulk and wall particles, the wall fouling formation mechanism was found to be similar. Between the two sizes of small particles tested, the 212-300 micron particles gained a higher net specific charge than 300-425 micron particles. Bipolar charging due to small and large particles contacts was detected within the bulk of the bed and the wall coating.

RÉSUMÉ

Dans les réacteurs à lit fluidisé gaz-solide, tels que ceux utilisés pour la production de polyéthylène, la génération de charges électrostatiques est presque inévitable. Ces charges électrostatiques sont générées en raison du contact inter-particulaire et le contact entre les particules et la paroi du réacteur. En effet, l'accumulation des charges électrostatiques porte à l'adhérence des particules sur la paroi du réacteur provoquant ainsi la formation de couches qui peuvent être problématiques pour l'industrie des polymères. Ces couches peuvent se briser et bloquer la plaque de distribution résultant en de longues périodes de fermeture et nettoyage menant à des pertes économiques en raison des coûts d'entretien plus élevés et de la diminution de production. L'objectif général de cette recherche est de mieux comprendre les mécanismes sous-jacents à la génération de charge dans les lits fluidisés gaz-solide pour être en mesure de trouver des moyens de réduire ou d'éliminer ce problème. En particulier, l'objectif spécifique de cette thèse est de déterminer l'effet de la taille des particules fluidisées sur le degré d'encrassement et de génération de charge. Le programme expérimental utilise des résines de polyéthylène obtenu directement de réacteurs industriels (ayant une grande distribution de taille variant de 20-1500 microns) ainsi que des grosses particules de même taille (600-710 microns) et des mélanges binaires de petites particules (200-300 microns et 300-425 microns) et de grosses particules (600-710 microns) pour les expériences de fluidisation. Ces expériences ont été mises en œuvre en utilisant des colonnes à fluidisation sous conditions atmosphériques comprenant deux coupes à Faraday pour mesurer le niveau de charge électrostatique. Pour toutes conditions expérimentales, la distribution de charge, de masse et de taille des particules encrassées sur la paroi du réacteur, ainsi que l'épaisseur de la couche a été mesurée et comparée. De même, lors de la fluidisation des résines de polyéthylène obtenu directement de réacteurs industriels, seules les particules ayant une taille de 400 µm ou moins ont contribué à l'encrassement. En effet, pour les mélanges binaires, les couches de particules sur la paroi de réacteur étaient composées principalement des plus petites particules. Bien que le niveau d'encrassement ait diminué à mesure que la quantité des particules plus petites a augmenté, les plus petites particules ont une charge nette spécifique beaucoup plus élevée, et donc ont remplacé les grosses particules sur la paroi. De telles charges élevées qui sont accumulées sur la paroi de la colonne à leur tour ont empêché la croissance de la couche puisqu'elles repoussaient les particules de charge opposée du mur. Bref, quelle que soit la charge des particules dans le lit et sur la paroi, le mécanisme de

formation de charge provoquant l'encrassement était similaire. En comparant les deux tailles de petites particules utilisées, les particules de 212-300 microns ont généré une charge spécifique nette supérieure aux particules de 300-425 microns. Finalement, la génération de charge bipolaire due au contact entre petites et grandes particules a été détectée à l'intérieur du lit et des couches sur la paroi.

TABLE OF CONTENTS

Abstract ..... **i**

Résumé ..... **ii**

Table of Contents ..... **iv**

List of Tables ..... **viii**

List of Figures ..... **ix**

Nomenclature ..... **xiii**

Acknowledgements ..... **xv**

Chapter 1. Introduction **1**

1.1 Gas-Solid Fluidization **2**

1.1.1 Fluidization Flow Regimes 3

1.1.2 Classification of Particles 4

1.1.3 An industrial application of gas-solid fluidization process: Polyethylene Production 5

1.2 Electrostatic Charging **6**

1.2.1 Triboelectric Charging 6

1.2.2 Induction Charging 12

1.2.3 Bipolar Charging 12

1.3 Electrostatic Charging and Wall Fouling in Gas-Solid Fluidized Beds **13**

1.3.1 Electrostatic Force 14

1.3.2 Image Force 14

1.3.3 Electrostatic Charging in Polyethylene Reactors 14

1.3.4 Electrostatic Charge Measurement Techniques 16

1.3.4.1 Electrostatic probe 16

1.3.4.2 Faraday cup 17

1.4 Effect of Fluidizing Particle Size on Electrostatics in Gas-Solid Fluidized Beds ... **19**

1.5 Effect of Binary Mixture of Particles on Gas-Solid Fluidized Beds Hydrodynamics 20
1.6 Thesis Objectives 22
1.7 Thesis Outline 23
Chapter 2. Experimental Apparatus, Method and Materials 24
2.1 Materials 24
2.1.1 Fluidizing Gas 24
2.1.2 Fluidizing Particles 24
2.2 Fluidization Experiments 28
2.2.1 Fluidization Column 28
2.2.1.1 Electrostatic Charge Measurement Technique 34
2.2.1.2 Instrumentation 36
2.2.1.3 Charged Particle Separator 37
2.2.2 Experimental Conditions and Procedure 39
2.3 Bench-Scale Shaking Experiments 42
2.3.1 Experimental Apparatus 42
2.3.2 Experimental Conditions and Procedure 43
2.3.2.1 Shaking experiments with PE_A particles used in fluidization experiments in small system 43
2.3.2.2 Shaking experiments with PE_B particles used in fluidization experiments in small system 44
2.3.2.3 Shaking experiments with PE_B particles used in fluidization experiments in large system 45
Chapter 3. Results and Discussion - Small Fluidization System 46
3.1 PE_A and PE_B Resins as Received 46
3.2 Binary Mixture of Small and Large Particles of PE_A Resin 47
3.2.1 Initial Particles 47
3.2.2 Bulk Particles 48
3.2.3 Wall Particles 50
3.2.4 Multiple Bulk Sample Test 55

3.2.5 Charged Particle Separator 57
3.2.6 Bench-Scale Shaking Experiments 60
3.2.6.1 Case (a) 60
3.2.6.2 Case (b) 62
3.2.6.3 Case (c) 63
3.3 Binary Mixture of Small and Large Particles of PE_B Resin 66
3.3.1 Initial particle 66
3.3.2 Bulk Particle 66
3.3.3 Wall particle 67
3.3.4 15 Minutes Fluidization and Multiple Sampling of Bulk for 20% PE_{BS-1} mixture. 71
3.3.4.1 15 Minutes Fluidization Experiments 71
3.3.4.2 Multiple Sampling of Bulk Particles 73
3.3.5 Bench-Scale Shaking Experiments 75
3.3.5.1 Case (a) 75
3.3.5.2 Cases (b) and (c) 75
3.4 Mechanism of Wall Layer Formation 76
Chapter 4. Results and Discussion - Large Fluidization System 79
4.1 PE_B Resin as Received 79
4.2 Initial Particles 80
4.3 Bulk Particles 80
4.4 Wall Particle 81
4.5 Charged Particle Separator 85
4.6 Bench-Scale Shaking Experiments 86
4.7 Summary 86
Chapter 5. Conclusions and Recommendations 89
5.1 Conclusions 89
5.2 Recommendations for Future work 91
Reference 92
Appendix 100

Appendix 1. The Pressure Signal Analysis for PE_B particles in Small System..... 100

LIST OF TABLES

Table 1.1: Triboelectric series, adapted from Adams, C.K, 1986. 8
Table 1.2: Work function of various materials, adapted from Tanoue & Masuda, 2006. 10
Table 2.1: Properties of polyethylene particles used in this work. 25
Table 2.2: The detail information of fluidization columns. 29
Table 2.3: Summary of the fluidization experimental conditions of PE_A and PE_B particles in small column. 40
Table 2.4: Summary of the fluidization experimental conditions of PE_B particles in large column. 41
Table 2.5: Values of U_{mf} measured in m/s for various mixtures of small and large particles of PE_A and PE_B particles. 41
Table 3.1: Results of Case (a) shaking experiments with PE_A particles without using CPS unit. 61
Table 3.2: The results of shaking tests for PE_B particles Case (a). 75
Table 3.3: Charging polarity of PE_{BL} and $PE_{BS\text{-}1}$contacted with a tube wall covered with the same particles. 76
Table 3.4: Generated net q/m of PE_{BL} and $PE_{BS\text{-}1}$ resins shaken in a tube covered with the same particles. 76

LIST OF FIGURES

Figure 1.1: Schematic of a typical gas-solid fluidization column. 3
Figure 1.2: Fluidization flow regimes, adapted from Kunii & Levenspiel, 1991. 4
Figure 1.3: Geldart classification of powders at ambient conditions, adapted from Geldart, 1973. 5
Figure 1.4: An example of commercial polyethylene production reactor, adapted from Goode et al., 1989. 6
Figure 1.5: The electrostatic charge generation mechanisms: (a) contact charging; and (b) frictional charging. 7
Figure 1.6: Electron potential energy for metal-metal contacts, adapted from Matsusakaa et al., 2010. 9
Figure 1.7: Schematic of hypothetical mechanism for mobile ion transfer, adapted from Gooding and Kaufman, 2014. 11
Figure 1.8: Mosaic of surface charge on one surface, adapted from Beytekin et al., 2011. 12
Figure 1.9: The induction charge generation mechanism. 12
Figure 1.10: Sheeting formation in industrial polyethylene reactors, adapted from Hendrickson, 2006. 16
Figure 1.11: Schematic of an electrostatic probe and its charge measurement mechanism. 17
Figure 1.12: Schematic of a Faraday cup and its charge measurement mechanism. 18
Figure 1.13: Gas-solid fluidized bed integrated with Faraday cup measurement technique. (a) Adapted from Fasso et al. (1982); (b) Adapted from Bartilucci et al. (1982); (c) Adapted from Ali et al. (1998): c1.Faraday cup grid; c2. Scopper. 19
Figure 1.14: Voidage at minimum fluidization vs. fines volume fraction, adapted from Formisani, 1991. 21
Figure 2.1: Schematic of the small column fluidization system. 30
Figure 2.2: Schematic of large column fluidization system. 31
Figure 2.3: Pictures of the fluidization columns: (a) small column; (b) large column; and (c) overview of large system. 33

Figure 2.4: (a) Image of the bench-scale Faraday cup; (b) Particles charge measurement in various regions of the fluidized bed; (c) Typical image of the particle layer left on the column wall upon the removal of the bulk particles. 36
Figure 2.5: (a) Schematic of charged particle separator (CPS); (b) Picture of charged particle separator. 38
Figure 2.6: (a) Schematic of CPS unit placed under the column; (b) Picture of CPS unit placed under the large column. 39
Figure 2.7: Image of shaking experiments apparatus. 43
Figure 3.1: Particles mass%, q/m, and dp_{50} collected from various regions of the small fluidization system after fluidizing PE_A and PE_B resins as received, as well as the particle size distribution of wall particles. 47
Figure 3.2: Initial particles net q/m, dp_{50}, and sauter mean diameter for binary mixture of PE_{AS} and PE_{AL} Particles. 48
Figure 3.3: Bulk particles mass%, net q/m and $dp_{(50)N}$ after fluidization of various binary mixtures of PE_{AS} and PE_{AL} resin in the small fluidization system. 49
Figure 3.4: Wall particles mass%, net q/m and $dp_{(50)N}$ after fluidization of various binary mixtures of PE_{AS} and PE_{AL} resin in the small fluidization system. 52
Figure 3.5: Images of wall layer coating after the fluidization of various binary mixtures of PE_{AS} and PE_{AL} particles, before and after tapping. 53
Figure 3.6: Particle size distribution of wall particles collected after fluidization of various binary mixtures of PE_{AS} and PE_{AL} particles. 54
Figure 3.7: Net q/m and dp_{50} of multiple samples taken from bulk $PE_{A:}$ (a) 0% PE_{AS}, (b) 20% PE_{AS}. 56
Figure 3.8: Charge, mass%, net q/m and $dp_{(50N)}$ of particles collected in the four Faraday cups of the CPS unit: (a) 0 % ,(b) 5 % ,(c) 7 % , (d) 10 % and (e) 20% PE_{AS}. 59
Figure 3.9: Size distribution of particles collected in the four Faraday cups of the CPS unit for 0, 5, 7, 10 and 20% PE_{AS}. PP stands for positive plate. 60
Figure 3.10: Mass% and q/m of PE_{AL} and PE_{AS} particles with CPS unit for shaking and non-shaking tests. 62
Figure 3.11: The net q/m of various mixtures of PE_{AL} and PE_{AS} particles, before and after shaking. 63

Figure 3.12: The PE_A particles mass%, net q/m, and PSD for case (c) of bench-scale shaking experiment with 0% $PE_{AS.}$ 64
Figure 3.13: The PE_A particles mass%, net q/m, and PSD for case (c) of bench-scale shaking experiment with 5% $PE_{AS.}$ 65
Figure 3.14: The PE_A particles mass%, net q/m, and PSD for case (c) of bench-scale shaking experiment with 10% PE_{AS}. 65
Figure 3.15: Initial particles net q/m, $dp_{(50)N}$ and sauter mean diameter for binary mixtures of PE_{BS-1} and PE_{BL} resin fluidized in the small system. 66
Figure 3.16: Bulk particles mass%, net q/m and $dp_{(50)N}$ collected after fluidization of various binary mixtures of PE_{BS-1} and PE_{BL} resin in the small fluidization system. 67
Figure 3.17: Wall particles mass%, net q/m and $dp_{(50)N}$ collected after fluidization of various binary mixture of PE_{BS-1} and PE_{BL} resin in the small fluidization system..... 69
Figure 3.18: Images of wall layer coating before and after the wall particles removal for fluidization of various binary mixtures PE_{BS-1} and PE_{BL} particles in the small fluidization system. 70
Figure 3.19: Bulk particles mass%, net q/m and $dp_{(50)N}$ for 15 and 60 minutes fluidization of binary mixture of 20% PE_{BS-1} and PE_{BL} particles..... 72
Figure 3.20: Wall particles mass%, net q/m and $dp_{(50)N}$ for 15 and 60 minutes fluidization of binary mixture of 20% PE_{BS-1} and PE_{BL} particles..... 72
Figure 3.21: Images of wall layer coating before and after tapping the column wall after the fluidization of PE_B particles (20% mixture) for different fluidization periods. (a) 15 min; (b) 60 min. 73
Figure 3.22: Bulk particles net q/m and dp_{50} found by multiple sampling of the 20% PE_{BS-1} and PE_{BL} mixture. 74
Figure 3.23: The net q/m vs dp_{50} of multiple bulk samples taken for 20% PE_{BS-1} and PE_{BL} mixture. 74
Figure 3.24: Schematic of wall fouling formation mechanism: (a) charge generation due to particle-particle and particle-wall contacts and formation of image force between the column wall and negatively charged particles; (b) Wall coating layer formation and growth. 77

Figure 4.1: Particles mass%, q/m and dp_{50} found in various regions of the larger fluidized bed after fluidization of the PE_B resin as received, as well as particle size distribution of wall particles. 79
Figure 4.2: Initial particles net q/m and $dp_{(50)N}$ for the two binary mixtures PE_B resin fluidized in the large fluidization system. 80
Figure 4.3: Bulk particles mass%, net q/m and $dp_{(50)N}$ after fluidization of various binary mixtures of PE_{BS} and PE_{BL} resin in the large fluidization system. 81
Figure 4.4: Wall particles mass%, net q/m and $dp_{(50)N}$ after fluidization of various binary mixtures of PE_{BS} and PE_{BL} resin in the large fluidization system. 82
Figure 4.5: Wall particles size distribution for various binary mixtures of PE_{BS} and PE_{BL} particles fluidized in the large system. 83
Figure 4.6: Average pressure drop and the standard deviation of pressure fluctuations measured during 1 hour fluidization of various binary mixtures of PE_{BS} and PE_{BL} particles in the large fluidization system. 84
Figure 4.7: Mass%, net q/m and $dp_{(50)N}$ of particles collected in the four Faraday cups of the CPS unit for 5% case: (a) PE_{BS-1}; (b) PE_{BS-2}. 85
Figure 4.8: net q/m of different PE_B particle size ranges before and after shaking in a stainless steel tube. 86
Figure 4.9: Schematic of wall fouling formation mechanism: (a) First positive wall layer formation caused by image force between column wall and charged particles; (b) Second negative wall layer formation. 88
Figure A.1: Standard deviation of pressure fluctuations measured during 1hour fluidization of various mixtures of PE_{BS-1} and PE_{BL} particles in the small fluidization system. 100

NOMENCLATURE

Symbol	Description	Units
A	Area	m^2
$\hat{A}$	Specific surface area	m^2/g
Db	Bubble size	m
d_P	Particle diameter	µm
$d_{P(50)\ N}$	Normalized particle diameter at the 50^{th} percentile	-
$\vec{F}_E$	Electrostatic force	N
$\vec{F}_i$	Image force	N
g	Gravitational force constant	m/s^2
L/D	Static bed height to column diameter ratio	-
P	Perimeter	m
q	Charge	nC
q/m	Specific charge	µC/kg
r	Distance between two point charges	m
u_{mf}	Minimum fluidization gas velocity	m/s
z_{PP}	Distance between two particles	m
z_{PW}	Distance between a particle and wall	m
$\mathbb{C}$	Circularity	-
ϕ	Sphericity	-
ε_f	Permittivity of the fluid	F/m
ε_{mf}	Bed porosity at minimum fluidization condition	-
ε_w	Permittivity of the wall	F/m
ρ_s	Density of particle	kg/m^3

Acronym	Description
AP	Pressure
CPS	Charged Particle Separator
DP	Differential Pressure
EI	Electrometer
FR	Pressure Regulator and Filter
KGV	Knife Gate Valve
LLPE	Linear Low-density Polyethylene
MFC	Mass Flow Controller
PC	Polycarbonate
PE	Polyethylene
PE_{AS}	Small particle (212-300 μm) of Polyethylene A resin
PE_{AL}	Large particle (600-710 μm) of Polyethylene A resin
PE_{BS-1}	Small particle (212-300 μm) of Polyethylene B resin
PE_{BS-2}	Small particle (300-425 μm) of Polyethylene B resin
PE_{BL}	Large particle (600-710 μm) of Polyethylene B resin
PTFE	Polytetrafluoroethylene
PVC	Polyvinylchloride
RH	Relative Humidity
SEM	Scanning Electron Microscopy

ACKNOWLEDGEMENTS

I would like to express my special appreciations to my supervisor Dr. Poupak Mehrani for her support and guidance during my thesis, and for her patience and motivation. She is also the most influential person for me in Canada. I could not have imagined having a better supervisor.

Many thanks also goes to Dr. Andrew Sowinski whose assistance made me feel confident when conducted experiments. I also would like to thank other group members including Di Song, Fawzi Salama and Jonny Matta for their help.

I would also like to thank the technical support staff of the Chemical Engineering Department: Louis Tremblay, Franco Ziroldo and Gérard Nina. This work could not be completed without their assistance.

I would like to thank my friends: Zuolong Chen, Xin Tian and others who made my life in Canada full of fun.

Furthermore, I would like to thank my parents for their continuous support. Last thanks are for my fiancée, Yuepeng Li for her patience and continuous encourage.

Chapter 1. Introduction

Gas-solid fluidization is a process by which solid particles are suspended in an upward stream of gas and behave like a fluid. Gas-solid fluidized beds are widely used in industry for processes such as combustion, catalytic cracking, drying, to just name a few.

There are numerous advantages of using gas-solid fluidized beds since they provide excellent mass and heat transfer characteristics as well as mixing. However, one problem that arises in some gas-solid fluidized beds is the occurrence of electrostatic charge generation. The first references to electrostatic charging of fluidizing particles dates back to 1940s and 1950s when the electrostatic charge was identified as a problem (Lewis et al., 1949; Miller and Longwinuk et al., 1951; Osberg and Charlesworth., 1951). In gas-solid fluidized beds, electrostatic charging occurs due to continuous contacts among fluidizing particles and the particles and the vessel wall. Thus, the generation of electrostatic charge is almost cannot be avoided in such processes however the extent of bed electrification varies depending on the nature of the fluidizing particles and those of the fluidization column and operating conditions. Fluidized bed electrification in turn affects the hydrodynamics of the fluidization by resulting in particle agglomeration and particle-vessel wall fouling. One industry that has significantly been affected by the electrostatic phenomenon is polyolefin industry and mostly in the gas-phase ethylene polymerization to produce polyethylene which is conducted in fluidized bed reactors. In polyethylene commercial reactors, generation of electrostatic charge results in polyethylene and catalyst particles to adhere to the reactor wall while the polymerization reaction is underway and thus resulting in a problem known as “sheeting” (Hendrickson, 2006). The dislodge of sheets off of the reactor wall can block the reactor distributor plate and thus requiring reactor shutdown for cleanup. This in turn results in significant economic loss.

To date although some industries have aimed at reducing the electrostatic charge generation, and in some cases finding charge reduction methods with examples of treating the column inner wall and additive injection (Bafrnec and Beña, 1972; Fulks et al., 1989; Goode et al, 2000; Servais and Bernot, 2000; Hagerty et al., 2005), the problem still exists. This is due to the fact that the mechanisms of electrostatic generation in fluidized beds are still not well understood. Therefore,

determining the underlying charging mechanisms and the understanding of the factors contributing to the charge generation and wall fouling in such reactors are essential in order to be able to assist the industry in reducing or eliminating this problem.

The goal of this research was to investigate the effects of fluidizing particle size on the degree of electrostatic charge generation and wall fouling in gas-solid fluidized beds. Relative topics are briefly reviewed in following sections.

1.1 Gas-Solid Fluidization

Gas-solid fluidization is a process by which solid particles are transformed into a fluid like state by an upward gas. The first application of fluidization technology dates back to 1942 with catalytic cracking (Kunii and Levenspiel, 1991). The most widely established industrial reactor for polyolefin production is known to be fluidized bed (Cross, 1987).

The schematic of a typical gas-solid fluidization column is shown in Figure 1.1. The fluidizing gas is fed from the bottom of the column through the windbox when it then passes through the distributer plate before travelling through the bed of solid particles. During the fluidization, if the gas velocity is higher than the terminal velocity of some particles, these particles will be entrained into the expanded section of the bed and with some leaving the system.

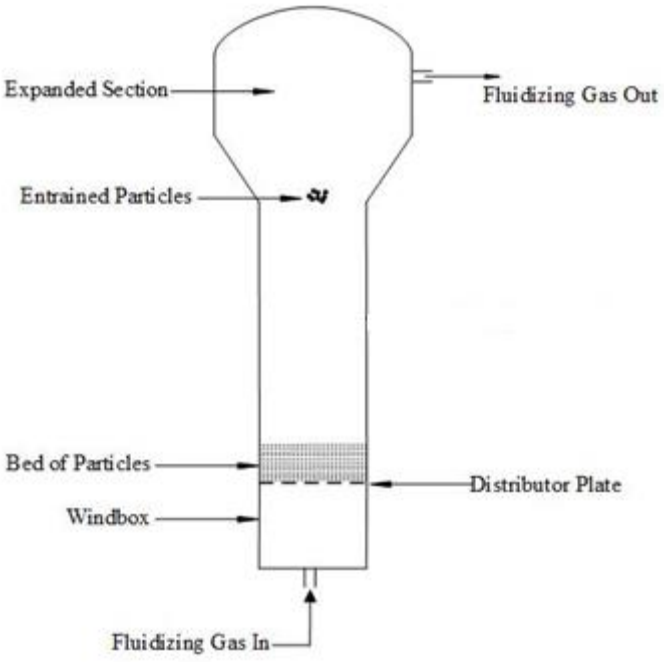

Figure 1.1: Schematic of a typical gas-solid fluidization column.

1.1.1 Fluidization Flow Regimes

The basic principle of gas-solid fluidization can be demonstrated by a simple force balance on the solid particles, namely the balance between drag force and gravitational force. When the drag force is equal to gravitational force, the bed reaches the fluidization state and the gas velocity at this condition is called minimum fluidization velocity.

At low gas velocity, the drag force is smaller than gravitational force; the bed will keep static (Fixed Bed). When fluidizing gas velocity reaches minimum fluidization velocity, the particles are become suspended by the gas. After that point, the particles start to move like a fluid. If the velocity is further increased, the hydrodynamics of the fluidized bed lead to different fluidization flow regimes (Figure 1.2). Beyond minimum fluidization, the excess gas forms bubbles at the distributor plate. Bubbles then rise to the top of bed and burst (Bubbling Fluidization). By increasing the gas velocity, the bubble size grows and if the column is narrow its size could take up the full diameter of the bed (Slugging Fluidization). When the gas velocity is significantly large, turbulent fluidization regime is reached.

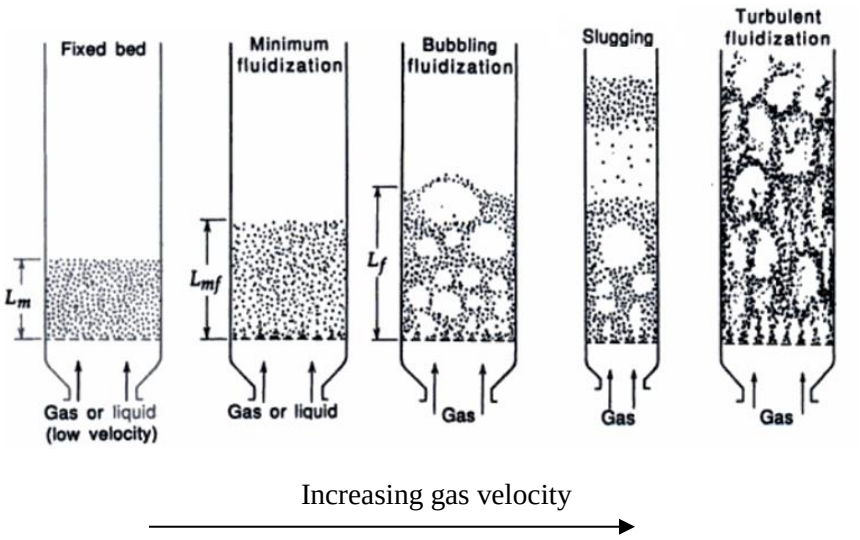

Figure 1.2: Fluidization flow regimes, adapted from Kunii & Levenspiel, 1991.

1.1.2 Classification of Particles

Presence of different particle density and mean diameters leads to various fluidization hydrodynamic behaviour. Thus, in 1973, Geldart proposed the most common particle classification where different types and size particles were divide into four groups (Figure 1.3).

- **Group C:** These particles are cohesive, fine (0-30 μm) and difficult to fluidize. The interparticle forces greatly affect the behaviour of these particles.
- **Group A:** These particles are aerabale and characterized by small particles size and small density, such as FCC, and milk flour.
- **Group B:** These particles are easily fluidized. The minimum bubbling fluidization velocity (U_{mb}) almost equal to minimum fluidization velocity (U_{mf}).
- **Group D:** These particles are either very large or very dense such as wheat and lead shot. They are difficult to fluidize.

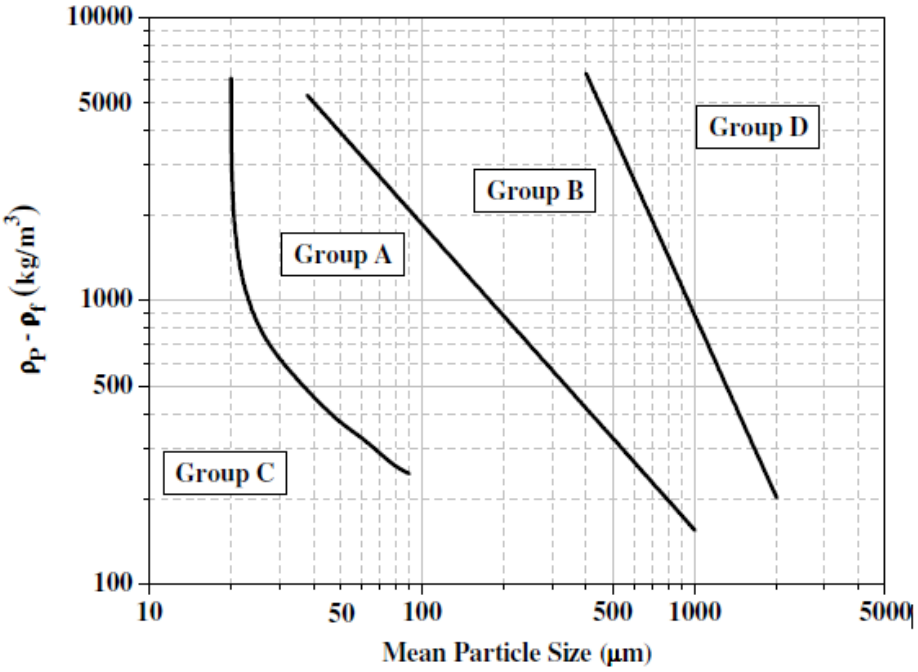

Figure 1.3: Geldart classification of powders at ambient conditions, adapted from Geldart, 1973.

1.1.3 An industrial application of gas-solid fluidization process: Polyethylene Production

One of the industrial applications of gas-solid fluidized beds is in catalytic ethylene polymerization to produce polyethylene. The first commercial polyethylene fluidized bed reactor was constructed by Union Carbide in 1968. A typical gas-phase polyethylene commercial reactor is shown in Figure 1.4 (Goode et al., 1989). The reactor is typically operated at pressures up to 30 atm and at temperature up to 110 ℃ (Beret et al., 1986; Chirillo et al., 1989; Mun 2005). Ethylene gas along with some comonomors is fed from the bottom of the reactor and evenly distributed by the distributor plate. The catalyst (Ziegler-Natta, metallocene, or others) is injected along the column with nitrogen where then a chain polymerization reaction occurs on the surface of the catalyst. Polymer chains grow and surround the catalyst particles forming large polyethylene granules. The unreacted catalyst particles, if any, are recycled with ethylene gas through the system by a compressor. Since ethylene polymerization is a highly exothermic reaction, in order to keep the operation condition stable, the recycled gas is cooled in a heat exchanger before introduced back into the reactor. When the polyethylene particles grow heavy enough, they will settle down at the bottom of the column close to the distributor plate where they are discharged as product (Fulks et al., 1985).

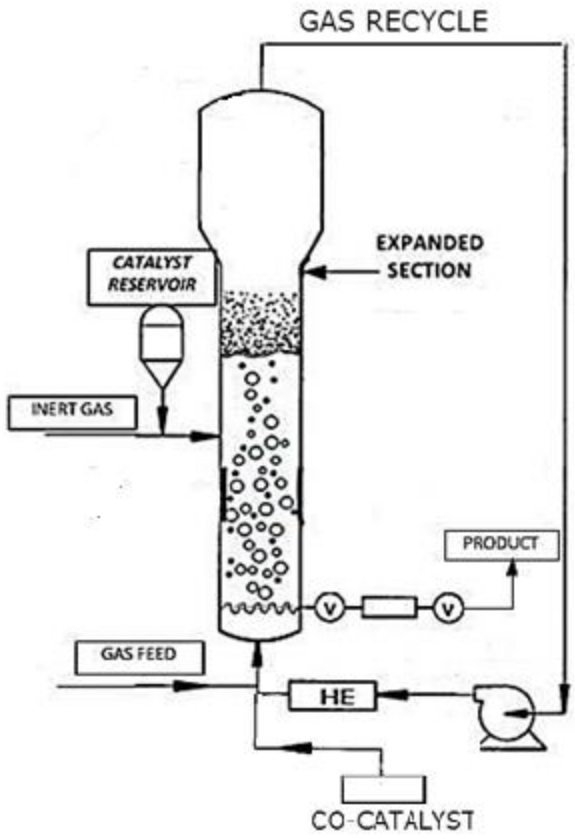

Figure 1.4: An example of commercial polyethylene production reactor, adapted from Goode et al., 1989.

1.2 Electrostatic Charging

Electrostatic charge results from electron loss or gain on an object surface, in turn making the surface to charge positively or negatively, respectively. There are several mechanisms for electrostatic charge generation where in gas-solid fluidized beds the focus will be on tribolelectric charging (contact and frictional charging) as well as induction charging. Induction charging only occurs in fluidization systems with columns made of a conductive material.

1.2.1 Triboelectric Charging

When two different or similar materials contact each other, charge transfer from one surface to the other results in charge generation. This mechanism is known as contact electrification (Figure 1.5a). Frictional charging arises from charge exchange between two surfaces when they are

rubbed against each other (Figure 1.5b). In practice, it is difficult to distinguish between these two contacting process. Thus, the term 'triboelectric charging' is used (Matsusakaa, et al., 2010).

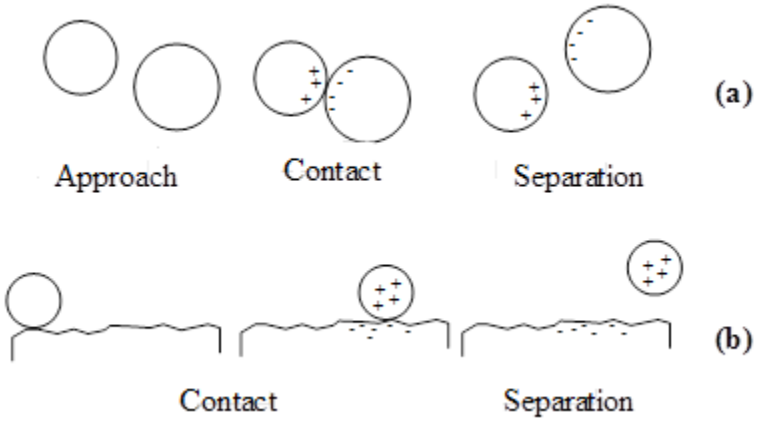

Figure 1.5: The electrostatic charge generation mechanisms: (a) contact charging; and (b) frictional charging.

Charge polarities of different materials contacting each other have been determined by some researchers and arranged in triboelectric series (Table 1.1), which are qualitatively ranked based on the amount of charge transferred from one material to another. Such series can be used to predict the charging polarity between two materials into contact. As presented in Table 1.1, materials at the top of the table become positively charged when contacted with a material at a lower location in the table.

Table 1.1: Triboelectric series, adapted from Adams, C.K, 1986.

Charge Polarity	Material
+	Glass
	Nylon
	Wool
	Lead
	Silk
	Aluminum
	Cotton
	Steel
	Nickel, Copper
	Brass, Silver
	Polyester
	Polyurethane
	Polyethylene
	PVC
−	Teflon

Based on the charge transfer, there are three main mechanisms for triboeletric charging: electron transfer, ion transfer and material transfer.

For contacts between two metals, electrostatic charging mechanism is well understood through electron transfer (Williams, 2012), which is due to the difference of the work functions of the two surfaces (Harper, 1967). Work function is the amount of energy required to move an electron from the Fermi energy level to vacuum (Cross, 1987); in other word it is the minimum energy required to release an electron from the object surface. When the metals contact each other, the electrons are transferred from lower work function surface to higher work function surface as shown in Figure 1.6 (Matsusakaa, et al., 2010).

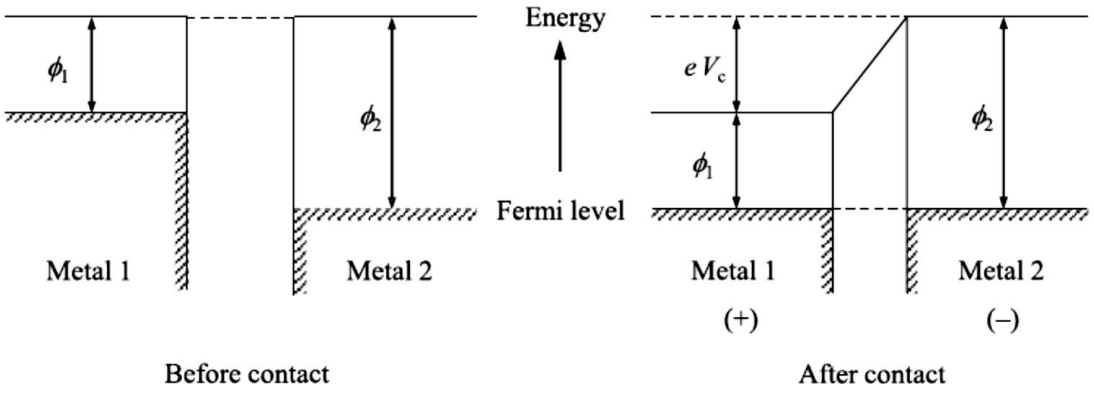

Figure 1.6: Electron potential energy for metal-metal contacts, adapted from Matsusakaa et al., 2010.

Although in insulators electrons have no free mobility, but the above mentioned mechanism has been extended to insulators. Davies (1969), Murata and Kittaka (1979) and Harper (1998) found that after an insolator contacted a metal, there was a linear relationship between charge density of insulator and metal work function. In this condition, it was assumed that insulator had an "effective work function". The driving force for charge transfer is the difference between work function of the metal and the effective work function of the insulator. The effective work function for polymers was detected based on insulator to metal contacts. Work function of various materials is shown in Table 1.2 (Tanoue and Masuda, 2006). In recent years, Wiles et al. (2003) developed a rolling-sphere tool to investigate the charge generation between metals and solid insulators. They found the charge on polymer surface grew sigmoidally in time, indicating that polymer has a charge saturation point. For insulator to insulator contacs, Liu and Bard (2008, 2009, 2010) provided a hypothesis as "there may be high energy cryptoelectrons that transfer between insulating materials and that these electrons are responsible for a range of reduction reactions that can occur at negatively tribocharged surfaces." But Piperno et al. (2011) suggested that such observation resulted from material tansfer. Until now, it is still unclear if electrons can be responsible for insulator to insulator charging.

Table 1.2: Work function of various materials, adapted from Tanoue & Masuda, 2006.

Material	Work function (eV)	Material	Work function (eV)
Zn	3.63	Polyethylene	5.23
Al	4.06-4.26	Polypropylene	5.49
Cu	4.25	Polystyrene	4.77
Fe	4.67-4.81	Teflon	5.75
Ag	4.25-4.74	PVC	5.13
Ti	4.33	Pylex7740	4.84

Over the last decades, numerous works were emerged for ion transfer. Kornfeld (1969) proposed that when two ion-coated surfaceres contact each others, ions transfer from one surface to the other due to different surfaces having different affinities for giving ions. By using this mechanism, he claimed that ion transfer is possible to explain charging between same materials.

Some other evidences for ion transfer come from electrophotography, where the external addition of ionic charge control agents is widely used. It is considered that materials contain the mobile ion. Therefore, mobile ion mechanism was proposed. Some studies supported this mechanism. Law et al., (1995) used x-ray pohtoelectron spectroscopy method to detect the charge transfer on toners coated with a ceium salt which acts as a charge control agent. They found that there was a linear correlation between the toner charge and the amount of cesium transferred. Diaz (1993) pointed that toner dyes containing a large organic cation and samll inorganic anion result in a positively charge toner. Contrastly, those contained a large organic cation and a mobile anion leading to negaticely charged toners. In this system, the mobile ion mechanism worked. McCarty et al. (2007) and McCarty and Whitesides (2008) contributed other significant evidence for mobile ions transfer by studying ploymers which contained covalently bound ions and mobile counterions. They also putted forward the hypothesis that when polymers which contain covalently bound ions and mobile couterions on their surfaces contact an insulator or conductor, some mobile counterions transfer between the surfaces as shown Figure 1.7. These results provided the evidence that charge carriers are ion.

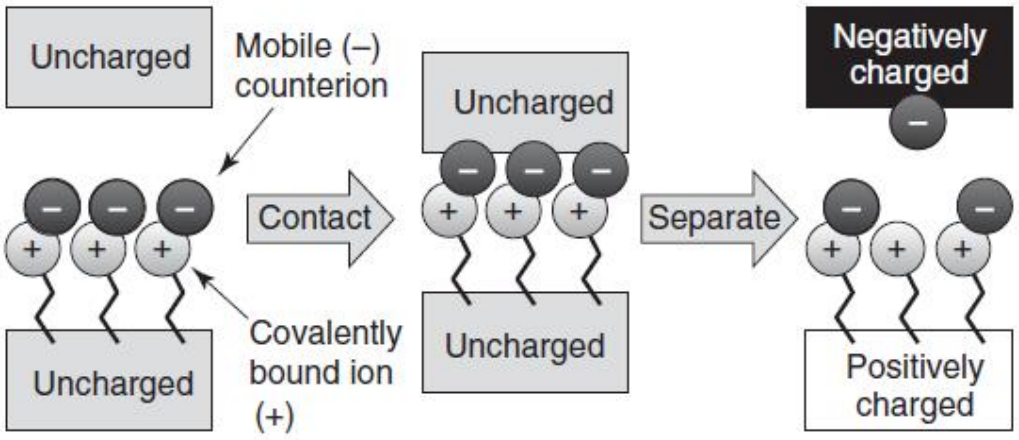

Figure 1.7: Schematic of hypothetical mechanism for mobile ion transfer, adapted from Gooding and Kaufman, 2014.

Material transfer mechanism considers minute amounts of material being transferred between contacting surfaces resulting in charge generation. Lowell (1977) concluded that, "material tranfer is not the primary mechanism of triboelectric charging, because it occurs to a large extent on the first contact and to a much smaller extent on subsequent contacts."

For a long time, it was believed that each surface chages uniformly, positviely or negatively, after contact charging. In 2011, Baytekin et al. found that although each surface gains a net positive or negative charge when two different insulators contact, but each surface could consist of local positively and negatively chaged regions as shown in Figure 1.8. This was also an important evidence for material transfer from one surface to another. Burgo et al. (2012) analyzed the contact regions between Polytetrafluoroethylene (PTFE) and Polyethelene (PE). It was found that charge polarties on polymer surfaces were not uniform but rather contained both positive and negative charged regions. Moreover, the positvely charged region on PTFE was formed by PE species, and the negatively charged regions on PE was formed by PTFE species, indicating that material transfer was respondible for charge transfer. The mechanism for both situations is similar: mechanical stress leads to covalent bond breakage resuling in radicals generations, followed by electron transfer from the hydrocarboradicals to the more electronegative fluorocarboradicals (Burgo et al., 2012).

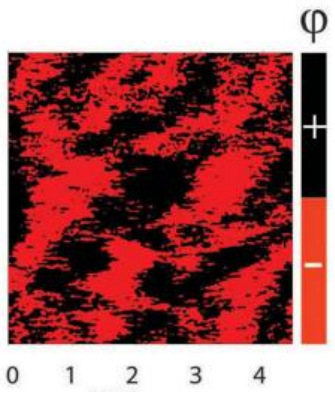

Figure 1.8: Mosaic of surface charge on one surface, adapted from Beytekin et al., 2011.

1.2.2 Induction Charging

Induction charging is generated when a charged object approaches a conductor as shown in Figure 1.9. The electric field of the object will redistribute the electrons and protons on the opposite sides of the conductor. In the case shown in Figure 1.9, since the object is charged positively, it will attract electrons to the closer side, leaving protons on the further side, resulting in both sides of the conductor being charged oppositely. If the further side is grounded, the positive charge of that side will be dissipated. After removing the charged object and the ground, the electrons will evenly distribute on the surface of the conductor. As a result, the conductor becomes negatively charged. Induction charging leads to an attractive force between the conductor and the charged object referred to as image force.

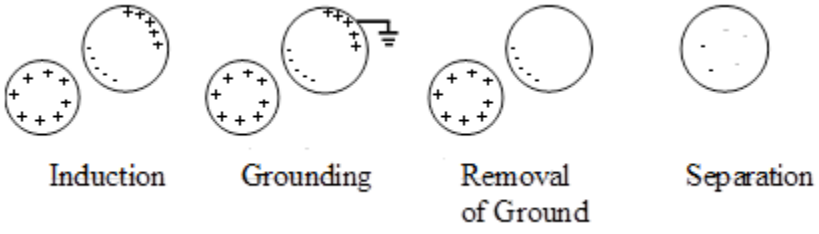

Figure 1.9: The induction charge generation mechanism.

1.2.3 Bipolar Charging

Based on the above mentioned discussions and triboelectric series, when two similar insulators contact each other, there should not be any charge generation. However, Komatus et al. (2004), Forward et al. (2009) and Apodaca et al. (2010) epxerimened contacting charging of identical

materials and found opposite charges on each surface. Lacks and Sankaran (2011) suggested that this could be due to some statistical variations in the actual material surface properties. Similar phenomenon has been reported in gas-solid fluidized beds with same metarials but different particle size (Ali et al., 1998; Cartwright et al., 1985; Mehrani et al., 2005; Sowinski et al., 2010; Zhao et al., 2003) where large and small particles charged oppositvely. This phenomenon is known as "bipolar charging".

1.3 Electrostatic Charging and Wall Fouling in Gas-Solid Fluidized Beds

Electrostatic charge generation in any gas-solid fluidized bed is almost unavoidable due to vigorous mixing of particles resulting in particles continuously contacting each other and the fluidized bed wall. In early 1940s, electrostatic charges in gas-solid fluidized beds were observed by adhesion of particles to the column wall (Lewis et al., 1949; Miller and Longwinuk et al., 1951). The presence of electrostatics not only has significant impacts on hydrodynamics of the fluidized bed due to particle agglomeration, but also causes a major problem which is reactor wall fouling. The degree of bed charging varies depending on the nature of the particles and the fluidized bed wall as well as the operating conditions including gas velocity (Sowinski et al., 2012) and relative humidity (Giffin and Mehrani, 2013), and operating pressure (Salama et al., 2013; Salama, 2013).

Electrostatic charging mechanisms in gas-solid fluidized beds include triboelectric charging and induction charging. Triboelectric charging results from contacts between particles as well as particles and the column wall. Induction charging only occurs in metal fluidization columns.

Previous studies in our research team have concluded that when particles gain a net charge due to triboelectric charging with the column wall, they generate induction charging on the metallic column wall and as a result, image forces are formed between the charged particles and metallic column wall (Salama, 2013). The image force is considered to be the main reason for reactor wall fouling formation. For the case of particle-particle triboelectrification, if no entrainment exists then the generated net charge within the bed will be zero. However, when entrainment is present, a net charge will be left behind within the bed consequently generating additional induction charging and images forces. This case would then further contribute to wall fouling. In

addition, as highly charged particles migrate and attach to the fluidized bed wall, they attract oppositely charged particles from the bulk of the bed and thus assisting in the growth of the wall coating.

Electrostatic force is not usually taken into account in gas-solid fluidized beds hydrodynamic studies. However, it plays an important role on particles movement and wall fouling formation.

1.3.1 Electrostatic Force

Assume a particle as a point, then the electrostatic force between two charged particles can be expressed with Coulomb's Law as shown in Equation 1.1.

$$\vec{F}_E = \frac{q_1 q_2}{4\pi\varepsilon_f r^2} \qquad (1.1)$$

Where q_1 and q_2 are the net charges of the two particles, ε_f is the permittivity of the medium or fluid, r is the distance between the particles.

1.3.2 Image Force

As a charged particle approaches a conductive wall, the net charge of the particle generates induction charging on the surface of the wall. Therefore, an attractive force, "image force", forms between the conductive surface and the charged particle. Image force can be calculated by Equation 1.2 (Masuda et al., 2006).

$$\vec{F}_i = \frac{1}{4\pi\varepsilon_f}\,\frac{\varepsilon_w - \varepsilon_f}{\varepsilon_w + \varepsilon_f}\,\frac{q_1^2}{(2z_{PW})^2} \qquad (1.2)$$

where q_1 is the charge of the particle, z_{PW} is the distance between the particle and the wall, and ε_w is the permittivity of the wall material.

1.3.3 Electrostatic Charging in Polyethylene Reactors

Polyethylene production industry has significantly suffered from electrostatic charging. During gas-phase ethylene polymerization, continuous contacts among catalyst, polyethylene resin and reactor wall lead to triboelectric charge generation. As a result, electrostatic and image forces are generated attracting the particles toward the reactor wall. Since ethylene polymerization is an exothermic reaction, the layer of catalyst particles sticking to the wall has negative effects on the

heat dissipation. In turn, some polyethylene particles melt, fuse together and form “sheets”. Song et al. (1995) found that a common sign indicating the onset of sheeting in the reactor is when the skin temperature at the reactor wall deviates from the reactor bed temperature up to 20 ℃. As shown in Figure 1.10, there are three types of sheeting based on the formation locations: dome sheeting, expanded section sheeting and wall sheeting. Wall sheeting formation typically occurs at locations approximately half the diameter of the fluidization column above the distributor plate (Goode et al., 1989), where the drag forces along the column wall are minimum. The sheets range from 0.00635 m to 0.0127 m in thickness, 0.0762 m to 0.457 m in width, and 0.305 m to 1.52 m in length (Goode et al., 1989). When the sheets become heavy enough, they will detach from the reactor wall and fall onto the distributor plate, blocking the distributor plate and potentially the product discharge pipe. When this problem occurs, the reactor needs to be shut down for clean-up (2-3 days). In some serious situations, the clean-up may take up to 30 days, resulting in large economic loss. The approximate economic loss of a plant, for example a large commercial plant with an approximate annual production of 750,000 metric ton could be in the range of 1.0 to 1.2 million USD/day. This indicates the severity of the electrostatic effects and the need for investigating this phenomenon and finding reduction or elimination methods.

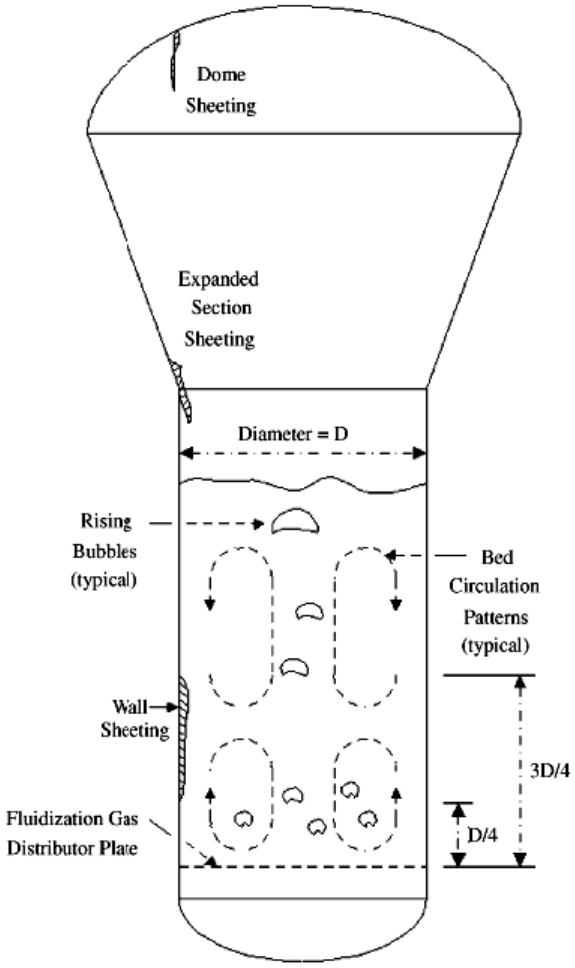

Figure 1.10: Sheeting formation in industrial polyethylene reactors, adapted from Hendrickson, 2006.

1.3.4 Electrostatic Charge Measurement Techniques

There are two main electrostatic charge measurement techniques employed in gas-solid fluidized beds: electrostatic probe and Faraday cup.

1.3.4.1 Electrostatic probe

As shown in Figure 1.11, an electrostatic probe consists of a conductive metallic bar or wire, surrounded with an insulating layer and a grounded outer conductive layer. The inner conductor is connected to an electrometer and outer grounded conductive layer prevents the outside electric fields affecting the measurement conducted by the inner piece. When charged objects are close to the tip of the probe, the electric field of objects induces an image charge on the probe. The induced charge which is equal to that of the objects is measured by the electrometer at the other

end of the probe. Electrostatic probes provide indirect electrostatic charge measurements. The measured signal can be electric potential, field or current.

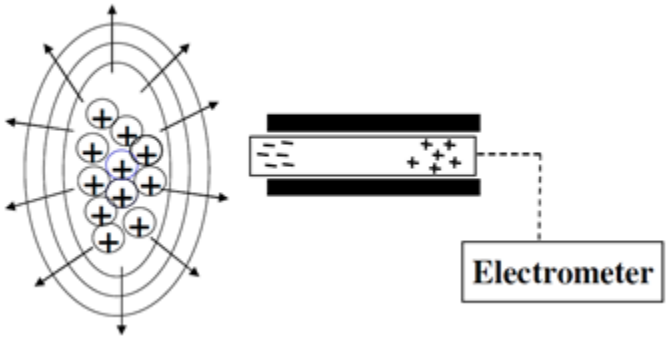

Figure 1.11: Schematic of an electrostatic probe and its charge measurement mechanism.

The probes are placed either vertically (parallel to the column axis) (Ciborowski and Wlodarski, 1962; Kiselnikov et al., 1967; Rojo et al., 1986) or horizontally (perpendicular to the column axis) (Boland and Geldart, 1972; Ham et al., 1992; Moughrabiah et al., 2009) within the fluidized beds. The probes can only provide charge measurement near the probe tip. Thus, they only detect a local charge. Moreover, these probes have been known to lose their accuracy due to particles adherence to the tip of the probe as fluidization progresses.

1.3.4.2 Faraday cup

A Faraday cup consists of two concentric metal cups: inner cup and outer cup as shown in Figure 1.12. They are isolated from each other with a piece of insulating material. The outer cup is grounded acting as an electrical shield to prevent outside electric fields. The inner cup is connected to an electrometer for charge measurement. When charged objects are placed inside the inner Faraday cup, the field of charge objects will redistribute the electrons and protons on opposite surfaces of inner cup wall, respectively. In turn they induce equal and opposite charge on the inner wall of the inner Faraday cup and this charge is measured by the electrometer. Faraday cup is a method of directly measuring electrostatic charge and provides the net charge of the objects placed within the cup.

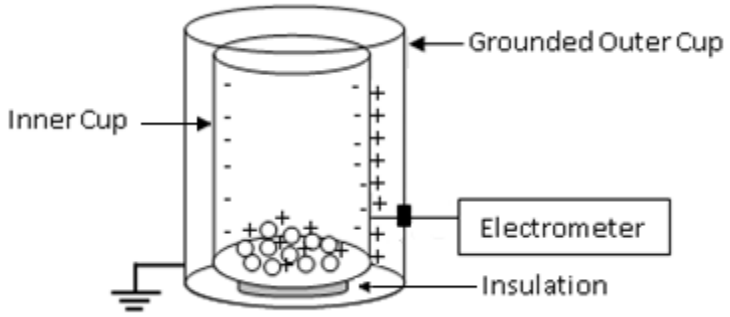

Figure 1.12: Schematic of a Faraday cup and its charge measurement mechanism.

The Faraday cup technique has been employed in gas-solid fluidized beds to measure the fluidizing particles charge. Fasso et al. (1982) placed a sampling port on the side of the reactor and utilized a vacuume pump to collect a few particles into the Faraday cup (Figure 1.13). Ali et al. (1998) used a scooper to remove a pellet sized group of particles form the fluidized bed and dropped these particles over a grid of Faraday cups. The mass, charge and particle size distribution were investigated. Bartilucci et al. (2003) modified the product discharge tank into a Faraday drum to measure the charge of particles when they reached the desired production conditions. Most previous works involing Faraday cups only measured the charge of particles in a specific region of the bed. Moreover, handling particles into Faraday cups through piping or tubing could generate additional charge which affects the charge measurement accuracy. Mehrani et al. (2005) constucted a gas-solid fluidized bed which acted as the inner cup of a Faraday cup. However, this system only provided the charge measurement of entrained fines. Finally, Sowinski et al. (2009) developed a fluidization system incorprated with two Faraday cups in an online unique way. This method provided charge, mass and size distribution measurements of particles in various regions of the fluidized bed, especially those that coated the fluidized bed wall, without any particles handling.

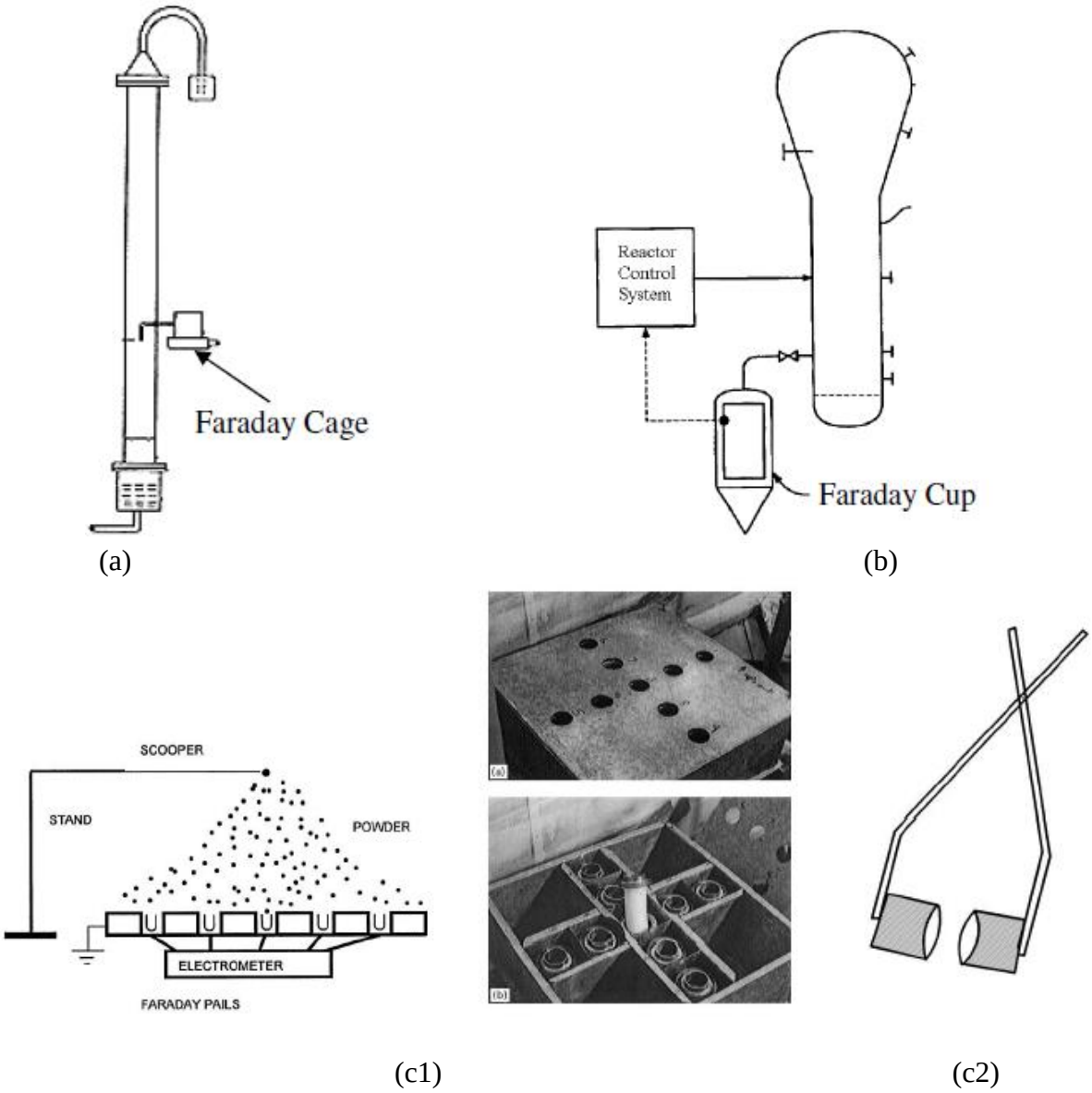

Figure 1.13: Gas-solid fluidized bed integrated with Faraday cup measurement technique. (a) Adapted from Fasso et al. (1982); (b) Adapted from Bartilucci et al. (1982); (c) Adapted from Ali et al. (1998): c1.Faraday cup grid; c2. Scopper.

1.4 Effect of Fluidizing Particle Size on Electrostatics in Gas-Solid Fluidized Beds

Boland and Geldart (1971/72), Gajewski (1985) and Guardiola (1996) found that the degree of fluidized bed electrification increases with the increase in fluidizing particles size. Sowinski et al. (2011) investigated the effect of fluidizing polyethylene particle size on charge generation and reactor wall fouling where the particles as received from commercial reactors (i.e., with a wide

particles size distribution of 20-1500 μm) and those sieved into narrow sized ranges (300-425 μm, 500-600 μm, 600-710 μm and 710-1000 μm) were tested. Their results indicated that the smaller particles would have a higher frequency of building up on the column wall. In addition, for the non-sieved resin with a size range of 20-1500 μm, particles which attached to the column wall were similar in size with the lowest narrowed size fraction of 300-425 μm and smaller. For all size ranges of sieved particles, the net charge-to-mass ratio (q/m) of particles forming the wall coating almost remained the same. However, the net q/m of non-sieved particles was twice than that of sieved particles. Moreover, they found that the larger particle size ranges (600 – 710 μm) formed an unstable wall coating, which can be found in some trials but not for others. However, it was difficult for particle sizes large than 710 μm to adhere to the column wall.

Mehrani et al. (2007) fluidized mono-size and binary mixture of glass bead particles consisting of relatively large (566 μm mean diameter) and fine (30 μm mean diameter) particles in a Faraday cup fluidized bed, which was 0.1 m in diameter and 2.1 m high, and made of copper. They concluded that the entrained fines were found to transport a net charge out of the fluidized bed, leaving a net charge of opposite polarity behind.

Yu et al. (2010) investigated the effect of the particle size on the electrostatic potential (measured by an electrostatic probe) of mixtures of different sizes of granular LLDPE particles (185 μm - 855 μm particles to the large ones 1275 μm) in a three-dimensional Plexiglas fluidized bed. Their study concluded that electrostatic potential increased by the increase in the fraction of additive. This observation was more obvious for smaller particles. Moughrabiah et al. (2012) empolyed binary mixture of small (45-90 μm) and large (600-850 μm) glass beads. The experiments were conducted in a three-dimensional stainless steel fluidization column and at elevated pressures of up to 1000 kPa (10 bar). Electrostatics was detected by electrostatic probes. It found that the degree of electrification increased as the proportion of small (65 μm) particles increased.

1.5 Effect of Binary Mixture of Particles on Gas-Solid Fluidized Beds Hydrodynamics

Formisani (1991) fluidized binary mixture of sieved glass beads ranging from 173 μm to 483 μm in a Perspex fluidization column of 0.101 m inner diameter. It was found that the mean particle size ratio (large particle size to small particle size) and volumetric fraction of smaller particles in

the mixture (Figure 1.14) had significant impacts on the viodage at minimum fluidization. Addition of small amount of fines, up to 40%, resulted in voidage reduction.

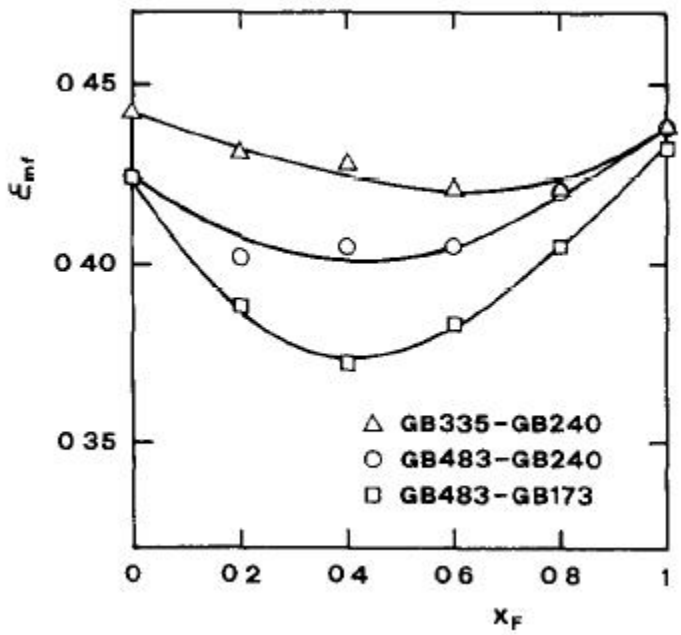

Figure 1.14: Voidage at minimum fluidization vs. fines volume fraction, adapted from Formisani, 1991.

Beetstra et al (2009) investigated the influence of fines on the fluidization behaviour of Geldart group A particles. Their experiments were conducted by fluidizing a mixture of porous alumina particles of 50 μm to 70 μm with fines of smaller than 45 μm in a small-scale stainless steel fluidized bed (0.073 m in diameter and 0.40 m in height). The fines fraction was varied from 0 to 50 wt%. In this work, the relative bubble size was detected by spectral decomposition of the measured pressure fluctuations. They found that at a gas velocity of $U = 2U_{mf}$, the bubble size increased with the addition of fines.

Lu and Gidaspow (2003), Lu et al. (2007), and Gao et al. (2009) found that for fluidization of binary particle mixures (Group A with Group D), segregation occurred where small particles (Group A) moved to the top of bed while the large particles (Group D) settled down to the bottom of the bed. In the wall region, the concentration of small particles showed a higher value. Moreover, both size particles flowed down near the wall. Vertical velocity, paralel to the column, of the small particles was larger than that of large particles.

Wu et al. (2007) analyzed the pressure fluctuation signals while fluidizing polyethylene particles of different size and particle size distribution in a bubbling gas-solid fluidized bed. They found that particle size distribution significantly impacts the gas-solid flow behavior. They proposed that the wider particle size ranges have the less chance to generate larger bubbles at the same superficial gas velocity ratio (U_g/U_{mf}).

X-ray tomography was employed to study the effect of fines content on bubble diameter and rise velocity inside a bubbling fluidized bed by Brouwer et al (2012). They fluidized a mixture particle of 77 μm catalyst SSCa-5/200 and 38 μm SCFa-230 with 600 μm polyethylene particles at various gas velocities in a stainless steel column with an inner diameter of 0.25 m. The results demonstrated that an increase in fines content led to smaller bubbles.

Chew et al. (2011) examined the bubbling performance of Geldart group B particles (sand) with continuous size distribution in a Plexiglass column (0.185 m in diameter). Continuous size distributions of the particles was defined as the ratio of standard deviation to sauter-mean diameter (σ/d_{sm}) and sauter-mean diameter (d_{sm}) was set to 375 μm. In this work, fiber optic probe was utilized to obtain information on bubble characteristics. All bubble parameters (chord length, velocity and frequency) were found to monotonically increase with increasing the range of the particle size distribution.

Tagami et al. (2009) employed three-dimensional discrete element model (DEM) for mono-disperse, binary and ternary systems of particles in a fluidized bed. The system with wide particle size distribution exhibited higher particle velocities around bubbles, resulting in faster bubble growth and its subsequent rise through the fluidized bed.

1.6 Thesis Objectives

The overall focus of our group is to better understand the underlying mechanisms of charge generation in gas-solid fluidized beds. And ultimately, to assist commercial operations such as those of polyethylene to find means to reduce or eliminate the negative effects of electrostatic charging. In order to achieve this goal, a fluidization system was previously developed by Sowinski et al (2009) housing an online Faraday cup charge measurement technique. This

system was then operated with various polyethylene resins to investigate the effects of various operating parameters such as fluidizing gas velocity and relative humidity, fluidizing particle size, column wall material, fluidization period, etc.

For all experiments where fluidization of different types of polyethylene resins (received from a commercial reactor with wide size distribution of 20-1500 μm) were performed, it was found that certain particle sizes, approximately 400 μm and smaller, generally fouled on the column wall. This finding lead to the specific objectives of this thesis were the effect of polyethylene fluidizing particle size, particularly the specific size rang of 400 μm and smaller on the degree of bed electrification and reactor wall fouling was investigated.

The investigation specifically focused on examining two types of polyethylen resin as received directly from commercial reactors as well as the mono-sized and binary mixture of the same resins sieved. The binary mixtures included small particles (smaller than 400 μm) and large particles (600-700 μm, which were of similar size to the mean particles size of resin as received).

Although the experiments conducted were in relation to polyolefin industry but results obtained from this research can assist in the overall understanding of electrostatics phenomenon in gas-solid fluidized beds.

1.7 Thesis Outline

The second chapter of this thesis describes the materials experimental apparatus and the measurement technique used in this reserach.

The third and fourth chapters present the results of the effect of fluidizing particle size and the mechanism of wall fouling formation.

The final chapter focuses on the overall conclusions of this work. It also discusses recommendations for future work.

Chapter 2. Experimental Apparatus, Method and Materials

This chapter describes the experimental apparatus and materials used, and the procedures followed to conduct two sets experiments: a) fluidization; and b) bench-scale shaking tests.

2.1 Materials

2.1.1 Fluidizing Gas

Fluidizing gas utilized in all experiments was compressed building air with relative humidity (RH) of 3.0±0.5% and temperature of 20±2 ℃.

2.1.2 Fluidizing Particles

Although results obtained from this research can assist in the overall understanding of electrostatics phenomenon in gas-solid fluidized beds, but the experiments conducted were in relation to one application related to polyolefin industry.

Fluidizing particles used in all experiments were linear low-density polyethylene (LLDPE) resins, which were produced using metallocene based catalysts and received from Univation Technologies, LLC (USA). Two types of polyethylene resins (PE_A and PE_B) were used in this work with properties summarized in Table 2.1. Experiments were first performed with both resins as received (i.e., having a larger particle size distribution). Then in order to evaluate the effect of presence of small particles (400 μm), resins as received were sieved into narrow size distributions and binary mixture of large and small particles were studied. The small particles sizes were 212-300 μm and 300-425 μm while the large particles were 600-710 μm,

Table 2.1: Properties of polyethylene particles used in this work.

		PE_A (as received)	PE_{AS} (Sieved) (Small Particles)	PE_{AL} (Sieved) (Large Particles)
Surface Properties				
Scanning Electron Microscope (SEM) Images		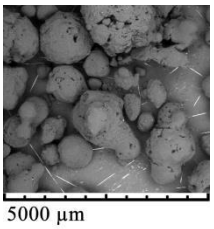	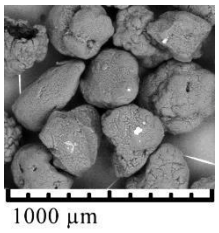	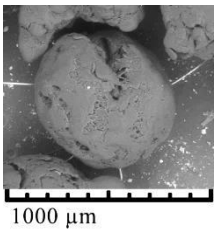
Sphericity		0.749	0.797	0.797
Morphology			Coarse	Coarse
Physical Properties				
Particle Density	kg/m^3	920		
Particle Size Distribution	µm	20-1500	212-300	600-710
Mean Particle Diameter	µm	625	263	713
Specific Surface Area ($\hat{A}$)	m^2/g	0.0124	0.0255	0.004
Geldart Group		B	B	B
Mean Particle Size Comparison				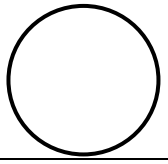
Chemical Properties				
Chemical Formula		$(C_2H_4)_n$		
Chemical Structure		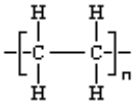		
Water adsorption		Hydrophobic		
Electrical Properties				
Work Function	eV	5.3		

		PE_B (as received)	PE_{BS-1} (Sieved) (Small Particles)	PE_{BS-2} (Sieved) (Small Particles)	PE_{BL} (Sieved) (Large Particles)
Surface Properties					
Scanning Electron Microscope (SEM) Images		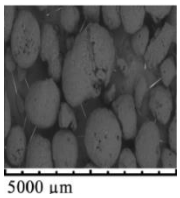	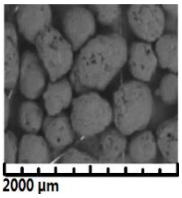	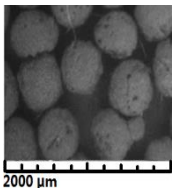	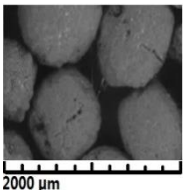
Sphericity		0.80	0.80	0.81	0.81
Morphology		Coarse	Coarse	Coarse	Coarse
Physical Properties					
Particle Density	kg/m^3	918			
Particle Size Distribution	µm	20-1500	212-300	300-425	600-710
Mean Particle Diameter	µm	654	268	398	696
Specific Surface Area ($\hat{A}$)	m^2/g	0.0120	0.0233	0.0156	0.0086
Geldart Group		B	B	B	B
Mean Particle Size Comparison					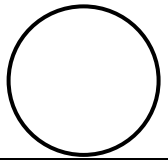
Chemical Properties					
Chemical Formula		$(C_2H_4)_n$			
Chemical Structure		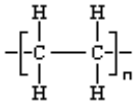			
Water adsorption		Hydrophobic			
Electrical Properties					
Work Function	eV	5.3			

Particle Surface Morphology and Sphericity

The qualitative measurement of particles surface morphology was conducted through SEM images. These images also enabled the calculation of the particles sphericity. The sphericity was assumed to be equal to circularity. The measurement of circularity was performed based on projected area seen in SEM pictures and using tools in Photoshop software. The circularity can be estimated by the following equation:

$$circularity = 4\pi\left(\frac{area}{perimeter^2}\right) \quad (2.1)$$

The sphericity values presented in Table 2.1 are the average of the circularity of many particles.

Particle Density

The density of the particles was provided by Univation Technologies, LLC.

Particle Diameter and Specific Surface Area

Particles size distribution was measured by the Malvern Mastersizer 2000 with Hydro2000S sampler. The measurements also provided the particles specific surface area.

Geldart Classification

Based on particles mean diameters and densities shown in Table 2.1, and the fluidizing gas density (1.2 kg/m^3), the particles Geldart classification was evaluated. For all particle size ranges, both resins (PE_A and PE_B) were found to be Geldart class B.

Work Function

The effective work function of polyethylene was found in literature to be 5.3 eV (Tanoue and Masuda, 2006)

2.2 Fluidization Experiments

Fluidization experiments were conducted in two pilot-scale systems as illustrated in Figure 2.1 and Figure 2.2, having column diameters of 0.10 m (hereafter refers to as "small column") and 0.15 m (hereafter refers to as "large column"). The fundamental design of the two systems was equivalent in which both consisted of a 3D fluidization column that housed an online Faraday cup measurement technique and numerous instrumentations. Pictures of the two systems are presented in Figure 2.3.

2.2.1 Fluidization Column

As can be seen in Figure 2.3, both the small and the large fluidization columns were metallic and made of carbon steel and stainless steel 316, respectively. Numerous ports were located at different heights along the columns to allow mounting different instrumentations such as differential pressure transducers. The details of both columns are presented in Table 2.2.

For both columns, the distributor plates were modified pneumatic knife gate valves, enabling the bulk of the bed particles to be automatically discharged from the column. For the small column, the knife gate valve was of Series G pneumatic knife gate valve supplied by the Red Valve Company Inc. (Pennsylvania, USA), while that of the large column was a ORBINOX Series 50 pneumatic knife gate valve, supplied by Meridian (Alberta, Canada). The valves blades consisted of two perforated plates fabricated from stainless steel 316 and a metal mash sandwich between them. A 32 μm mesh placed between the two plates prevented particles from falling through the holes of the plates.

For both systems, as will be seen in section 2.2.2, it was necessary to easily open and close the top and bottom of the fluidization columns. Thus the larger column that was designed to operate at high pressures of up to 2500 kPa, consisted of two manways located at the top and bottom of the fluidization column.

Table 2.2: The detail information of fluidization columns.

Apparatus	**Parameter**	**Small Column**	**Large Column**
Column	Inner diameter (m)	0.10	0.154
	Fluidization section (m)	1.3	2.5
	Total Height (m)	2.4	4.5
Filter bag	Diameter (m)	0.102	0.178
	Height (m)	0.178	0.229
Bottom Faraday cup	Inner cup diameter (m)	0.152	0.254
	Inner cup height (m)	0.254	0.305
	Inner cup material	Copper	Copper
	Outer cup diameter (m)	0.254	0.356
	Outer cup height (m)	0.305	0.610
	Outer cup material	Copper	Stainless steel
Top Faraday cup	Inner cup diameter (m)	0.127	0.254
	Inner cup height (m)	0.330	0.305
	Inner cup material	Copper	Copper
	Outer cup diameter (m)	0.152	0.356
	Outer cup height (m)	0.406	0.610
	Outer cup material	Copper	Stainless steel

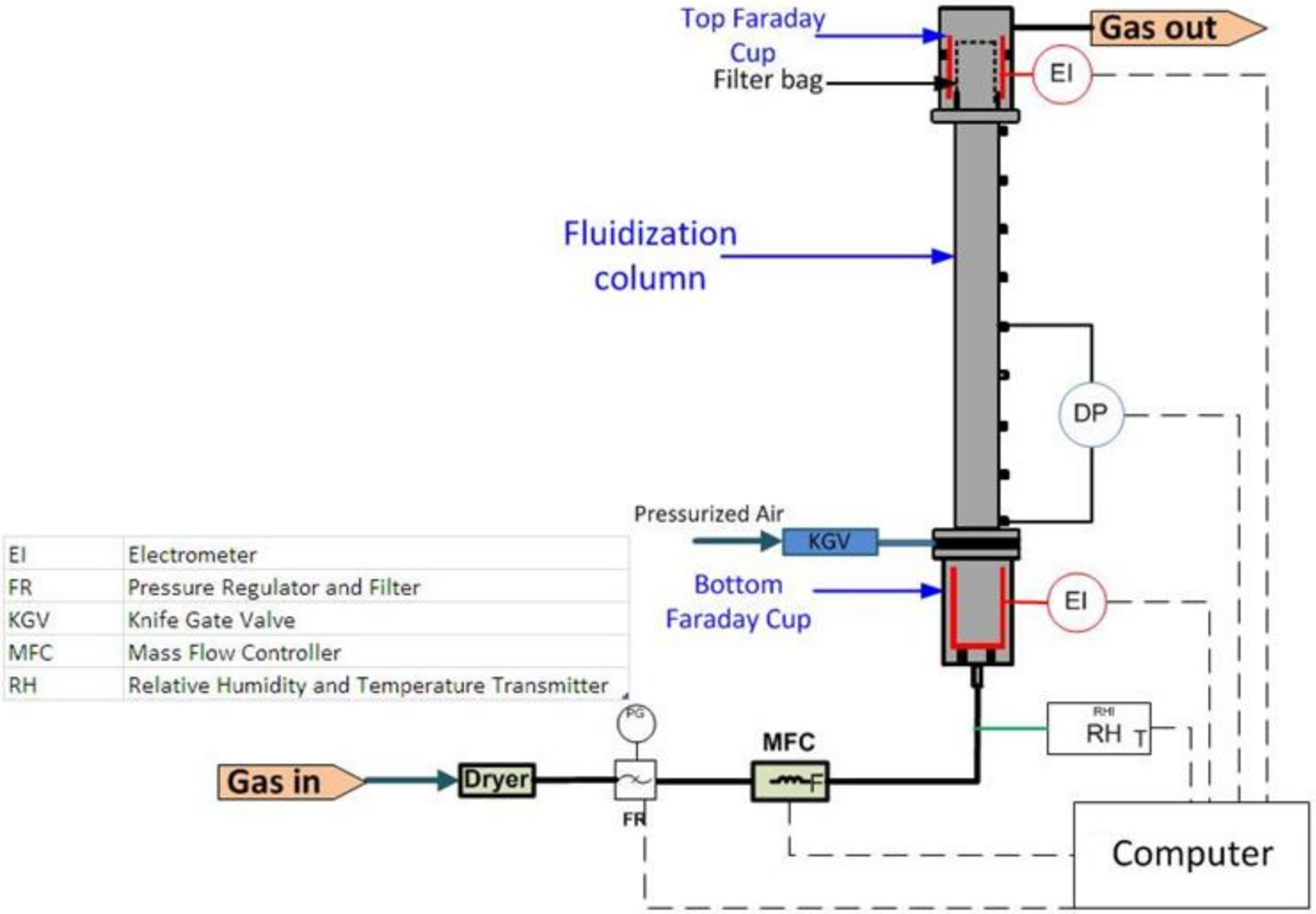

Figure 2.1: Schematic of the small column fluidization system.

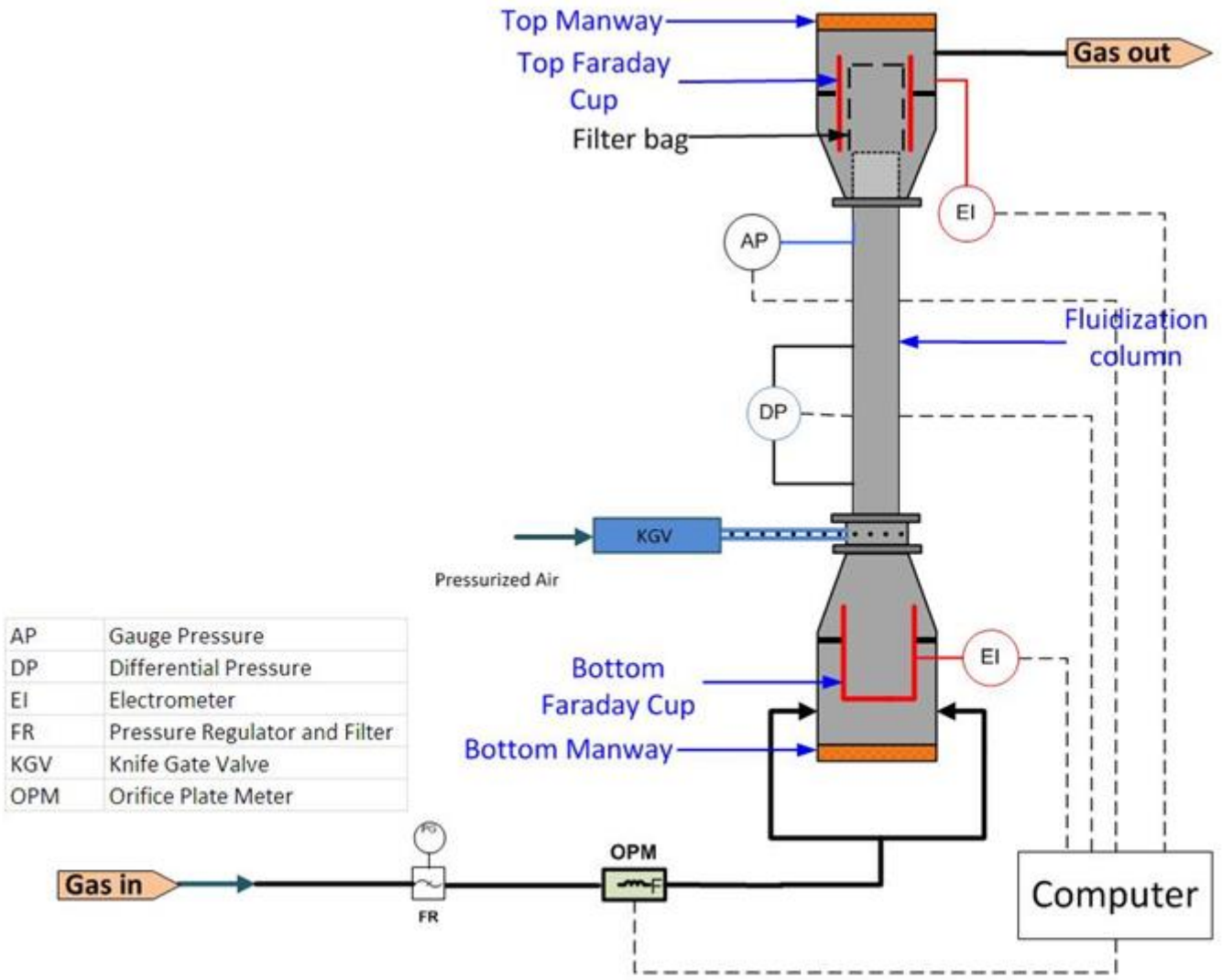

Figure 2.2: Schematic of large column fluidization system.

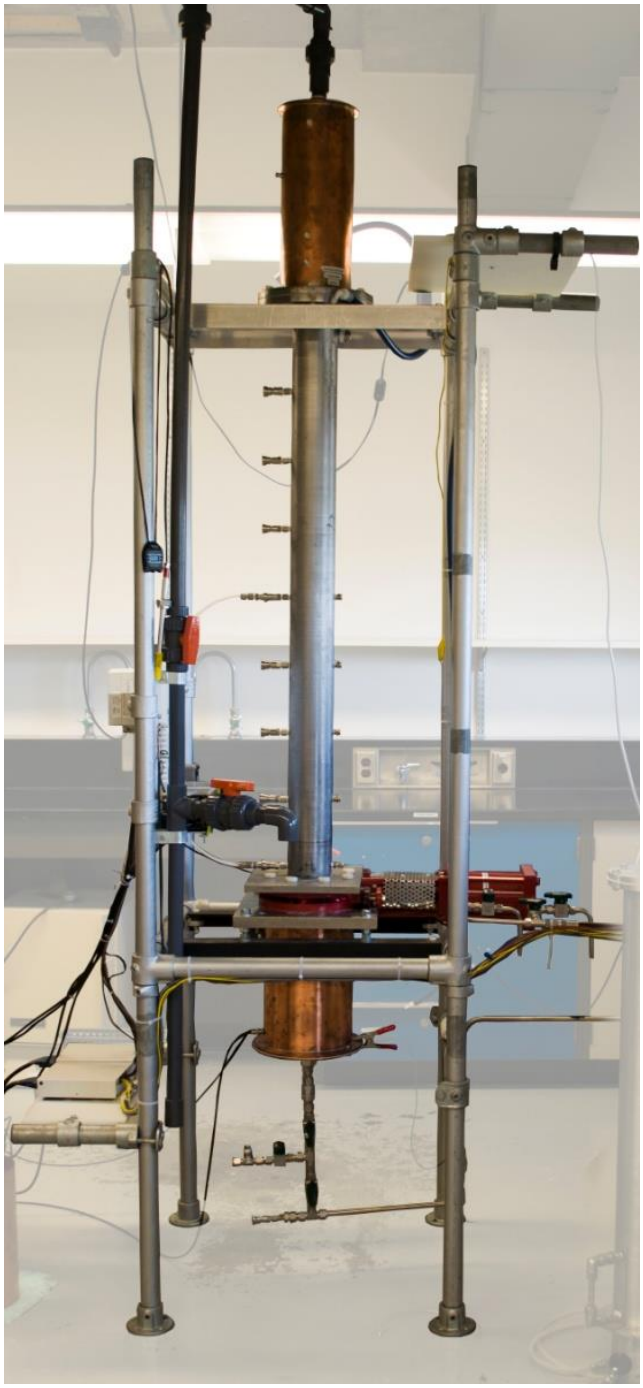

(a)

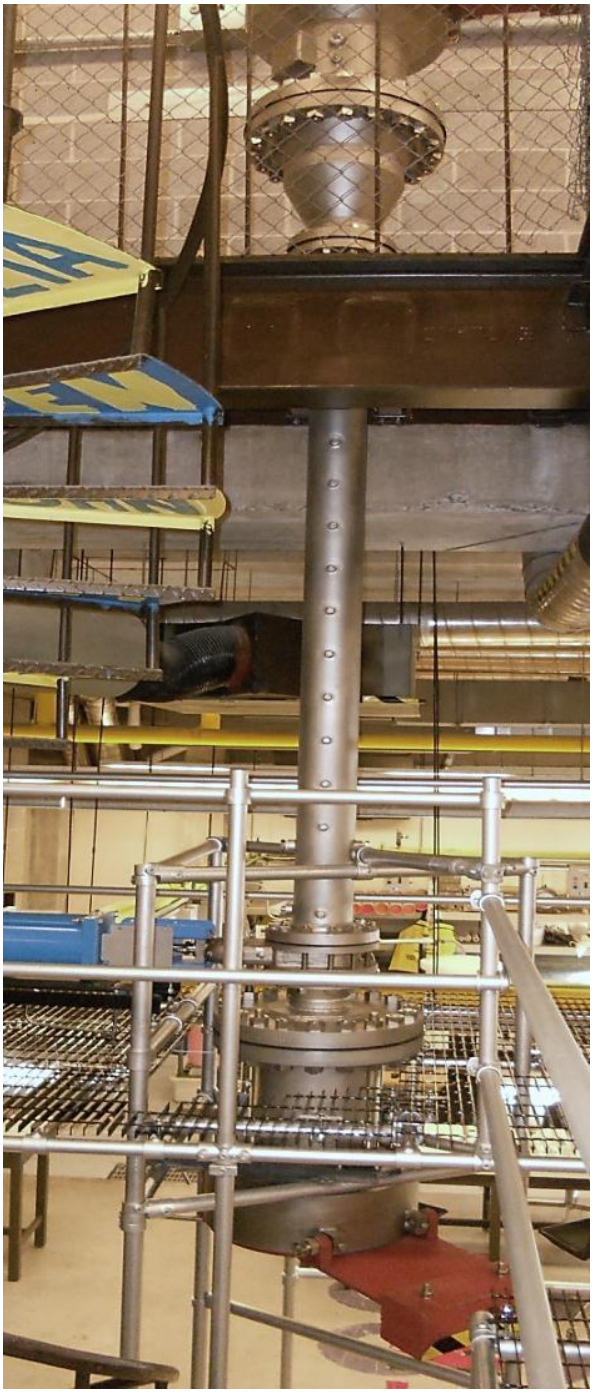

(b)

(c)

Figure 2.3: Pictures of the fluidization columns: (a) small column; (b) large column; and (c) overview of large system.

2.2.1.1 Electrostatic Charge Measurement Technique

Electrostatic charge measurements were conducted through an online Faraday cup technique that was previously developed in our research group by Sowinski et al. (2009). The measurement technique consisted of two Faraday cups located at the top and bottom of the fluidization column as seen in Figure 2.1 and Figure 2.2. These Faraday cups enabled the measurement of particles mass and charge in various regions of the fluidized bed, particularly the mass and charge of the particles adhering to the column wall.

All Faraday cups consisted of two concentric metal cups (an inner cup and an outer cup) which were isolated from each other with Teflon connectors. For the small column, all the inner and outer cups were made of copper while for the large column only the inner cups were fabricated of the same material. For the larger column, the body of the fluidization column at the top and bottom simply acted as the outer Faraday cup. For both systems, the fluidization column and the outer cups were grounded. The outer cups were grounded to prevent the inner cup measurement to be affected by any electric field present in the lab environment.

Top Faraday cups in both columns contained a filer bag attached to the top of the columns with a Teflon adapter. The filter bags were filled with four layers of Dustlock filter supplied by BC Air Filter (BC, Canada) to capture the entrained particles during fluidization. The inner Faraday cups were each connected to a Keithley digital electrometer Model 6514 enabling the measurement of the cumulative net charge of entrained particles during fluidization.

The measurement of the charge and the mass of particles within the bulk of the bed and those adhered to the column wall was conducted by the bottom Faraday cups. The inner cups of the bottom Faraday cups were connected to a Keithley digital electrometer Model 6514 allowing the measurement of the net charge of particles discharged from the fluidization column into these cups at the end of each fluidization run. As presented earlier, the removal of the particles without any handling was achieved by the modified knife gate valves.

This technique can provide the measurement of charge, mass and particle size distribution in various regions of the bed. The general operating procedure is as follow:

The desired mass of particles to be fluidized (hereafter refer to as “initial”) was measured and a sample of initial particles was taken for particles size distribution analysis. The charge of these

particles was measured by a bench-scale Faraday cup (Figure 2.4a) followed by pouring the particles into the fluidization column.

The mass of the filter bag was then measured followed by filling it with four layers of Dustlock filters. The bag was then attached to the top of column and the top Faraday cup was assembled. With the larger system, the top manyway was closed and locked. The top Faraday cup was connected to the electrometer.

Fluidization gas was then introduced into the column by slowly increasing the gas flow until the desired flowrate was reached. Particles were then fluidized at this flowrate for 60 minutes. During fluidization, the entrained particles ("fines" as shown in Figure 2.4b) were collected by filter bag and their cumulative net charge was continuously measured by top Faraday cup. After the fluidization period was completed, the top Faraday cup was removed followed by the filter bag. The mass of the filter bag containing the entrained fines was measured. A sample was taken from the particles for PSD analysis.

The bottom Faraday cup was then connected to the electrometer and after one minute background signal measurement, the knife gate was opened allowing the bulk of the bed particles (referred to as "bulk" as shown in Figure 2.4b) to drop into the cup so that their charge to be measured. The bottom cup was then removed and the mass of the bulk particles collected was measured while taking a sample for PSD testing.

Before putting the cleaned bottom Faraday cup back on the column, the inner column wall was inspected for any fouling and a picture was taken of the particles adhered to the column wall (referred to as "wall" particles in Figure 2.4c). The image would provide qualitative measurement of position and degree of the wall layer coating. The bottom Faraday cup was then assembled and connected to the electrometer. In the case of the larger column, the bottom manway was closed. After one minute of background signal measurement, in small column case, the column was lightly taped to dislodge the wall particles and this was continued until there was no change in the measured charge by the electrometer. These particles were referred to as "loosely bound". Then the bottom cup was removed to measure the mass of the particles collected and a picture was taken again to determine whether any highly charged particles still remained adhere to the wall (these particles referred to as "tightly bound"). Samples of loosely

and tightly bound particles were taken for PSD analysis. In the case of the large column, the removal of the wall particles was achieved by injecting a small stream of dry air thorough a stainless steel tube inserted into the column from the top. In this case, no distinction of the loosely and tightly bound particles was made and thus all particles were referred to as "wall".

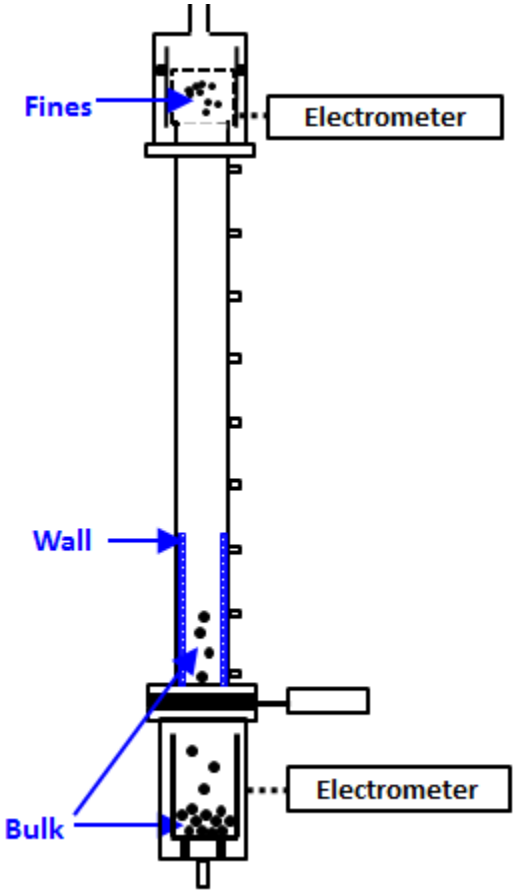

(b)

(a)

(c)

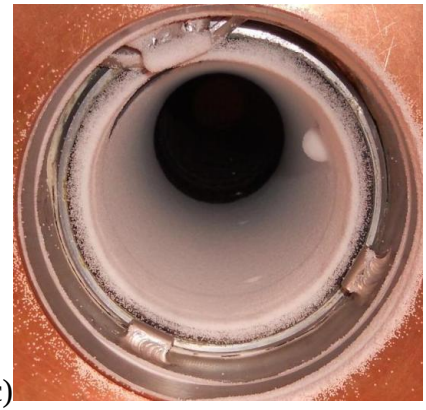

Figure 2.4: (a) Image of the bench-scale Faraday cup; (b) Particles charge measurement in various regions of the fluidized bed; (c) Typical image of the particle layer left on the column wall upon the removal of the bulk particles.

2.2.1.2 Instrumentation

Several instrumentations were used in both systems to measure and control various operating conditions. The pressure drop across the bed was detected by a differential pressure transducer (Omega PX654 transducer in the small column and an ABB 2600T transducer in the large

column). A pressure regulator (also housing a filter) was used to regulate the inlet gas (compressed building air) pressure. The fluidizing gas flowrate was measured and controlled by a mass flow controller in the smaller system while it was measured by an orifice plate meter in the larger unit. A Vaisala temperature and humidity transmitter (HMT338) was used to measure the relative humidity and temperature of the inlet gas. Since the inlet gas supply of two systems was the same, the conditions of fluidizing gas were similar. The temperature and relative humidity of the laboratory was also monitored by a second Vaisala temperature and humidity transmitter.

As presented earlier, electrostatic charge measurements were conducted by Keithley digital electrometers Model 6514. Various charge measurement ranges were available with this unit but for most charge measurements a range of 20 μC was used.

Particle size distribution measurement was conducted through two methods. One method was using a Malvern Mastersizer model 2000 with Hydro2000S sampler. Particles were suspended in solution (40% water and 60% ethanol) for this measurement. The other method was sieving.

All measurement devices and controllers were connected to a PC, and all data collection and recording was performed by the LabView software. Data was sampled at a frequency of 10 Hz with the exception of the minimum fluidization velocity measurement which was performed at 100 Hz.

2.2.1.3 Charged Particle Separator

The online Faraday cup measurement technique used in this research enables the net charge measurement of particles in various regions of the bed. Thus, in order to investigate the particles charge distribution within each region and to better understand the charging mechanisms, a charged particle separator (CPS) was used (Figure 2.5).

The CPS unit consisted of four Faraday cups (FC1, FC2, FC3 & FC4) located under two copper plates (0.457 m length and 0.305 m wide). The two plates were connected to a high voltage source (Ultravolt HVwith 40 kV maximum voltage). As shown in Figure 2.5a, one plate charged positively and the other negatively. As charged particles fall in between the two plates, positively charged particles would be attracted towards the negative plate and fall into FC3 and FC4 and negatively charged particles would be attracted towards the positive plate and thus falling into

FC1 and FC2. Each of the Faraday cups was connected to an electrometer to measure the particles charge. The separation efficiency depends on the magnitude and polarity of the particles. This unit was placed directly under the two fluidization columns as can be seen in Figure 2.6 for the analysis of charge distribution of the particles adhered to the column wall.

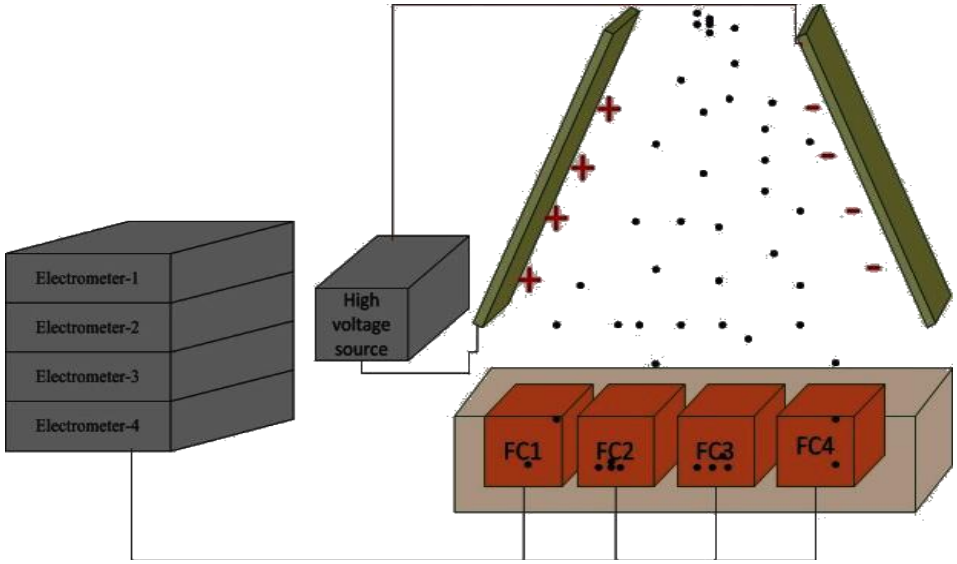

(a)

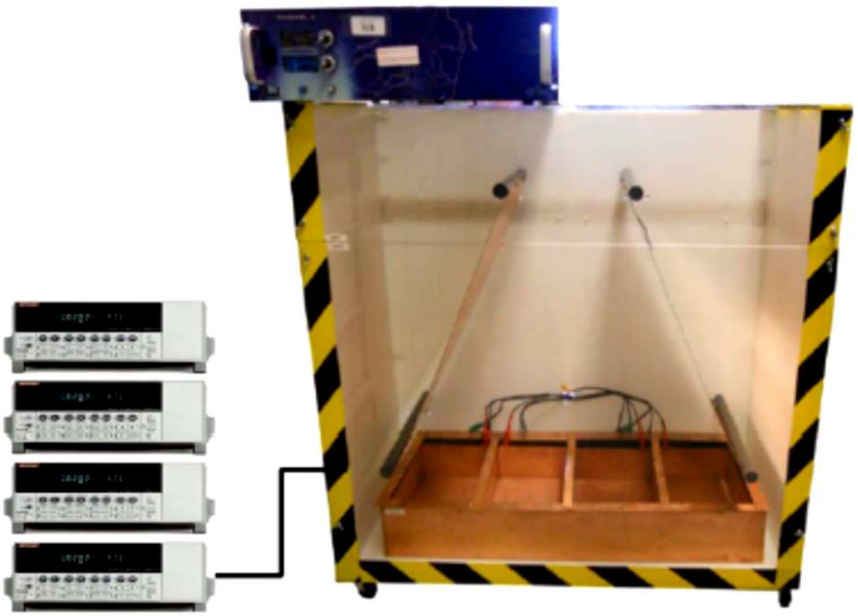

(b)

Figure 2.5: (a) Schematic of charged particle separator (CPS); (b) Picture of charged particle separator.

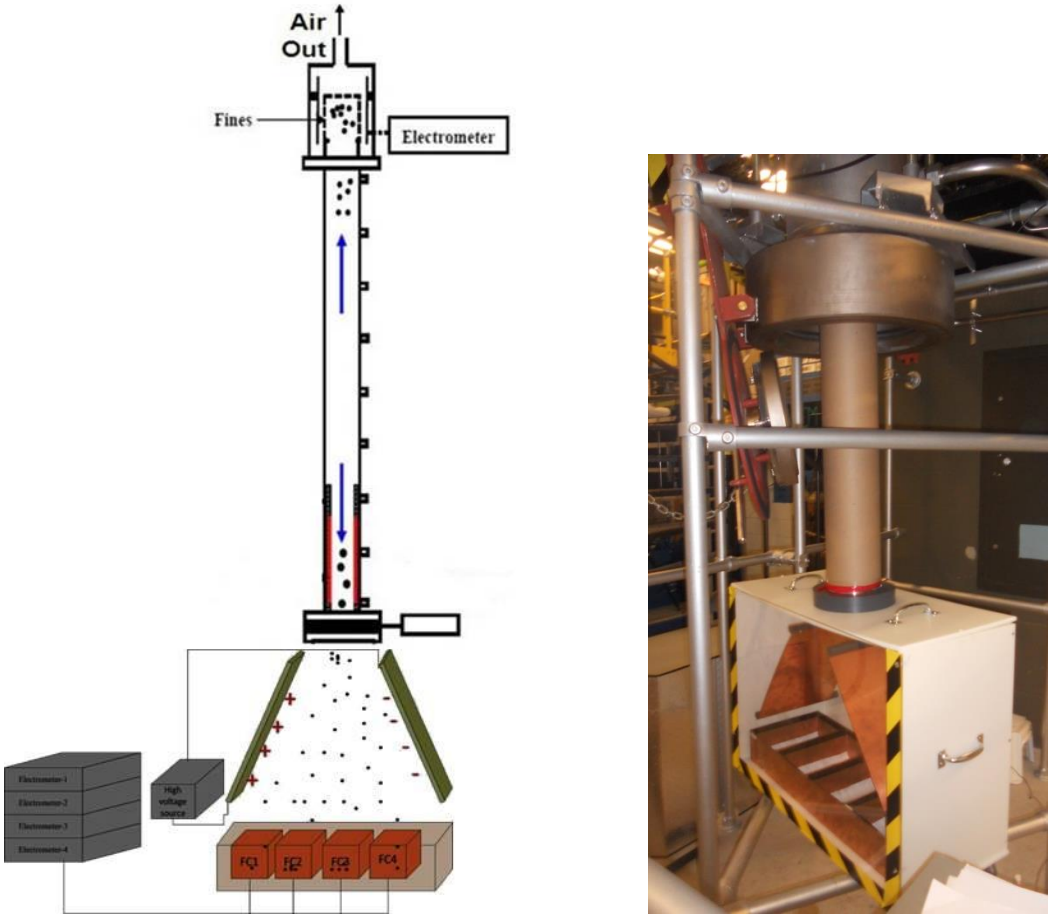

(a) (b)

Figure 2.6: (a) Schematic of CPS unit placed under the column; (b) Picture of CPS unit placed under the large column.

2.2.2 Experimental Conditions and Procedure

Fluidization experiments were first conducted with two types of polyethylene resin as received (PE_A and PE_B). However, in order to investigate the effect of particle size of 400 μm and smaller on the degree of bed electrification and wall fouling, as received polyethylene resins were sieved into different size ranges including 212-300 μm (mesh No. 70), 300-425 μm (mesh No. 50) and 600-710 μm (mesh No. 30). The binary mixture of sieved particles of small (PE_{AS} & PE_{BS-1} PE_{BS-2}) and large sizes (PE_{AL} & PE_{BL}) were then evaluated.

The detailed experimental conditions used in this work for fluidization trials are summarized in Table 2.3 and 2.4. For the binary mixture experiments, the fraction of smaller particles in the

mixture was evaluated from 0% to 20%. The later was chosen based on the fact that the resins as received had approximately 20 w% of 450 μm and smaller particles.

The minimum fluidization velocity, U_{mf}, was measured experimentally (by measuring the pressure drop across the bed while the fluidizing gas velocity was varied) and values are summarized in Table 2.3.

Table 2.3: Summary of the fluidization experimental conditions of PE_A and PE_B particles in small column.

Parameter	**value**	**value**
Fluidizing Particles		
Type	PE_A	PE_B
Size Range (μm)	212-300 (PE_{AS})	212-300 (PE_{BS})
	600-710 (PE_{AL})	600-710 (PE_{BL})
Fluidizing Gas		
Velocity	$1.5U_{mf}$	$1.5U_{mf}$
Temperature (^oC)	20 ± 2	20 ± 2
Relative Humidity (%)	3	3
Operating Conditions		
Column Height-to-Diameter (L/D)	4	4
Fluidization Time (min)	60	60
Mass percentage of small particles added (%)	0, 5, 6, 7, 8, 9, 10, 20	0, 5, 10, 20

Table 2.4: Summary of the fluidization experimental conditions of PE_B particles in large column.

Parameter	**value**	**value**
Fluidizing Particles		
Type	PE_B	PE_B
Size Range (μm)	212-300 (PE_{BS-1})	300-425 (PE_{BS-2})
	600-710 (PE_{BL})	600-710 (PE_{BL})
Fluidizing Gas		
Velocity	$1.5U_{mf}$	$1.5U_{mf}$
Temperature (^oC)	20 ± 2	20 ± 2
Relative Humidity (%)	3	3
Operating Conditions		
L/D	2.2	2.2
Fluidization Time (min)	60	60
Mass percentage of small particles added (%)	0, 5, 10, 20	0, 5, 10, 20

Table 2.5: Values of U_{mf} measured in m/s for various mixtures of small and large particles of PE_A and PE_B particles.

Mass percentage of small particles in the mixture (%)	0	5	10	20
PE_{AS}	0.173	-	0.161	0.134
PE_{BS-1}	0.190	0.169	0.151	0.133
PE_{BS-2}	0.190	0.174	0.158	0.146

The fluidization experimental procedure is previously explained in section 2.2.1.1. It is important to add that prior to each experiment, the column and distributor plate were thoroughly cleaned. Each experimental condition was repeated at least three times to ensure the reproducibility of results.

In order to investigate the fluidizing particles charge distribution, in some trials, the bottom Faraday cup was replaced by the CPS apparatus. In such a case, after taking a picture of wall particles, the bottom Faraday cup was removed and the CPS unit was placed under the column while the centre of the CPS was kept aligned with the centre of column. The high voltage source was then turned on and adjusted to the desirable voltage. After one minute of background signal measurement by all four electrometers, the loosely bound wall particles would be dislodged until no change in the measured charge by the electrometers was observed. After turning off high voltage source, the mass of particles collected in each of the four Faraday cups was measured and samples were taken for PSD testing.

2.3 Bench-Scale Shaking Experiments

In order to better understand the charge generation mechanism in fluidization experiments and to further investigate the triboelectrification charging behaviour of PE_A and PE_B particles, bench-scale shaking experiments were conducted.

2.3.1 Experimental Apparatus

The apparatus used for the shaking experiments is shown in Figure 2.7. The main components of the system included a shaker machine (portable Ce Tyler sieve shaker), and a clamp with insulated tips. A carbon steel tube 0.03175 m (1.25 inch) in diameter and 0.1016 m (4 inch) in length was used for shaking PE_A particles while for PE_B particles a stainless steel tube 0.01905 m (3/4 inch) in diameter and 0.3048 m (12 inch) in length with stainless steel caps was employed.

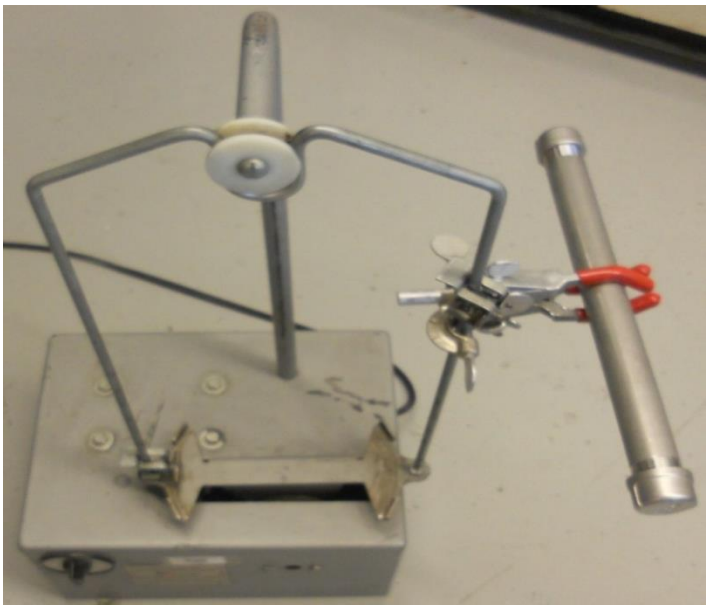

Figure 2.7: Image of shaking experiments apparatus.

2.3.2 Experimental Conditions and Procedure

The following section describes the operating conditions and procedures for various Bench-Scale experiments performed in this work.

For all experiments, the tubes were washed with ethanol and water and dried prior to each trial. Each test condition was repeated at least 3 times to ensure reproducibility. The generated charge on the particles due to shaking was calculated by subtracting the particles initial charge from their final charge.

2.3.2.1 Shaking experiments with PE_A particles used in fluidization experiments in small system

In these experiments, samples of the small (PE_{AS}) and large (PE_{AL}) particles, same as those used in the fluidization runs, were examined to determine which of the mechanisms; particle-wall or particle-particles contacts are dominant. Three types of experiments were conducted including:

Case (a): In order to detect the charging behaviour of these two size range particles in contact with the carbon steel fluidization column wall, 4 g of PE_{AS} and PE_{AL} particles were each shaken for 10 minutes. The mass of particles was small enough to consider the collisions between particles and tube wall as the main charging method during the shaking. In addition, two other

experiments were designed: **(a)** PE_{AS} and PE_{AL} particles were poured directly into the CPS unit without shaking; and **(b)** PE_{AS} and PE_{AL} particles were poured into CPS unit after shaking.

Case (b): In order to investigate the effects of addition of smaller particles on degree of charging, shaking experiments were also performed with binary mixtures of small and large particles. In this case, a total mass of 20 g of mixture was shaken for 10 minutes. Various fractions of PE_{AS} (0%, 5%, and 10%) were tested. Particles were then poured directly into the bench scale Faraday cup.

Case (c): To investigate the charge transfer between the small and large particles during the shaking process, experiments in case (b) were repeated using CPS unit after all trials instead of Faraday cup.

Prior to conducting the shaking tests, particles initial net charge and charge distribution were measured by the bench-scale Faraday cup and CPS unit, respectively. The CPS unit was operated with the high voltage source adjusted to 30 kV. Particles mass and PSD were measured from each Faraday cup.

In some trials, in order to better understand the charging polarity of the particles, their charge distribution was measured by the CPS unit upon the completion of the shaking period. The high voltage source was set to 25 kV for these tests. Samples of particles were then taken from each Faraday cup for PSD analysis.

In all trials, the empty tube was inserted into the bench-scale Faraday cup after each experiment to measure its charge upon shaking the particles.

2.3.2.2 Shaking experiments with PE_B particles used in fluidization experiments in small system

Three types of shaking experiments were performed with PE_B particles.

Case (a): 5 g of PE_{BS} and PE_{BL} particles were each shaken for 5 minutes. This type of testing aimed at detecting the charging behaviour of these two particle size range while in contact with the carbon steel fluidization column wall.

Case (b): In order to simulate particle-particle contacting especially for those of large and small particles and the charge polarity gained upon contact, a layer of PE_{BS} particles was applied to a scotch tape which was then folded into a 1 inch diameter and inserted inside the shaking tube, making the tube inner wall covered by PE_{BS} particles. Then 10 g of PE_{BS} and PE_{BL} particles were shaken separately in this tube for 10 minutes. Fresh layer of particles used for each repetition. The ends of the tube were also sealed by PE_{BS} layer. CPS unit was utilized in some runs to examine the particles charge distribution.

Case (c): Case (c) was similar to Case (b) with the exception that a layer of PE_{BL} particles were used on the tape instead of small particles and PE_{BS} particles were shaken in the tube.

The initial charge of particles was measured via the bench-scale Faraday cup prior to each trial. For cases (b) and (c), a layer of PE_{BS} or PE_{BL} particles were applied to scotch tape and it was ensured that particles tightly adhered to the tape and no particles were falling off. The mass of particles upon removal at the end of the shaking period was measured to ensure there were no particles sticking to the tape while shaking.

In some trials, in order to better understand the charging polarity of the particles, their charge distribution was measured by the CPS unit upon the completion of the shaking period.

2.3.2.3 Shaking experiments with PE_B particles used in fluidization experiments in large system

Five g of PE_{BS}-$_1$, PE_{BS}-$_2$, and PE_{BL} particles were each shaken for 5 minutes in the stainless steel tube to detect the charging behaviour of these two size range particles in contact with the stainless steel fluidization column wall.

Chapter 3. Results and Discussion - Small Fluidization System

This chapter presents the measurement results of particles mass, specific charge and size distribution in different regions (Initial, Bulk, Wall and Fines) found in the small fluidization system. Since the particles were sieved and had narrow size ranges, in all trials the amount of fine particles collected in the top Faraday cup was negligible, and therefore, no data regarding the entrained fines is presented here.

3.1 PE_A and PE_B Resins as Received

Both types of resins, as received, were fluidized in the small column. As can be seen in Figure 3.1, the wall and fine particles charged oppositely indicating the presence of bipolar charging within the bed. Although the mass% and q/m of two resins in various regions were different, the mean particle sizes (dp_{50}) of wall particles were similar and were smaller than 400 μm. In addition, the wall particles size distributions for both cases were also similar, indicating that particles of a certain size to form the column wall coating. These results signify the importance of the investigation of the effects of particle size, and especially those of smaller than 400 μm, on the extent of wall fouling and bed electrification.

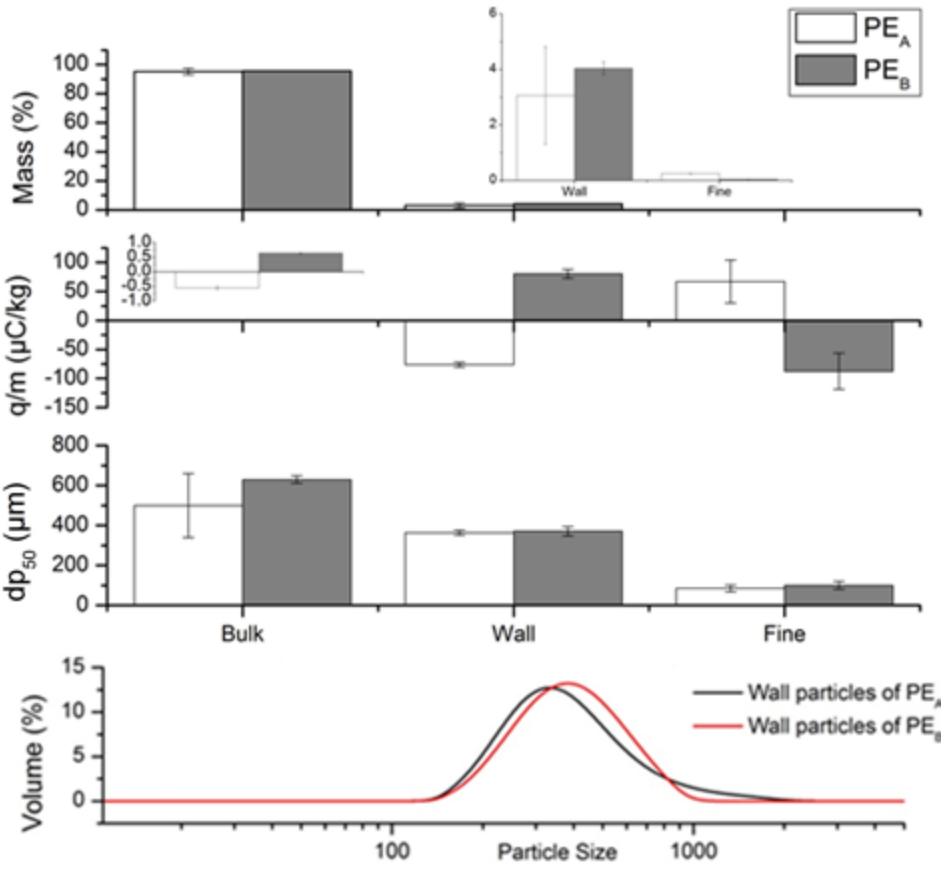

Figure 3.1: Particles mass%, q/m, and dp_{50} collected from various regions of the small fluidization system after fluidizing PE_A and PE_B resins as received, as well as the particle size distribution of wall particles.

3.2 Binary Mixture of Small and Large Particles of PE_A Resin

3.2.1 Initial Particles

The initial particles charge-to-mass ration (q/m), normalized mean particle sizes ($dp_{(50)N}$) andsauter mean diameter are presented in Figure 3.2. The net initial charge of all mixtures was negative. Although the fraction of PE_{AS} was different, all the trials started with similar net q/m. Since particles size measurements performed by Malven were not able to detect the small particles in the mixtures, the sauter mean diameter of each mixture was calculated and presented here. Results show a decrease by increasing the fraction of PE_A particles.

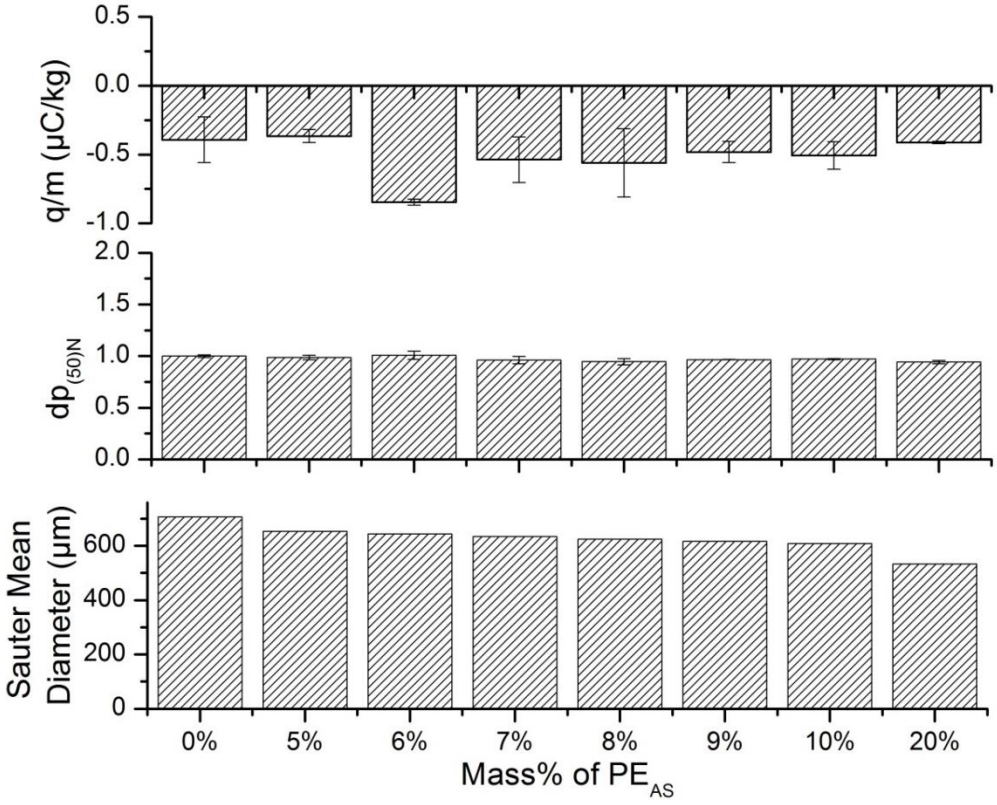

Figure 3.2: Initial particles net q/m, dp_{50}, and sauter mean diameter for binary mixture of PE_{AS} and PE_{AL} Particles.

3.2.2 Bulk Particles

As can be seen in Figure 3.3, the mean size of bulk particles remained similar to those of the initial particles. The percentage of mass of bulk particles was fluctuating when various fractions of PE_{AS} particles was added. It declined gradually (approximately 3%) from 0% to 7% PE_{AS} cases. For 7 and 8% trials, it reached to the lowest value. After that, there was an increase until 20% trial. This is an indication that for the cases with the highest percentage of small particles, less particles to be found on the column wall. On average there was a declining tendency in bulk particles net q/m as wt% of PE_{AS} particles increased. In comparison, the average net q/m of the cases with higher PE_{AS} content (10% and 20%) was nearly half of those with low PE_{AS} content (0%, 5% and 6%). This means that the magnitude of the particles charge for higher PE_{AS} fractions must have decreased to almost half, compared to that of low PE_{AS} fractions.

The less charge detected for higher PE_{AS} fractions could have been due to various possibilities. First, there could have been less charge generation in these cases. However, this cause was

negated by the analysis of the degree of electrostatic charge generation of the wall particles that were the highest for this case. Secondly, for higher PE_{AS} fractions, the quick formation of a tightly bound layer on the column wall would prevent the bulk particles contacting the wall and thus reducing the charge generation due to this effect. Revel et al. (2003) found that the mount of particles to wall contacts would decrease after particle-wall layer formation. Another possibility was the bipolar charge generation. As the fraction of PE_{AS} particles increased, the fluidization of the particles would have been consisted of two distinct particle size ranges resulting in more small and large particles contacting each other, leading to a bipolar charge distribution, namely the particles obtaining opposite polarity (Ali et al., 1998; Zhao et al., 2000; Sowinski et al., 2010). This effect then would have resulted in reducing the net negative charge of the bulk particles, or increasing their positive charge.

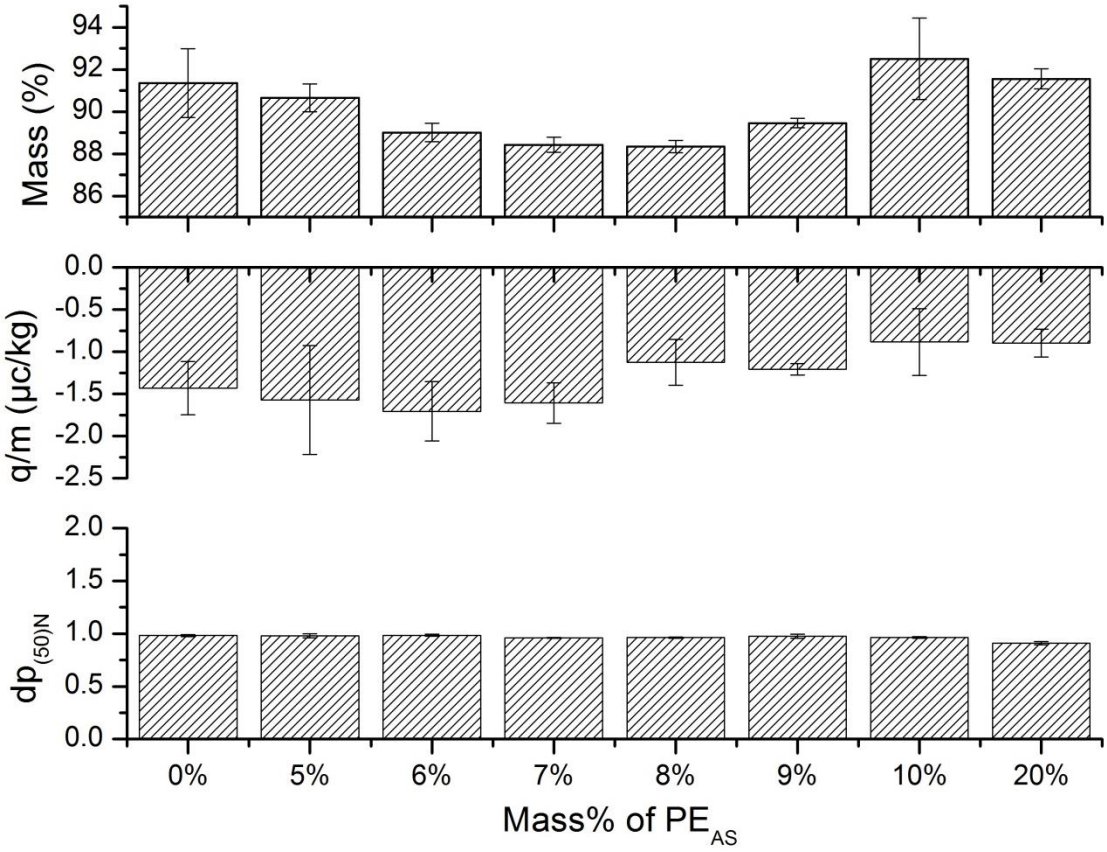

Figure 3.3: Bulk particles mass%, net q/m and $dp_{(50)N}$ after fluidization of various binary mixtures of PE_{AS} and PE_{AL} resin in the small fluidization system.

3.2.3 Wall Particles

Figure 3.4 presents the results of mass%, net q/m and $dp_{(50)N}$ of wall particles. The total mass of wall particles was the sum of loosely, very loosely and tightly bound particles. It can be seen from Figure 3.4 that the loosely bound layer formed the principle part of the wall particles and both of loosely and tightly bound layers had the same changing tendency. Obviously, there was a magnitude transition of wall fouling as the PE_{AS} increased. The total mass rose from 0% to 7% of PE_{AS}, reaching a peak at 7% and 8% trials. Then, it declined until 10% followed by a small increase in the 20% case. The maximum wall fouling occurred when concentration of PE_{AS} in the mixture was approximately 8%. The mass of tightly bound particles was negligible (almost 0) for the cases which had less than 10% of small particles. However, it amplified only in higher fraction of PE_{AS} cases where the 10% and 20% trials had the most tightly bound particles. This significant difference is also clearly visible in Figure 3.5, where at 10 and 20 case%, after tapping the column wall a large amount of particles still remained adhered on the wall. Interestingly, for 6% case, it was observed that there were some particles falling from the column wall during the period between bulk particles and loosely bound particles removal. Thus, these particles were called "very loosely bound". It was difficult to measure these particles charge.

The charge polarity of bulk and loosely bound particles for all fractions was negative. This can be attributed to the particle-wall contacts that occurred throughout the fluidization period resulting in PE_A particles to become negatively charged in comparison to the carbon steel column wall. For each case, the q/m of tightly bound particles was higher than that of loosely bound. These translate to the fact that electrostatics force due to the highly charged particles far exceeded gravitational forces, resulting in these particles to still remain adhered to the wall after tapping. Clearly, the net q/m of loosely bound particles remained constant from 0 to 9% trials, fluctuating around -30 μC/kg. Thus, the total charge of the wall increased as adding smaller particles until 8%. Comparing with 8% case, for the 10 and 20% PE_{AS} cases the net q/m nearly doubled in magnitude. This may be caused by the changes in the bed hydrodynamic when small particles are added could have influenced the degree of charging. Gao et al., (2009) while fluidizing binary mixture of small and larger particles found that the concentration of small particle was higher in the wall region. Such effect thus allows small particles to have more chances to become charged through contacts with the column wall. Since the mass% decline was

not in the same factor as net q/m increase, there must have been an elevation of charge of loosely bound particles. Furthermore, the tightly bound particles had higher charge than loosely bound particles where 10 and 20% trials contained more of such particles. Consequently, the total charge of wall particles must have increased resulting in the degree of electrostatic charge generation increasing with increasing the m% of 212-300 µm particles in the mixture. These findings may be due to increase in small particles concentration which have higher specific surface area. Ahuja (1976), Elsdon & Mitchell (1976) and Wolny & Opalinski (1983) concluded that the contact charges are proportional to contact surface area.

It can be seen from Figure 3.6 that after adding PE_{AS} particles the wall particles size distribution became wider from approximately 100 µm to 1100 µm, suggesting that the loosely bound particles consisted of both PE_{AS} and PE_{AL}. As the portion of smaller particles increased, the wall particles mean diameter shifted to the left, indicating that the smaller particles were occupying the major fraction of the loosely bound particles. Results also illustrate that for 10% and 20% cases, the PSD curves are comparable to those for the PE_{AS} alone (black line in 0% graph), confirming that the majority of loosely bound layer consisted of small particles.

In all trials, except for 0%, tightly bound particles had similar $dp_{(50)N}$, approximately 0.4 (Figure 3.4). This illustrates that not only the tightly bound particles had the same $dp_{(50)N}$ as of the $PE_{AS,}$ but also they had the same particle size distribution range, indicating that all of these particles were PE_{AS}. These particles were highly charged due to smaller particles having higher specific surface area, thus allowing for more opportunities for contacting the column wall and obtaining a higher charge. Since these particles had a higher tendency to adhere to the wall, they reduced the large particles-wall contacts. This in turn resulted in more PE_{AS} and PE_{AL} contacts within the bulk of the bed. This could then be the reason as why at 10 and 20% trials wall particles had a higher net q/m while the net q/m of bulk particles was lower. For 6% case, the particles size of very loosely bound was larger than that of loosely bound. Based on the collection order and particles size distribution of different samples, it was proposed that smaller particles adhere to the wall first due to being highly charged, followed by the larger particles.

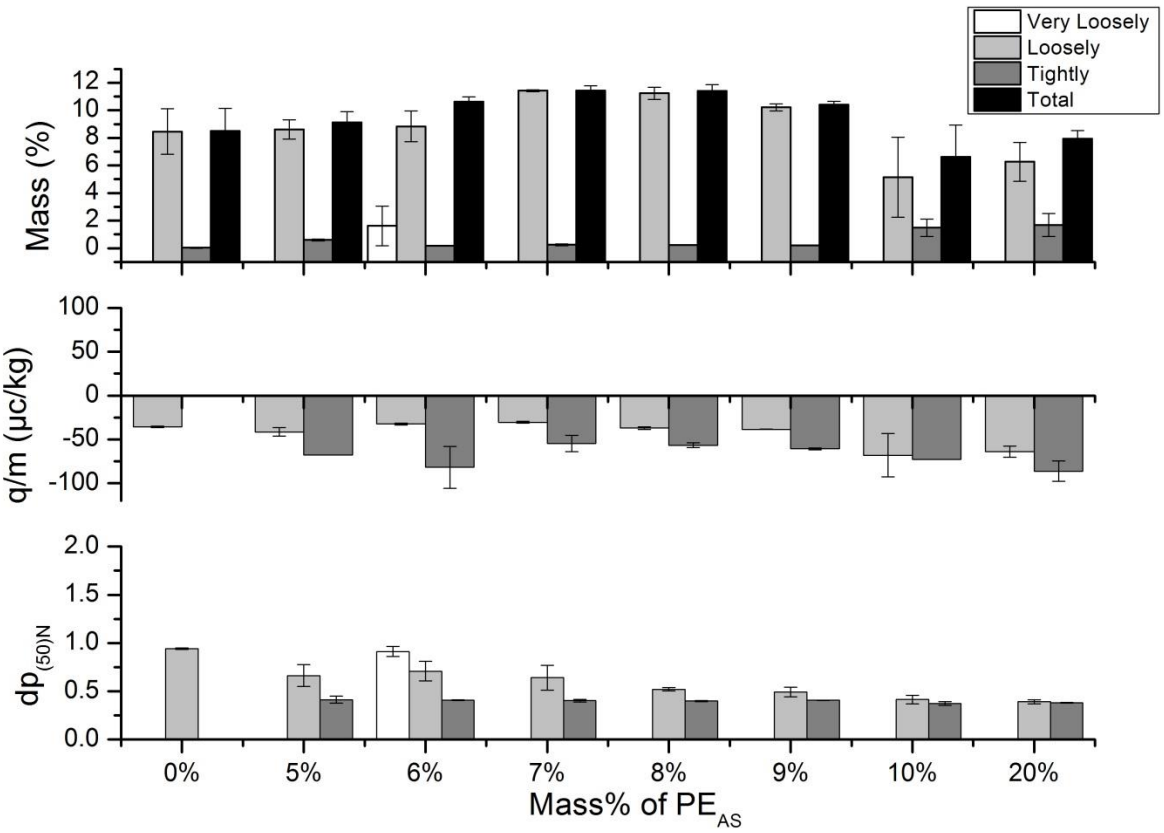

Figure 3.4: Wall particles mass%, net q/m and $dp_{(50)N}$ after fluidization of various binary mixtures of PE_{AS} and PE_{AL} resin in the small fluidization system.

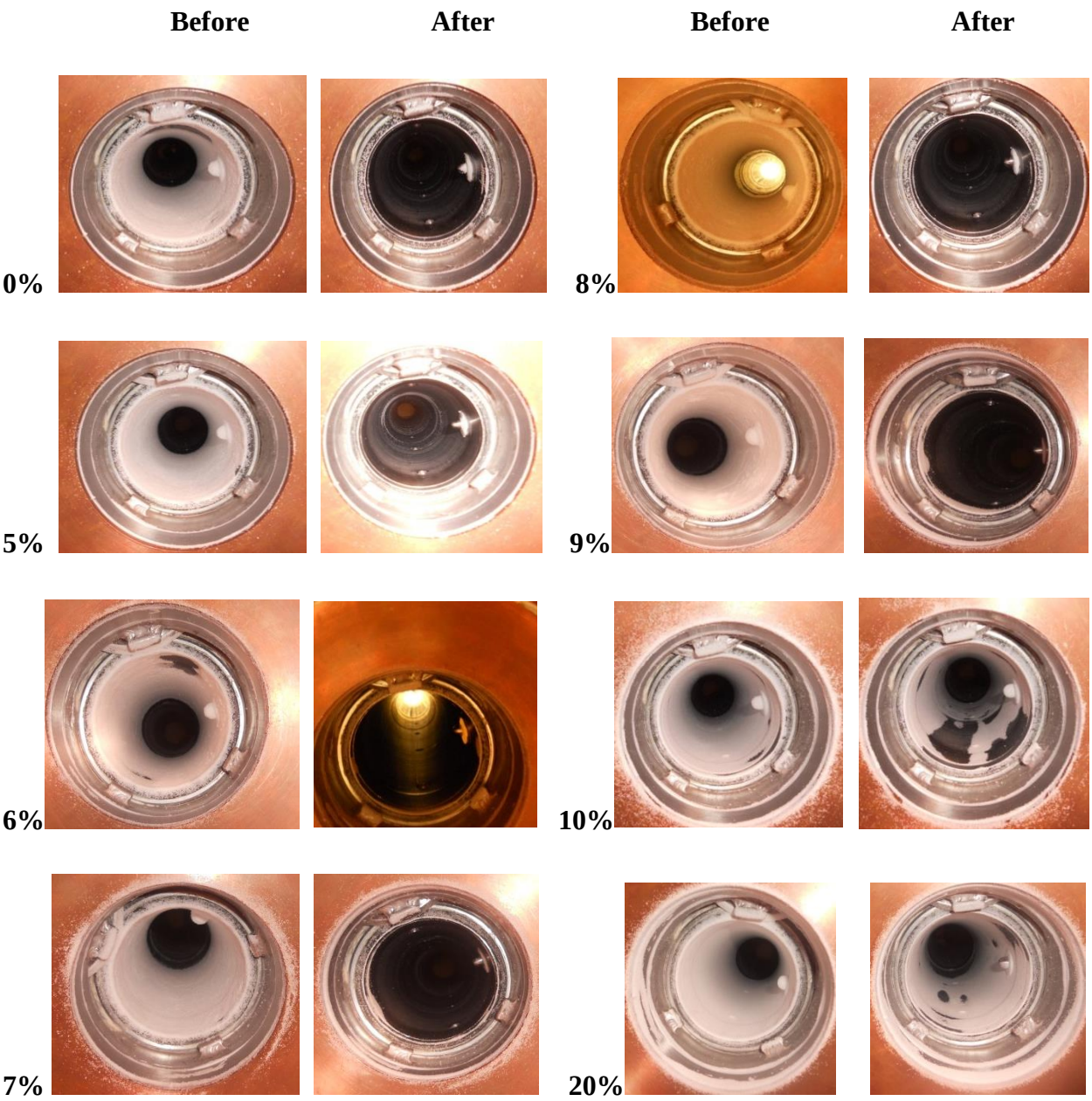

Figure 3.5: Images of wall layer coating after the fluidization of various binary mixtures of PE_{AS} and PE_{AL} particles, before and after tapping.

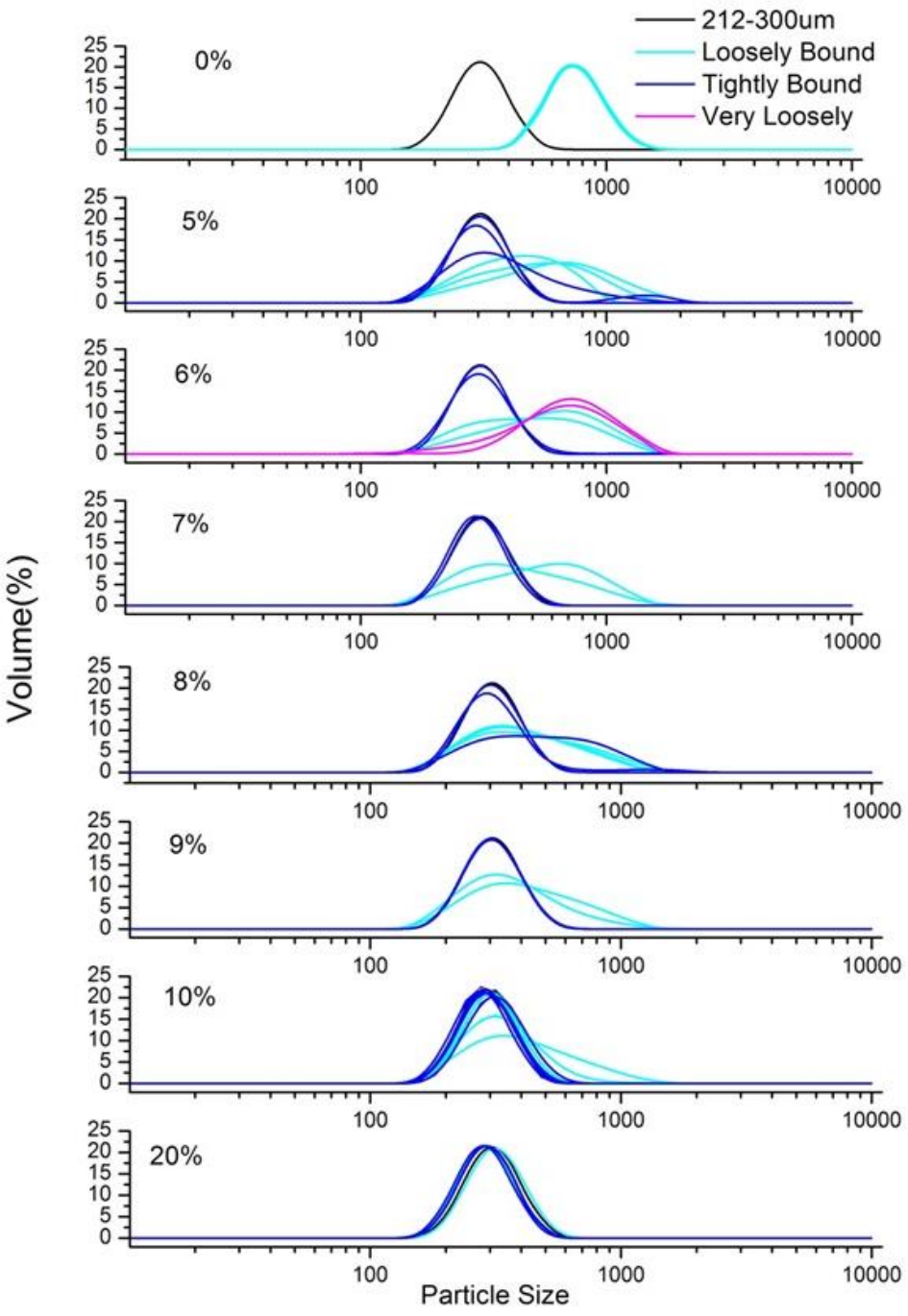

Figure 3.6: Particle size distribution of wall particles collected after fluidization of various binary mixtures of PE_{AS} and PE_{AL} particles.

3.2.4 Multiple Bulk Sample Test

In order to further examine the charge distribution of the bulk particles and the bipolar charging effects, in some trials the CPS unit was utilized instead of the bottom Faraday cup.

- The CPS unit was connected to the high voltage source and set at 30 kV.
- The knife gate valve was then opened and closed very quickly to allow only a portion of the bulk particles to drop into the CPS unit.
- The net charge and mass of particles collected in each Faraday cup was then measured.
- A sample was taken from each Faraday cup for PSD analysis.
- This procedure was repeated until there was no bulk particles left.

Figure 3.7 presents the results of multiple measurements of bulk particles by CPS unit for the 0% and 20% cases. In results presented previously in section 3.1.3, the net charge of bulk particles was negative. However, it can be seen form Figure 3.7 that for both cases, bulk particles consisted of both positively and negatively charged particles.

For both fractions, FC4 and FC1 collected mostly positively and negatively charged particles, respectively. Particles collected in FC3 were barely charged. There was not much difference of magnitude of q/m of FC1, FC2 and FC3 between two fractions of small particles. But it is apparent that positive particles collected in FC4 for 20% trial were charged higher than that of 0%.

In 20% trial, dp_{50} decreased as the sample number increased specifying that smaller particles moved to the top and large particles sank to the bottom of the bed, indicating segregation occurred at higher fraction of PE_{AS} trials. However, dp_{50} of each sample almost remained similar to the 0% case.

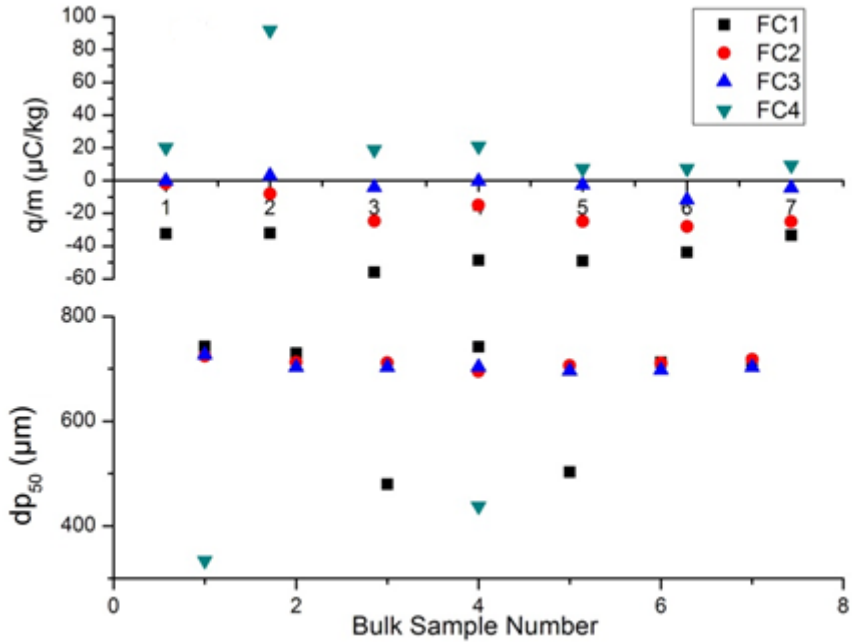

(a)

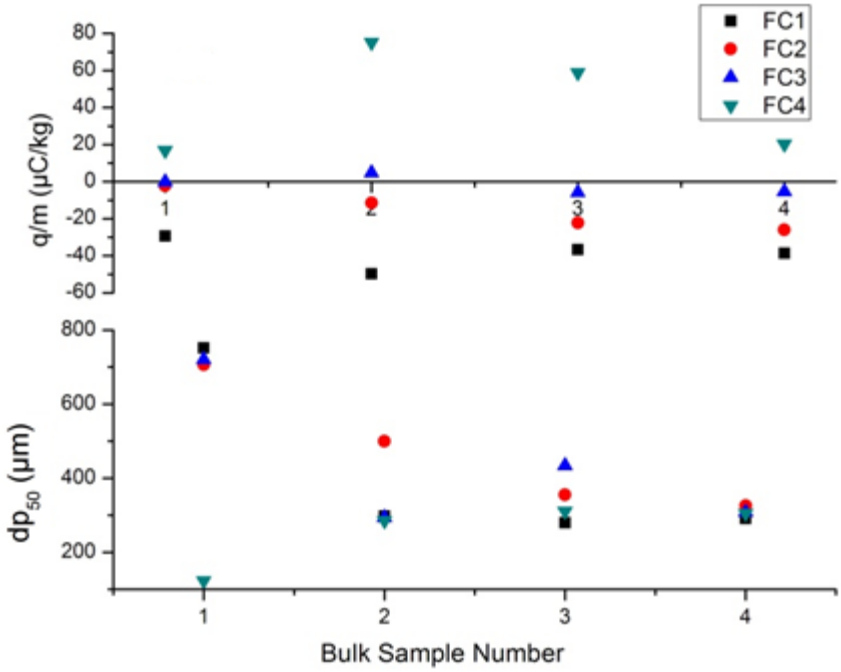

(b)

Figure 3.7: Net q/m and dp_{50} of multiple samples taken from bulk $PE_{A:}$ (a) 0% PE_{AS}, (b) 20% PE_{AS}.

3.2.5 Charged Particle Separator

To better understand the wall particles charge distribution, experiments were repeated where the bottom Faraday cup was replaced by the CPS unit when wall particles were removed. For all trials, the high voltage source was set at 30 kV. Results are shown in Figure 3.8. There were seldom particles collected in FC4 for all trials and thus not enough particles for PSD analysis. Thus, the particle size of FC4 was not shown in some cases.

In theory, FC1 and FC2 should collect negatively charged particles while other cups to collect the positively charged particles. However, in this case, the net charge of first three Faraday cups was negative and particles collected in FC4 charged positively. This indicted that the wall particles consisted of both positive and negative particles with the majority being charged negatively. The positive charges may have been generated by particle-particle contacts. The reason that FC3 particles to be charged negatively was due to the particles being charged less and the gravitational force influence. The net charge and mass of particles collected in FC2 for all cases occupied the majority of the wall particles and the particles $dp_{(50)N}$ in this cup was also higher than others. However, the net q/m of particles in FC1 for all trials was the highest. As adding small particles, it can be seen from Figure 3.9 that particles in FC1 were small particles suggesting that highly negatively charged particles were smaller in size.

In 0% case, there were only large particles. The net q/m of FC3 particles decreased along with the portion of PE_{AS} rising. At 5% PE_{AS}, particles collected in FC3 had a considerable wider size range (Figure 3.9) indicating that particles collected in this cup consisted of both PE_{AL} and $PE_{AS.}$ And the net q/m of these particles was approximately -15 μC/kg. For PE_{AS} content of higher than 5% (7, 10 and 20% trial), there was no large particles but only PE_{AS} particles collected in FC3 with lower net q/m around -10 μC/kg. These results indicated that some particles being collected in FC3 due to being charged positively. The particle-to-particle contacts (i.e., bipolar charging) contributed to the particles positive charge. This translates to wall layer formation to be a results of particle-to-particle contacts and particle to wall contacts.

During the experiments with the CPS apparatus, some particles adhered to the positive plate (PP), suggesting that these particles were highly negatively charged where electrostatic forces far exceeded gravitational forces, making them stick to the positive plate. Although, due to the high

charge of these particles it was difficult to collect them and measure their mass or charge, it was obvious from observations that the mass of these particles increased as the proportion of PE_{AS} increased. This is an indication that the smaller the particles were, the higher was their negative charge. Moreover, according to Figure 3.9, size of these particles was found to be smaller than those collected in FC1.

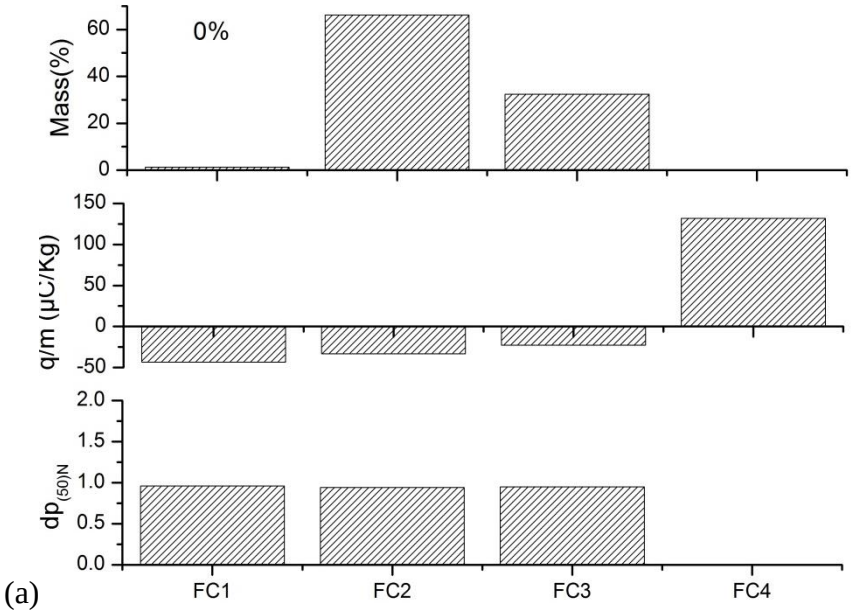

(a)

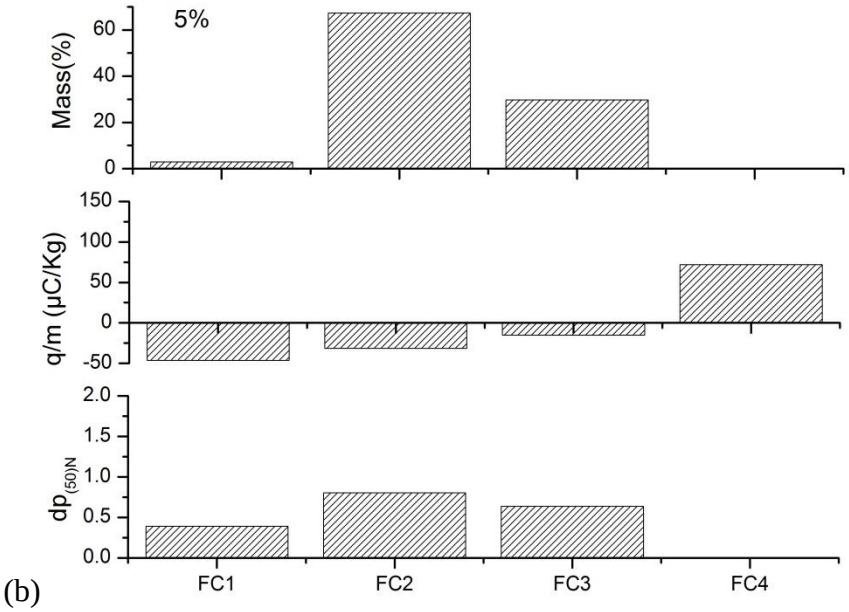

(b)

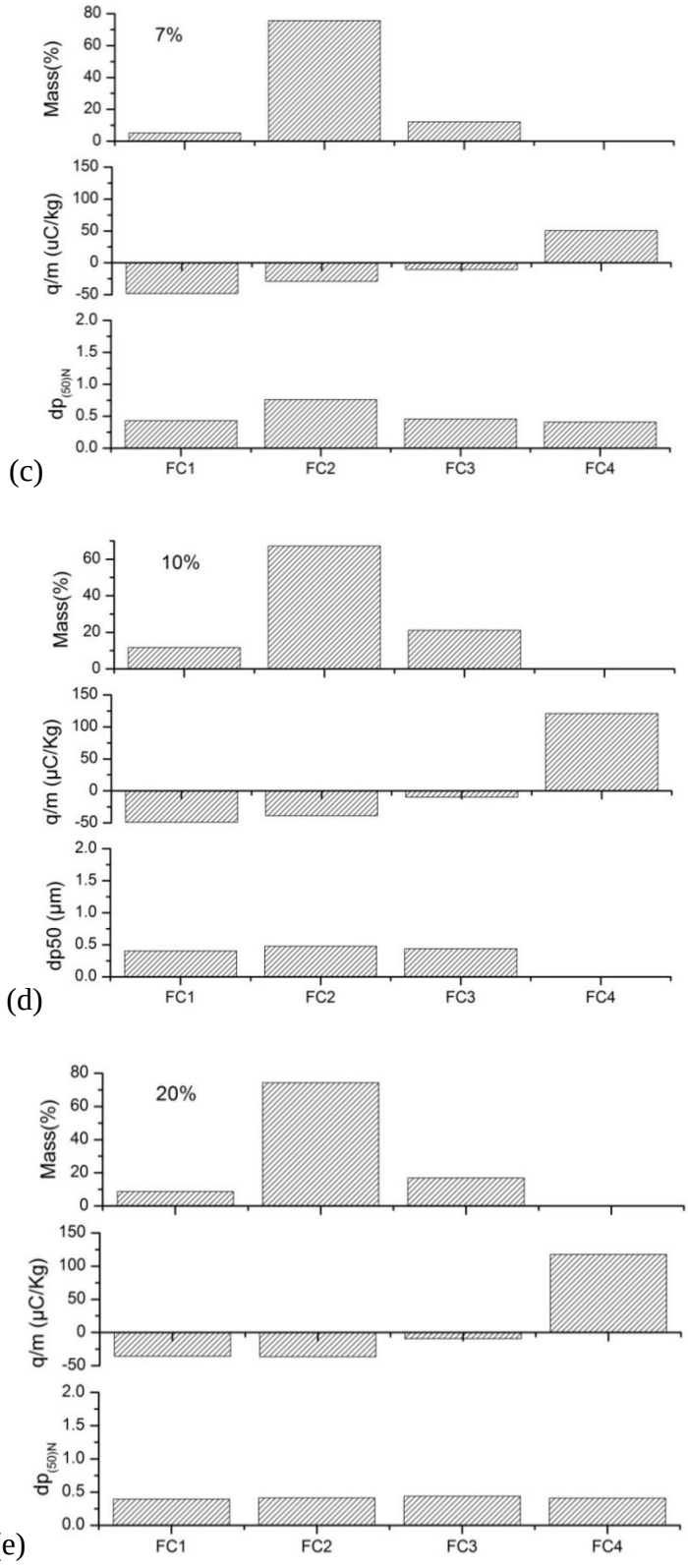

Figure 3.8: Charge, mass%, net q/m and $dp_{(50N)}$ of particles collected in the four Faraday cups of the CPS unit: (a) 0 % ,(b) 5 % ,(c) 7 % , (d) 10 % and (e) 20% PE_{AS}.

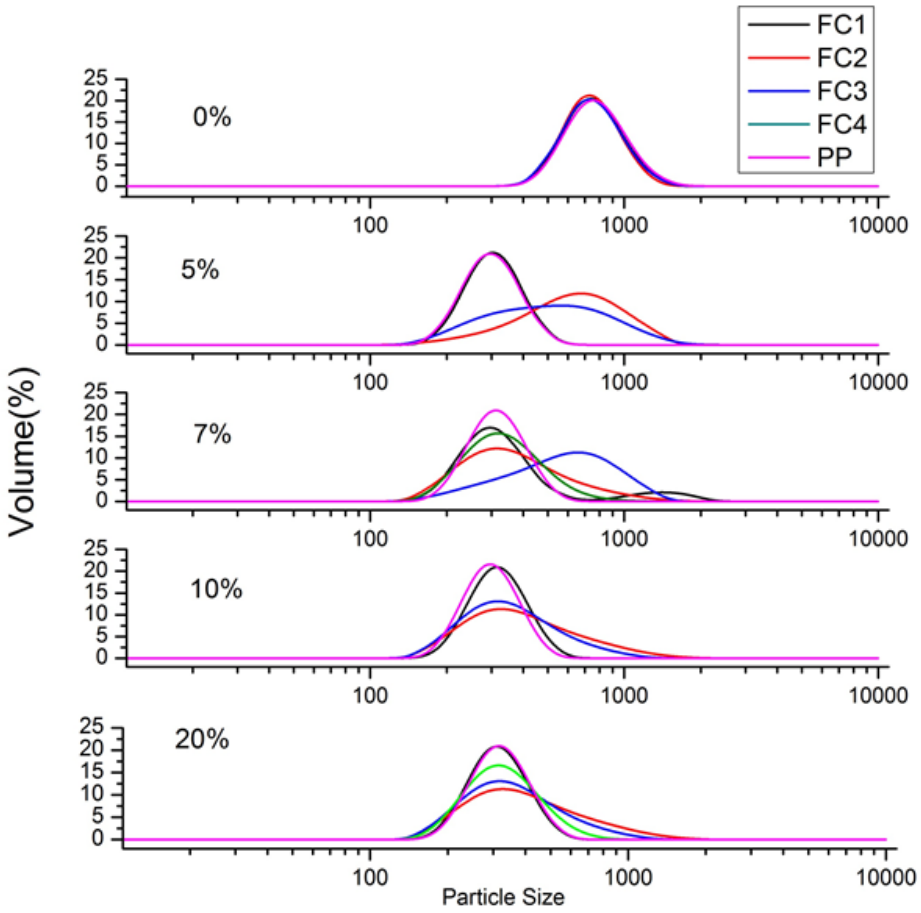

Figure 3.9: Size distribution of particles collected in the four Faraday cups of the CPS unit for 0, 5, 7, 10 and 20% PE_{AS}. PP stands for positive plate.

3.2.6 Bench-Scale Shaking Experiments

In order to better understand the results from fluidization runs and distinguish between particle-wall and particle-particle charging mechanisms, as well as finding the charge polarity on the different particle sizes, bench-scale experiments were conducted.

3.2.6.1 Case (a)

Since the mass of the particles was small enough comparing with the volume of the tube, the main charging mechanism was considered to be from particle-wall contacts. As shown in Table 3.1, the initial q/m of both particle sizes was quite similar. Due to shaking, both particles sizes

became negatively charged, which was consistent with the results of PE_A particles fluidization results, while smaller particles on average became more charged than the larger particles.

For both PE_{AS} and PE_{AL} trials with CPS unit (Figure 3.10), the mass% of the negatively charged particles was larger while the positive particles fractions were decreased after shaking. This suggests that during shaking, more of the initially positively charged particles became negatively charged. The results of runs without CPS unit showed that after shaking both particle sizes were negatively charged. This agrees with the fact that the contacts between different materials, having different work functions, results in one material to donate electrons and the other receive electrons.

Table 3.1: Results of Case (a) shaking experiments with PE_A particles without using CPS unit.

	Tube	PE_{AL}	PE_{AS}
Mass (g)	-	4.10	4.10
Initial q/m (μC/kg)	neutral	-0.20 ± 0.038	-0.16 ± 0.051
Average Generated q/m (μC/kg)	+ve	-9.75 ± 1.87	-11.15 ± 2.16

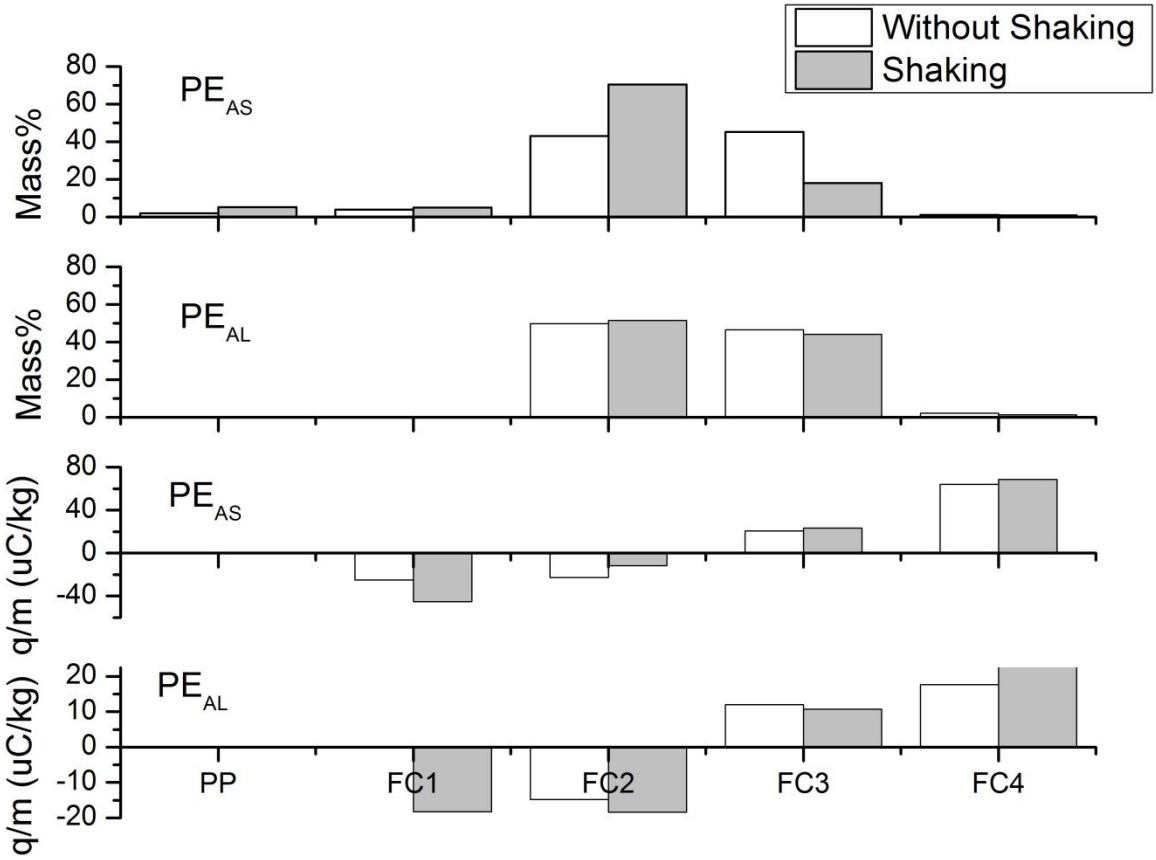

Figure 3.10: Mass% and q/m of PE_{AL} and PE_{AS} particles with CPS unit for shaking and non-shaking tests.

3.2.6.2 Case (b)

When the binary mixtures of small and large particles were tested, the net q/m of initial particles for each experiment was similar according to the Figure 3.11. However, as the proportion of PE_{AS} increased, the gained net q/m of mixtures also increased. Since the total mass of particles for all trials was kept constant (20 g), the net charge of particles must have increased. Although two different size particles would create bipolar charging due to contacts between themselves, the Faraday cup just measures the net charge of these particles. Thus, the increase in net charge observed as the percentage of smaller particles increased should be due to particle-wall contacts.

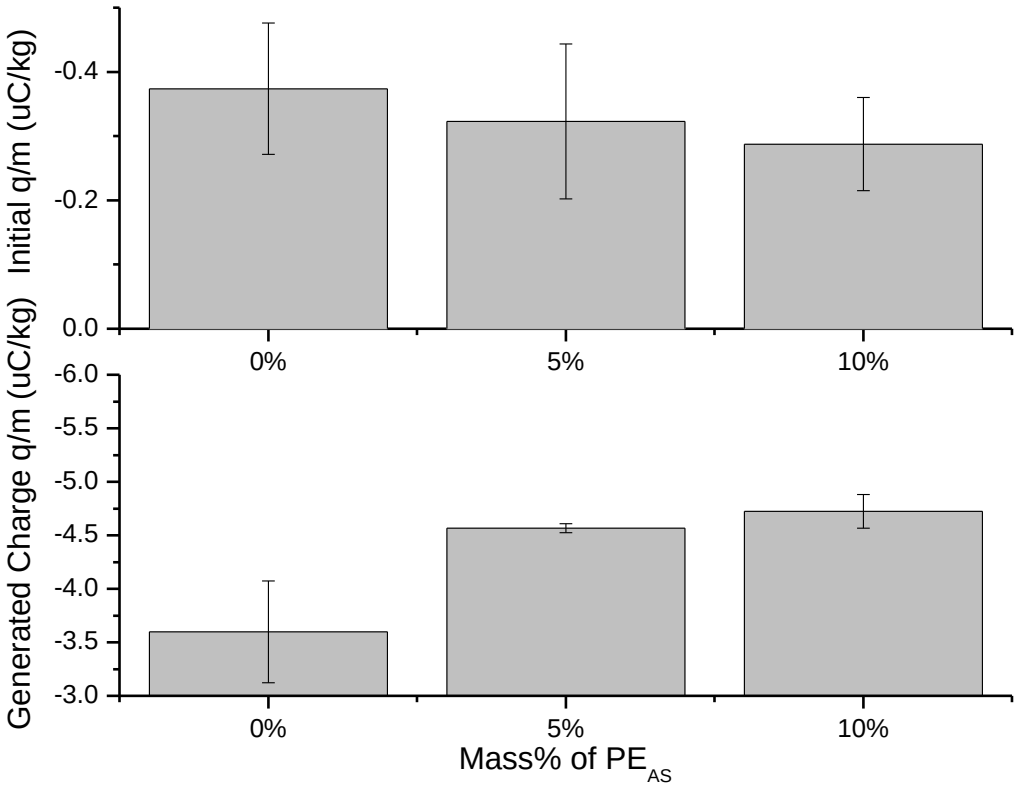

Figure 3.11: The net q/m of various mixtures of PE_{AL} and PE_{AS} particles, before and after shaking.

3.2.6.3 Case (c)

To better distinguish between particle-wall and particle-particle charging mechanisms and to find the charge polarity on different particle sizes, mixtures of small and larger particles were shaken while CPS unit was used for charge measurements.

For PE_{AL} only particles (Figure 3.12), there were no particles sticking to the positive plate. The particles collected in FC2 and FC3 occupied majority of the initial particles. Moreover, mass percentage of FC2 and FC3 was almost the same. It is apparent from results that after adding small particles, mass distributions of the four Faraday cups were totally different from PE_{AL} trial. For 5% and 10% cases (Figure 3.13 and Figure 3.14), there were particles collected on the positive plate. According to the particle size distribution results, these particles were the small particles (PE_{AS}). Although the mass percentage of FC4 was quit small, the net q/m increased

after adding small particles. Moreover comparing therresults with those of case (a), it is apparent that some smaller particles were charged positively during the shaking process. Based on the result of Case (a), the contacts between PE_{AS} and the tube wall will lead to the smaller particles to be charged negatively. Thus, the positive charge was derived from the particle-particle contacts; smaller particles becoming more positively charged after PE_{AL} and PE_{AS} contacts. In addition, FC1 particles were gradually replaced with $PE_{AS.}$ In 10%, case only PE_{AS} particles were collected in FC1.

Although, the particle-particle contacts resulted in bipolar charging, the net charge calculated from CPS experiments was negative, suggesting that particle-tube wall contacts were dominant throughout the entire shaking process. The same situation occurred in fluidization experiments (discussed earlier) where the particle-wall contacts played a significant role in generating a net negative charge.

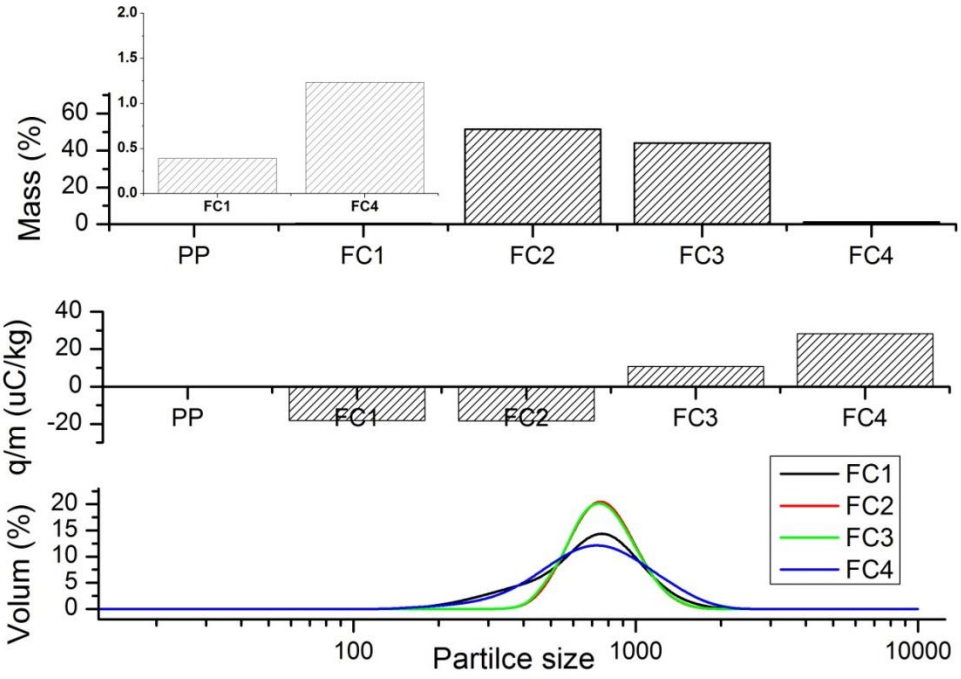

Figure 3.12: The PE_A particles mass%, net q/m, and PSD for case (c) of bench-scale shaking experiment with 0% $PE_{AS.}$

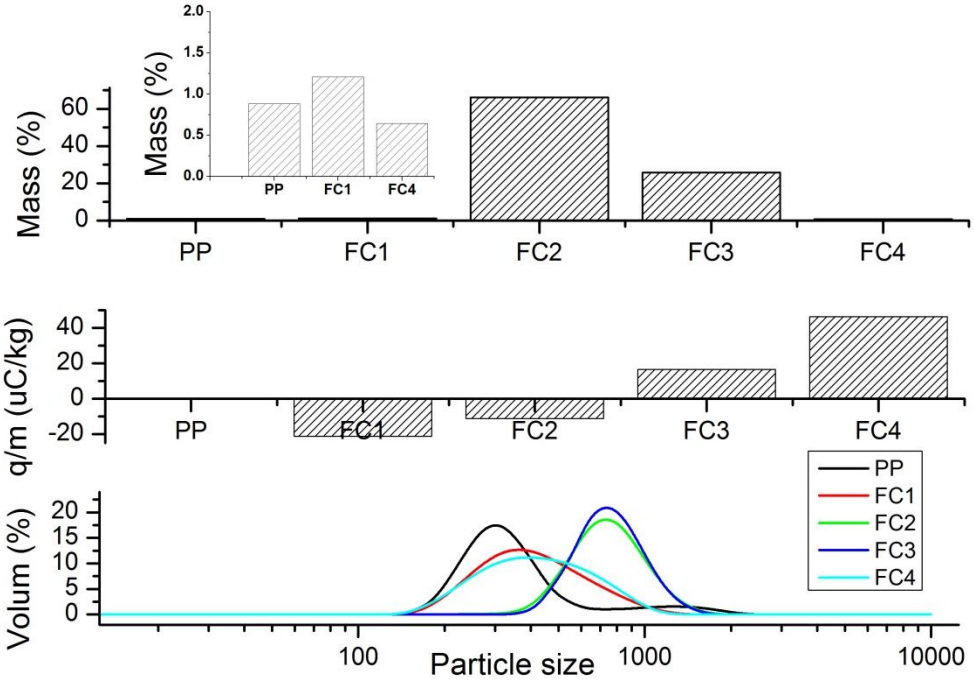

Figure 3.13: The PE_A particles mass%, net q/m, and PSD for case (c) of bench-scale shaking experiment with 5% PE_{AS}.

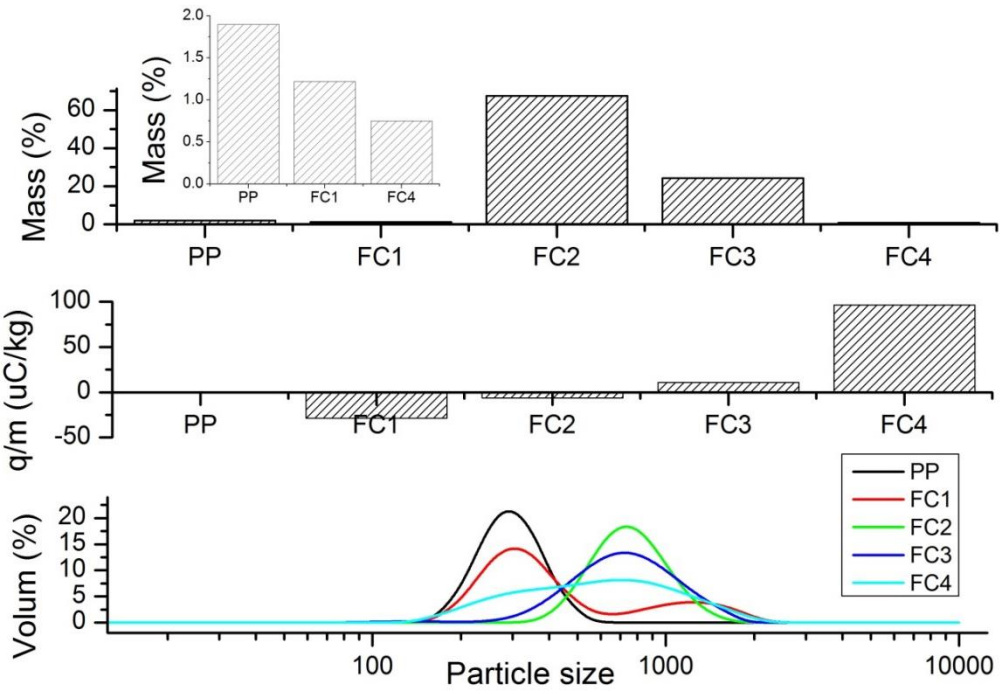

Figure 3.14: The PE_A particles mass%, net q/m, and PSD for case (c) of bench-scale shaking experiment with 10% PE_{AS}.

3.3 Binary Mixture of Small and Large Particles of PE_B Resin

Similar fluidization experiments as those presented in section 3.2 were conducted with PE_B particles with the exception that only binary mixtures of 5, 10, and 20% of small (PE_{BS-1}, 212-300 μm) and large (600-710 μm) particles were examined.

3.3.1 Initial particle

Figure 3.15 presents the results of initial particles charge-to-mass ratio (q/m), normalized mean particles size ($dp_{(50)N}$) and sauter mean diameter. It is apparent that all experiments started with similar small initial net specific charge while the sauter mean diameter decreased by adding PE_{BS-1} particles.

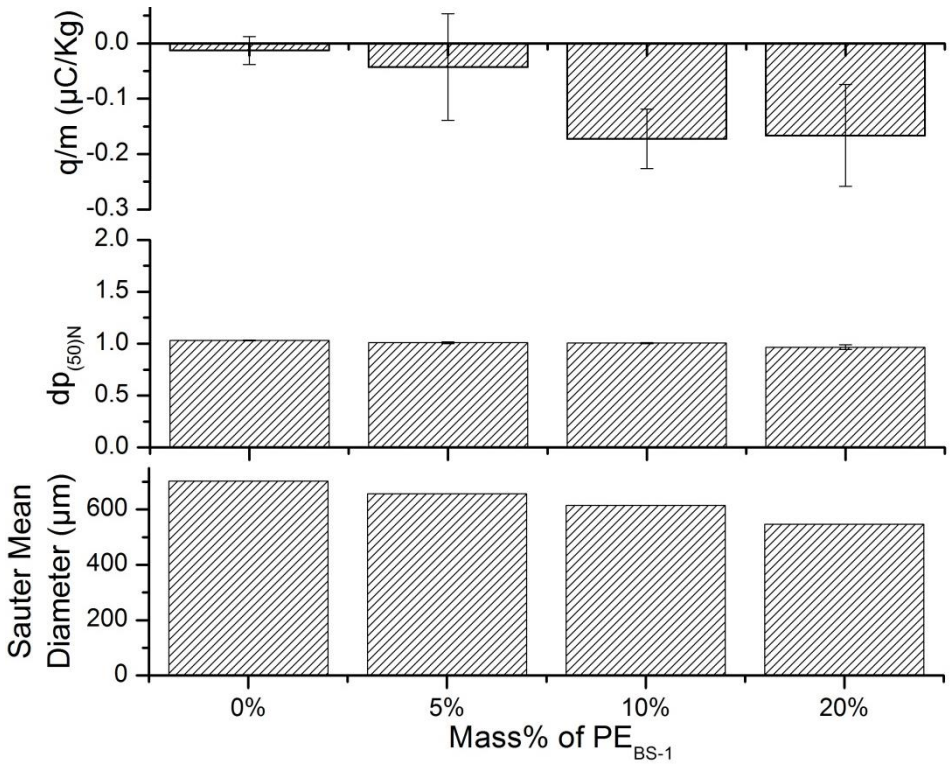

Figure 3.15: Initial particles net q/m, $dp_{(50)N}$ and sauter mean diameter for binary mixtures of PE_{BS-1} and PE_{BL} resin fluidized in the small system.

3.3.2 Bulk Particle

The mass%, net q/m and $dp_{(50)N}$ of bulk particles are shown in Figure 3.16. For all trials the average mass of bulk particles collected was similar, approximately 95% of the initial particles.

In cases of 0%, 5% and 10% mixture, the net charge of the particles for three mixtures were similar. However, the bulk particles net q/m for the 20% mixture was negligible. Since the mass collected for this case was similar to the other cases, then the net change of the particles must have reduced. The charge reduction was found to be due to two possibilities. Firstly, the quick formation of the wall layer could have resulted in fewer particles to contact the carbon steel wall and thus a lower particle charging occurred. Secondly, the particle-particle contacts increased by increasing the amount of smaller particles. And this in turn resulted in bi-polar charging effect causing the particles net charge to decline.

Comparing to initial particles, bulk particles had similar $dp_{(50)N}$, suggesting that bulk particles comprised of the majority of the bed particles.

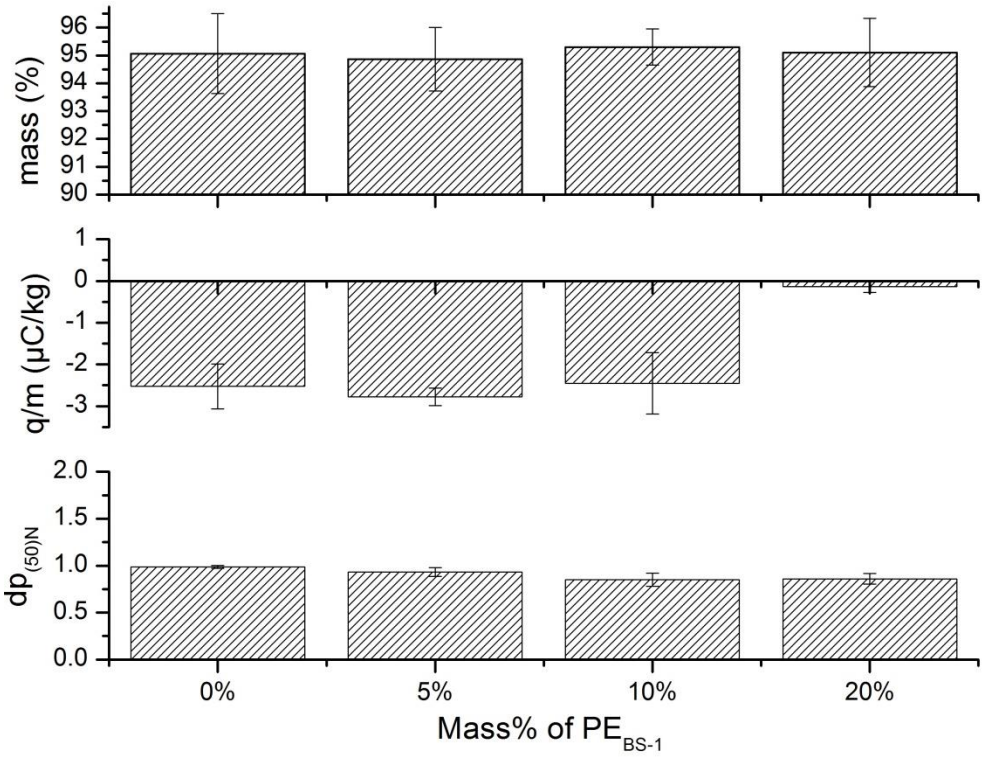

Figure 3.16: Bulk particles mass%, net q/m and $dp_{(50)N}$ collected after fluidization of various binary mixtures of PE_{BS-1} and PE_{BL} resin in the small fluidization system.

3.3.3 Wall particle

The results show that the total mass of wall particles was similar regardless of the magnitude of the smaller particles present (Figure 3.17). The total mass constituted of very loosely, loosely

and tightly bound particles. For all trials, very loosely bound particles were collected however, the charge of these particles was difficult to detect. Except for the tightly bound, the results for all other portions of the wall particles remained the same for various mixtures. The amount of tightly bound particles slightly increased as the percentage of PE_{BS-1} particles increased. Although the mass of tightly bound particles was small, it was obvious that after tapping the column to remove the loosely bound, there were still some particles sticking to the column wall (Figure 3.18).

Figure 3.17 presents the net q/m of loosely and tightly bound particles. The charge polarity of dropped, loosely and tightly bound particles for all experiments kept consistent and was negative. Moreover, the tightly bound particles obviously had higher net q/m than loosely bound particles which are similar to results found with PE_A resin. Clearly, the net q/m of loosely bound particles increased with increasing the weight fraction of PE_{BS-1} particles where for the 20% PE_{BS-1} case it was approximately double of that of the 0% case. As discussed in section 3.2.3, the high specific surface area of small particles and changes in bed hydrodynamics after adding small particles contributed to the high net q/m. Since the m% of all runs remained constant, then loosely bound particles charge must have elevated with increasing the weight fraction of small particles. Furthermore, similar trends were observed for the tightly bound particles. Consequently, the total charge of wall particles must have increased due to higher degree of electrostatics charge generation by increasing the amount of small particles in the mixture. Since the wall layer of 20% consisted of particles with high specific charge, the electric field of this layer would repel negative particles to the bulk and prevents the growth of the wall coating. That is the reason why at 20% the mass of wall fouling kept constant.

It can be clearly seen from Figure 3.17 that the wall particles mean particle diameter declined with increasing the m% of smaller particles. For 10% and 20% mixtures, the majority of wall particles consisted of 212-300 μm particles, which means that the smaller particles had higher tendency to migrate and adhere to the column wall. This effect is confirmed with the fact that they also had a higher charge.

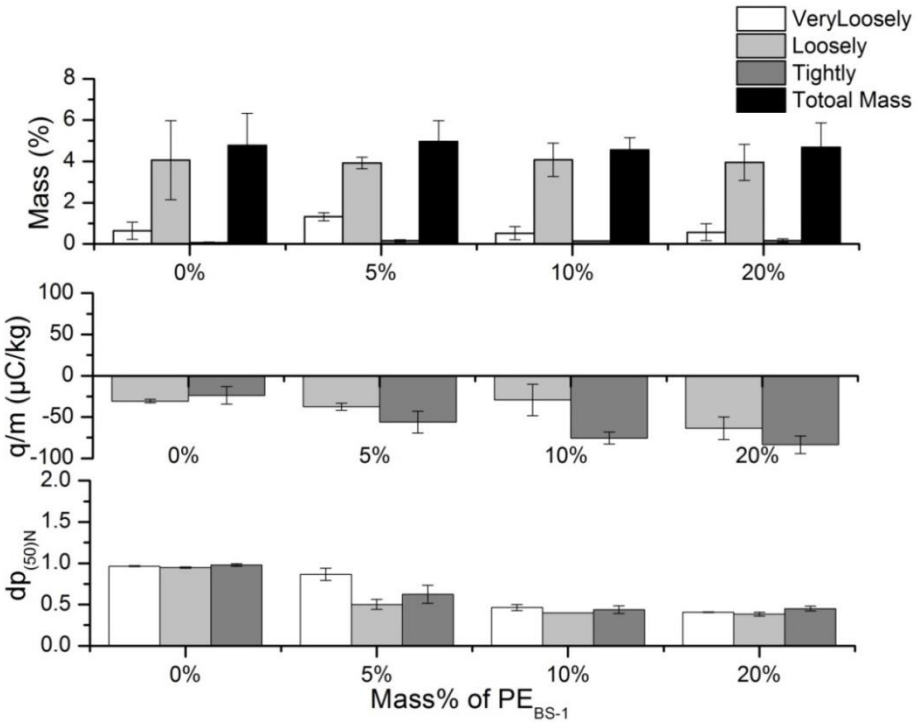

Figure 3.17: Wall particles mass%, net q/m and $dp_{(50)N}$ collected after fluidization of various binary mixture of PE_{BS-1} and PE_{BL} resin in the small fluidization system.

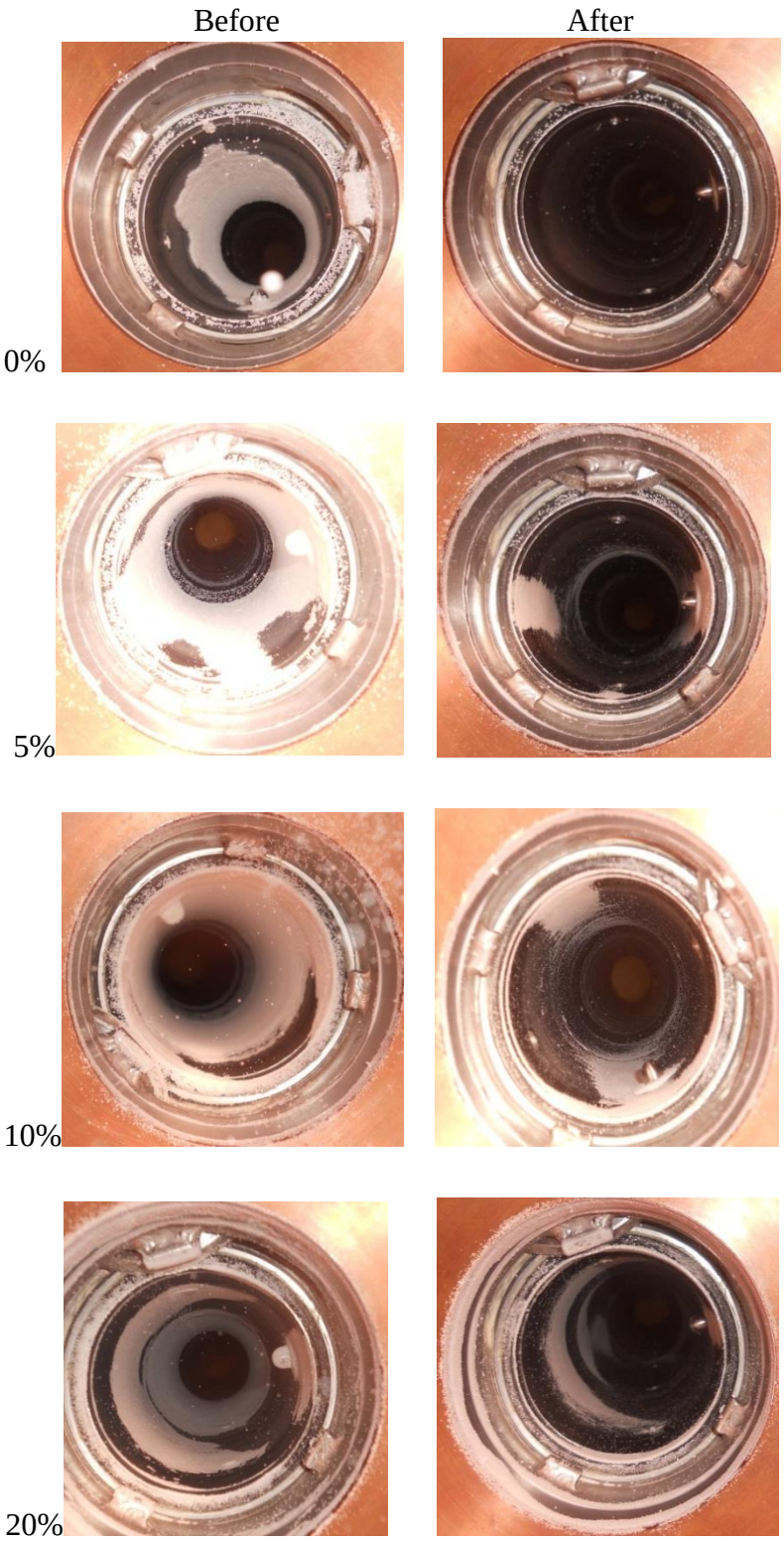

Figure 3.18: Images of wall layer coating before and after the wall particles removal for fluidization of various binary mixtures PE_{BS-1} and PE_{BL} particles in the small fluidization system.

3.3.4 15 Minutes Fluidization and Multiple Sampling of Bulk for 20% PE_{BS-1} mixture

In order to investigate the reasons for the negligible net charge-to-mass ratio of bulk particles found in the 20% mixture case, further experiments were conducted. They included: (a) 15 minutes fluidization trials; and (b) multiple sampling of the bulk particles.

3.3.4.1 15 Minutes Fluidization Experiments

Figure 3.19 presents the results of bulk particles collected mass%, net q/m and mean particle diameter for two fluidization time periods of 15 and 60 minutes. The comparison of results indicates that for the shorter fluidization time the amount of bulk particles was slightly larger, but the other parameters almost remained the same. This means that there was no significant change beyond 15 min of fluidization. According to Figure 3.20, the total mass of the wall particles for the 60 min fluidization was on average approximately 2 percentage larger than that of 15 min trial and the net q/m was comparable for both cases. Thus, the majority of charge of the wall particles was generated in the first 15 minutes of fluidization. The only difference is that no "very loosely bound" particles were observed in 15 min fluidization trial, indicating that this part of wall was formed after 15 min. It is therefore could be concluded that the wall layer coating formed during the first 15 minutes (Figure 3.21) could have prevented the remaining bulk particles from contacting the metal wall to result in further charging.

$Dp_{(50)N}$ of wall particles for both fluidization periods were similar indicating that the majority of wall particles constituted of smaller particles and these particles had higher movement tendency towards the column wall.

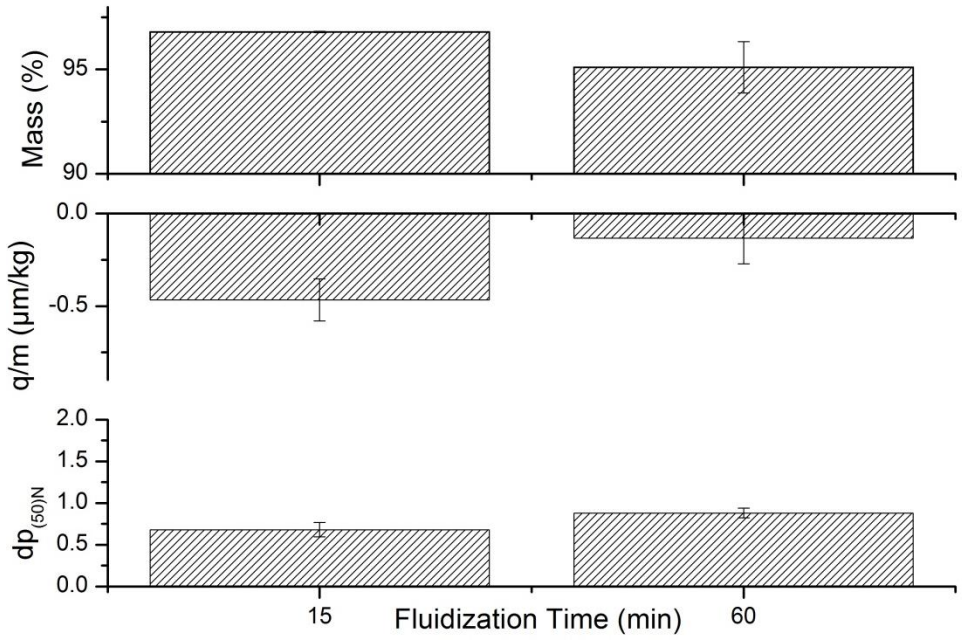

Figure 3.19: Bulk particles mass%, net q/m and $dp_{(50)N}$ for 15 and 60 minutes fluidization of binary mixture of 20% PE_{BS-1} and PE_{BL} particles.

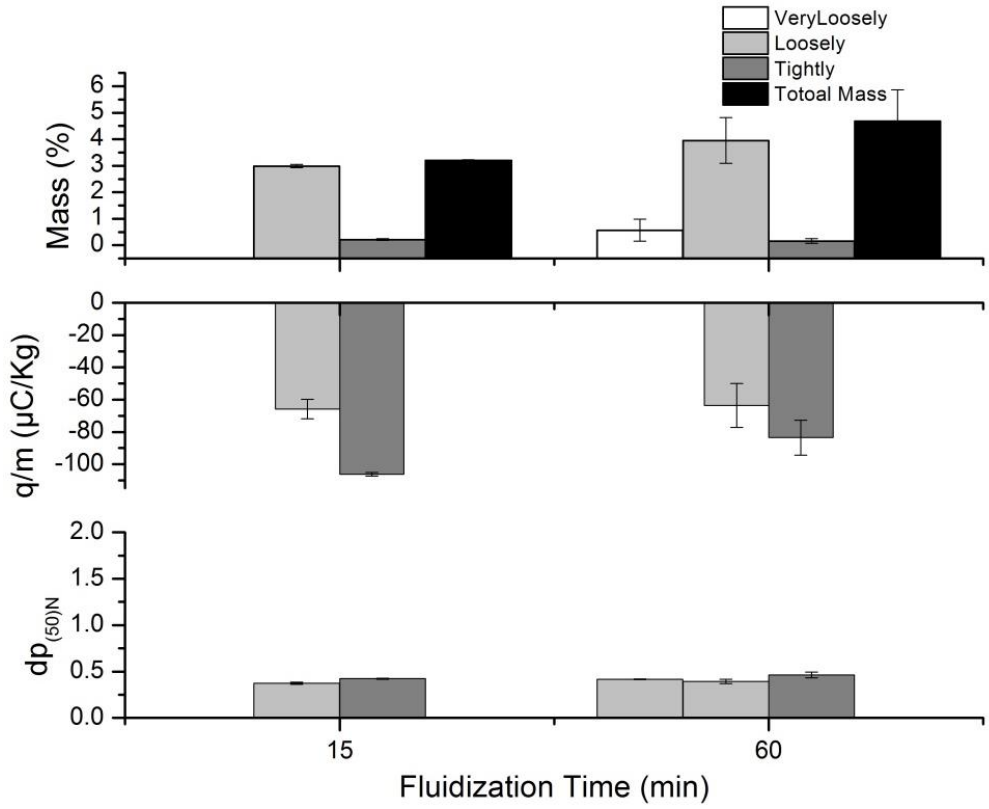

Figure 3.20: Wall particles mass%, net q/m and $dp_{(50)N}$ for 15 and 60 minutes fluidization of binary mixture of 20% PE_{BS-1} and PE_{BL} particles.

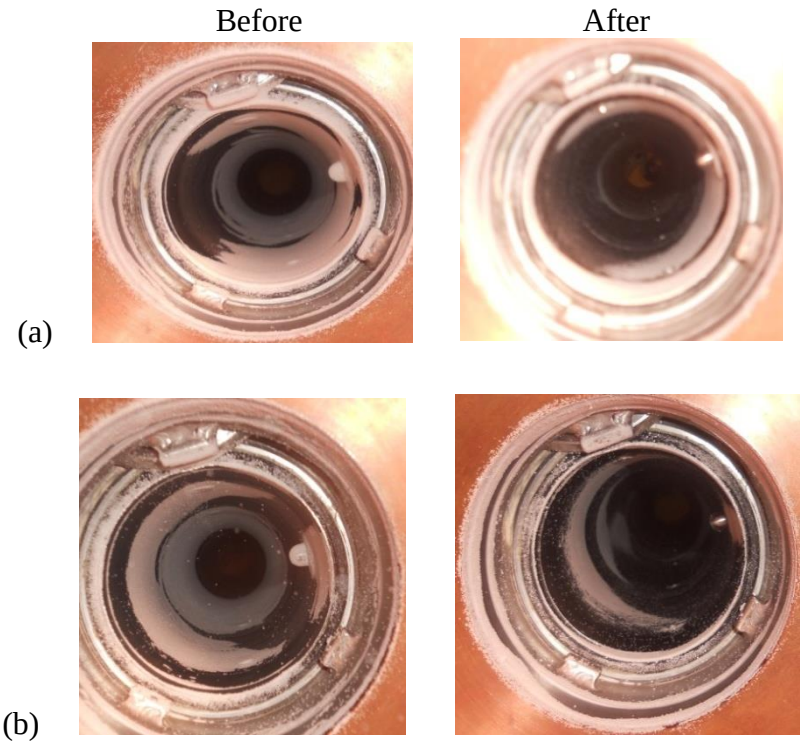

Figure 3.21: Images of wall layer coating before and after tapping the column wall after the fluidization of PE_B particles (20% mixture) for different fluidization periods. (a) 15 min; (b) 60 min.

3.3.4.2 Multiple Sampling of Bulk Particles

This experiment was conducted where the bulk particles were discharged into the CPS unit by opening and closing the knife gate valve numerous times (8 times). As can be seen the particles mass percentage in each Faraday cup almost kept constant. FC3 collected most of particles, approximately 75%, followed by FC2 having approximately 25%. The particles in FC1 and FC4 were very few. In results previously presented in Section 3.3.2**,** the bulk particles of 20% mixture had a negligible net q/m. However, as can be seen from Figure 3.22, with multiple sampling the net q/m of bulk particles consisted of both positively and negatively charged particles. FC4 and FC1 collected mostly positively and negatively charged particles. It is apparent that positive particles collected in Faraday cup 4 were charged significantly higher. For the first two samples, most of particles collected by all Faraday cups were large particles (600-710 micron). However, in the subsequent samples, smaller particles were collected. That means that the larger particles sank to the bottom of the bed while the smaller particles moved to the top (i.e., bed segregation occurred).

Figure 3.23 showes the net q/m vs dp_{50} obtained for particles collected in each Faraday cup for each sample taken. Both large and small particles had more variation in positive or negative polarity. However, the large particles charged less than the smaller particles, regardless of their charge polarity.

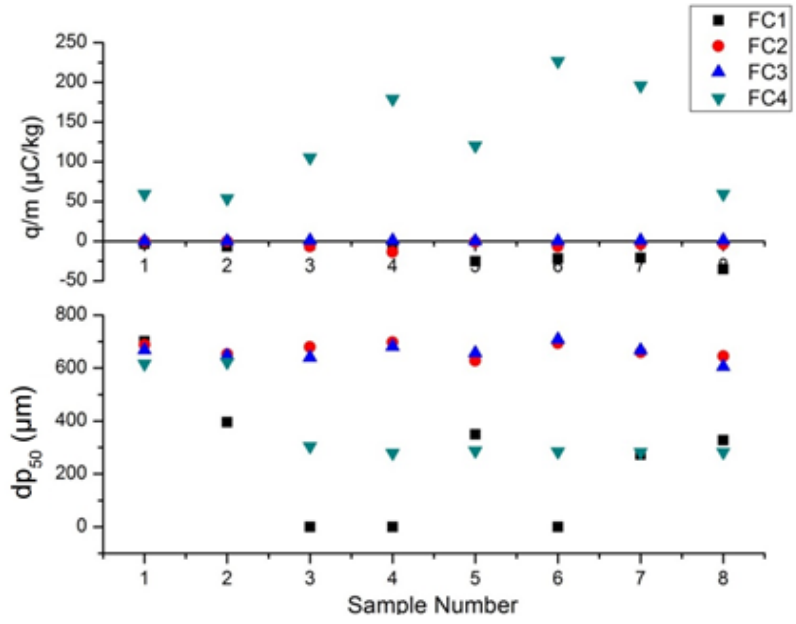

Figure 3.22: Bulk particles net q/m and dp_{50} found by multiple sampling of the 20% PE_{BS-1} and PE_{BL} mixture.

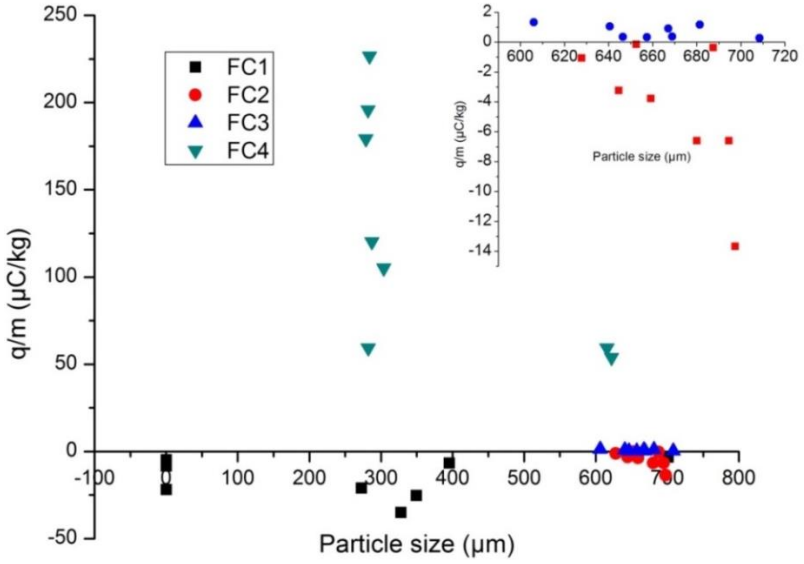

Figure 3.23: The net q/m vs dp_{50} of multiple bulk samples taken for 20% PE_{BS-1} and PE_{BL} mixture.

3.3.5 Bench-Scale Shaking Experiments

3.3.5.1 Case (a)

Since small amount of particles were used for these experiments, the main charging mechanism was assumed to be dominated by particle-tube wall contacts. The results are shown in Table 3.2.

Table 3.2: The results of shaking tests for PE_B particles Case (a).

	Tube	PE_{BL}	PE_{BS-1}
Mass (g)	-	5	5
Initial q/m (µC/kg)	neutral	-0.065 ± 0.005	-0.41 ± 0.3
Average Generated q/m (µC/kg)	+ve	-7.49 ± 2.7	-12.3 ± 4.7

The net initial q/m of both sizes of particles was small. After shaking, both types of particles were charged negatively which was consistent with results of fluidization experiments. In addition, the small particles were charged higher than the large particles. These results conclude that the particles to wall contacts were the main contributors to the charges generation through fluidization.

3.3.5.2 Cases (b) and (c)

In order to investigate the particle to particle contact charging mechanism and to avoid the effects of tube wall, a uniform layer of particles were attached to a tape and placed inside the tube. This case made the tube wall to be of polyethylene particles rather than being a metal surface. The polarity of the tape along with the particles attached to it upon the completion of the shaking period was detected by the bench-scale Faraday cup. Results of the charge gained by the particles and their polarity upon shaking are shown in Table 3.3 and Table 3.4.

Overall, contacts between PE_{BL} and PE_{BS-1} particles resulted in the larger particles becoming positively charged and smaller particles becoming negatively charged. The large particles were barely charged in contacts with large particles layer on the tube wall (PE_{BL} on Tube Wall). Clearly, the smaller particles gained negative charge in both of the cases. These results confirm

the formation of bipolar charging for small particles-large particles contacts. This could also explain the source of positive charging of the bulk and wall particles in the fluidization process.

In section 3.3.4.1, it was known that the wall layer coating almost formed in first 15 minutes of fluidization, resulting in fewer particles to wall contacts in 20% case. However, the amount of the wall particles slightly increased after 15 min. Thus, these particles charging might be the results of particle-particle contacts.

Table 3.3: Charging polarity of PE_{BL} and PE_{BS-1}contacted with a tube wall covered with the same particles.

	PE_{BS-1} on Tube Wall	**PE_{BL} on Tube Wall**
PE_{BL}	+/-	neutral
PE_{BS-1}	-/+	-/+

Table 3.4: Generated net q/m of PE_{BL} and PE_{BS-1} resins shaken in a tube covered with the same particles.

	Generated net q/m (µC/kg)	**Standard Deviation (µC/kg)**
PE_{BL} / PE_{BS-1}Layer	0.545	0.305
PE_{BS-1}/ PE_{BS-1}Layer	-0.500	0.048
PE_{BL} / PE_{BL} Layer	-0.044	0.229
PE_{BS-1}/PE_{BL} Layer	-2.258	0.195

3.4 Mechanism of Wall Layer Formation

The wall coating formation is due to electrostatic charging of fluidizing particles. Image force, which is generated between the column wall and charged particles, is the dominating reason for the initiation of the wall fouling. At incipient phase of fluidization, the charge generation results from particle-particle and particle-wall contacts. Since the particle-particle contacts make two

particles to be charged oppositely, the resulted net charge would be zero. Therefore, the net charge of the bed at incipient phase of fluidization will be due to particle-wall contacts.

Results presented earlier showed that the fluidization of PE_A and PE_B resins generated a net negative charge due to particles contacting with the column wall during fluidization. As shown in Figure 3.24, this net negative charge of the bed particles would then generates positive charge on the inner surface of the column due to induction charging, which then creates image force between column wall and the particles. As a result, the positive inner column wall will attract the negative particles while repelling the positive particles. The first negative particles layer is then forms. As the negative wall layer grows, the field of this layer will repel negative particles and attract positive particles. In turn, some positive particles will migrate and adhere to the column. Consequently, the wall coating will consist of a bipolarly charged layer. Results of the CPS trials also confirmed this phenomenon.

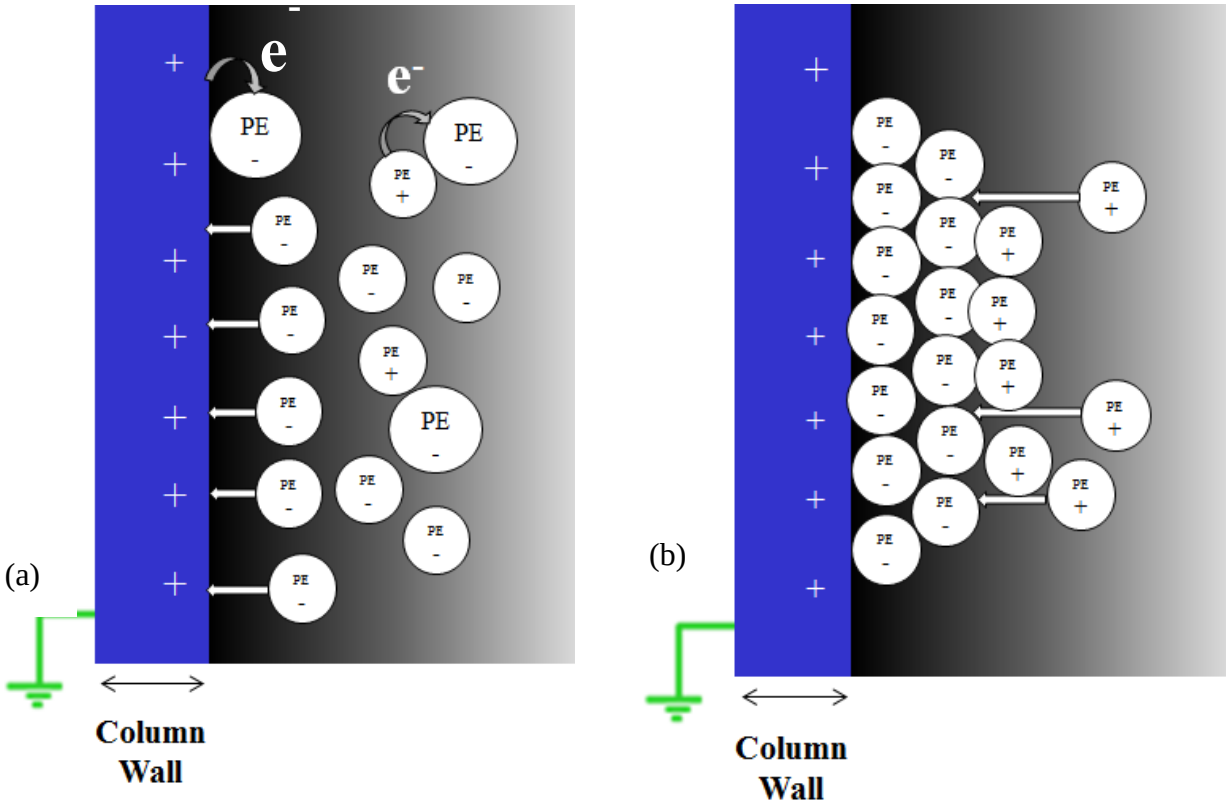

Figure 3.24: Schematic of wall fouling formation mechanism: (a) charge generation due to particle-particle and particle-wall contacts and formation of image force between the column wall and negatively charged particles; (b) Wall coating layer formation and growth.

With the small fluidization system, two types of polyethylene resins (PE_A and PE_B) were examined in which both produced similar results with some exceptions.

In bulk region, at higher smaller particle content (20% PE_{AS} and PE_{BS-1}), the net charge-to-mass ratio was lower than other fractions. This was found to be due to two possible reasons. Firstly, the quick formation of a wall layer preventing the bulk of the particles contacting the column wall and thus reducing the net charge generation of the bulk. Secondly, by adding more small particles, two distinct size particles lead to more particles to particles contacts, resulting in bipolar charging where some particles became negatively and some positively charged. In this case, some of the negative particles could have been attracted toward the column wall and contributed to the wall coating growth. Consequently, both effects reduced the net negative charge of the bulk particles, or increasing their positive charge.

In the wall region, for both resins it was found that the net specific charge of wall particles rose by increasing the fraction of small particles. In addition, the composition of the wall fouling transitioned from being only large particles to only small particles, namely small particles replaced the large particles within the wall coating. This is consistent with the previous study that certain size particles adhere to the fluidization column wall (Sowinski, et al., 2010). Finally, it was found that the electrostatic charge generation degree of the wall layer increased as proportion of small particles increased. Although there is no distinct relationship between magnitude of wall fouling and the fraction of small particles, comparing to the large particles, small ones easily became highly charged and thus had a higher tendency to being attracted towards the column wall, resulting in easier wall layer formation. Furthermore, while collecting the wall particles, it was obvious that highly charged particles (tightly bound) were difficult to be removed from the column. It was also found that although both bulk and wall particles had a net negative charge, in fact they consisted of both negatively and positively charged particles. Based on the collection order and particles size distribution of different samples, it was proposed that smaller particles adhere to the wall first due to their higher charge, followed by the larger particles.

Additionally, it was found from 15 minutes fluidization results that the high proportion of small particles will accelerate wall coating formation. Therefore if this occurs in industrial reactors, it will increase the frequency for shut down and cleanup.

Chapter 4. Results and Discussion - Large Fluidization System

The results presented in this chapter are of PE_B particles mass%, specific charge and mean particle size in different regions of the large fluidization system (Initial, Bulk, Wall and Fines). Since the PE_B particles were sieved and had narrow size ranges, the amount of fine particles collected in the top Faraday cup was negligible, and therefore, no data regarding the entrained fines is presented here. With the large fluidization system, two types of binary mixture of particles were examined, namely PE_{BL} with PE_{BS-1}, and PE_{BL} with PE_{BS-2}.

4.1 PE_B Resin as Received

As shown in Figure 4.1, the wall and fine particles charged oppositely indicating the presence of bipolar charging within the bed. The net q/m of bulk particles was quit low comparing to that of the wall and fine particles. Results illustrate that the wall layer mean particle size was approximately 400 µm, which was similar to what was found in the small fluidization system.

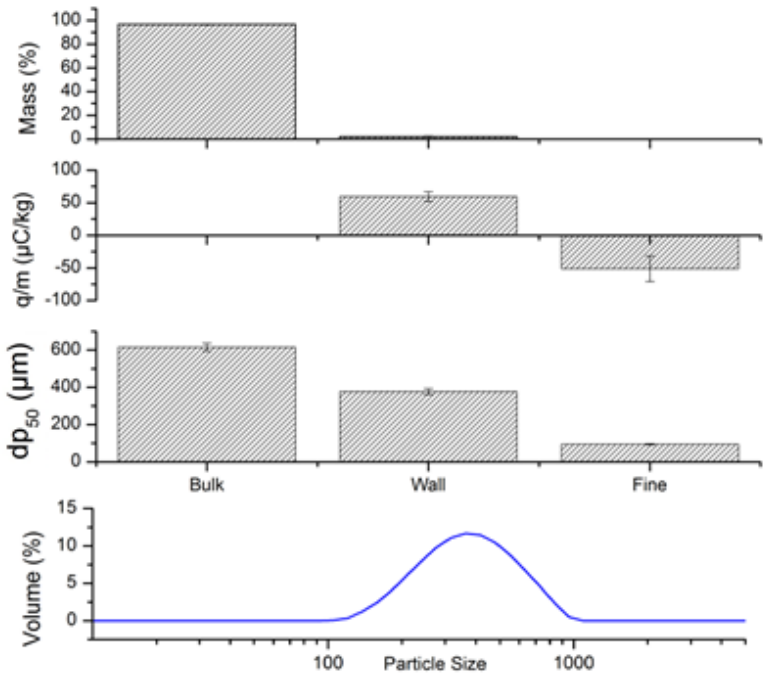

Figure 4.1: Particles mass%, q/m and dp_{50} found in various regions of the larger fluidized bed after fluidization of the PE_B resin as received, as well as particle size distribution of wall particles.

4.2 Initial Particles

Figure 4.2 shows the results of net charge-to-mass ratio and normalized mean particles diameter of initial particles of the two types of binary mixtures. All experiments started with negligible and similar initial charge.

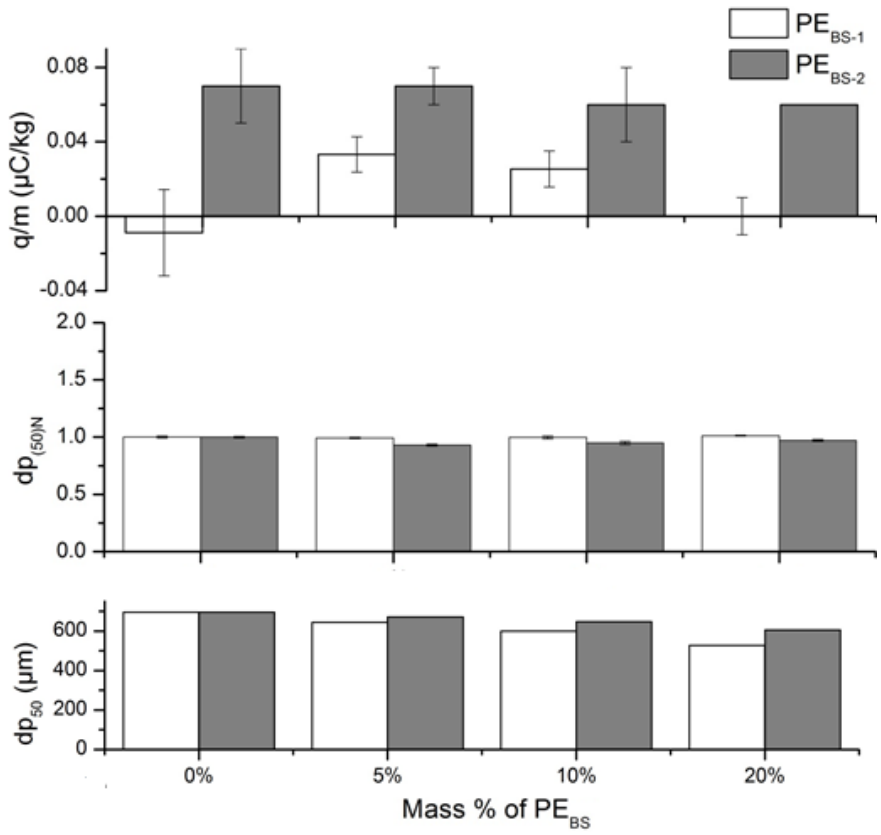

Figure 4.2: Initial particles net q/m and $dp_{(50)N}$ for the two binary mixtures PE_B resin fluidized in the large fluidization system.

4.3 Bulk Particles

The mass%, net q/m and $dp_{(50)N}$ of bulk particles are shown in Figure 4.3. For both binary mixtures, the mass of bulk particles showed similar trends in which gradually increased from 0% to 10% case and then plateaued (with approximately 97.5%).

In PE_{BS-1} case, the net q/m of bulk particles was similar for 0%, 5% and 10% trials. However, it suddenly decreased to zero for 20% mixture, which was similar to the observations made in the

small fluidization column for the same particles. For PE_{BS-2} mixture, the net charge of all fractions remained the same at approximately 0.3 μC/kg.

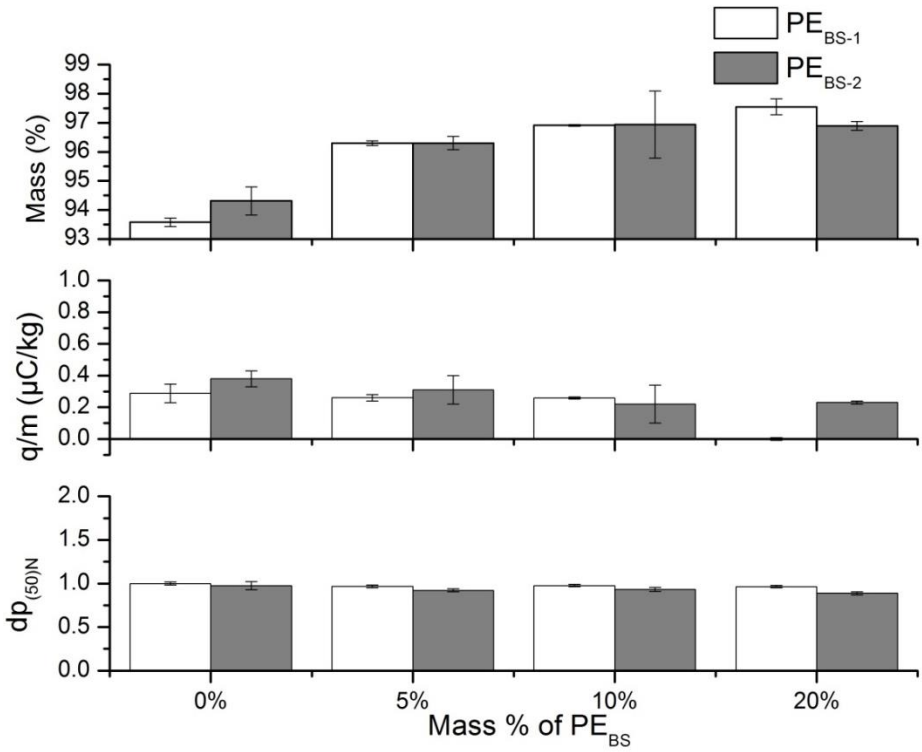

Figure 4.3: Bulk particles mass%, net q/m and $dp_{(50)N}$ after fluidization of various binary mixtures of PE_{BS} and PE_{BL} resin in the large fluidization system.

4.4 Wall Particle

Figure 4.4 presents the results of mass%, net q/m and $dp_{(50)N}$ of wall particles for both type of binary mixtures. It is apparent that both PE_{BS-1} and PE_{BS-2} cases displayed similar results. The bulk and wall particles obtained positive charge, which is an indication of particles to wall contacts. It can be seen from Figure 4.5 that there is a particle size transition for the wall particles. $Dp_{(50)N}$ of wall particles decreased and the mean particle diameters shifted to the left along with rising the fraction of small particles (Figure 4.4). For 10 and 20% cases, majority of wall particles were the small particles. In another words, when the bed consisted of certain fraction of smaller particles, the small particles replaced the large particles in forming the wall coating.

As can be seen in Figure 4.4, the particles net q/m increased as the mount of small particles rose. At 20% case, the net q/m was three times of that of PE_{BL} only particles (0% case). As previously discussed in section 3.2.3 the addition of small particles could affect the fluidized bed hydrodynamics by increasing the presence in the smaller particles in the wall region and thus generating more contact charging with the column wall. In addition, smaller particles gain a higher charge per specific surface area. Both reasons resulted in small particles obtaining a higher charge–to–mass ratio. Although the specific charge of the wall particles increased as the fraction of small particles increased, but the mass of the wall coating declined. This may be due to small particles higher charge which then would create an image force on the column wall making these charged particles to adhere to the wall. However, if the wall layer formed by highly charged particles, it will generate an electric filed which will repel the similarly charged particles to the bulk. In turn, this would prevent wall coating growth. This is true for 5%, 10% and 20% cases which had a significantly larger net q/m. Since the mass% decline was not in the same factor as net q/m increase after adding small particles, there must have been an elevation of charge of wall particles, which is similar to Yu et al. (2010).

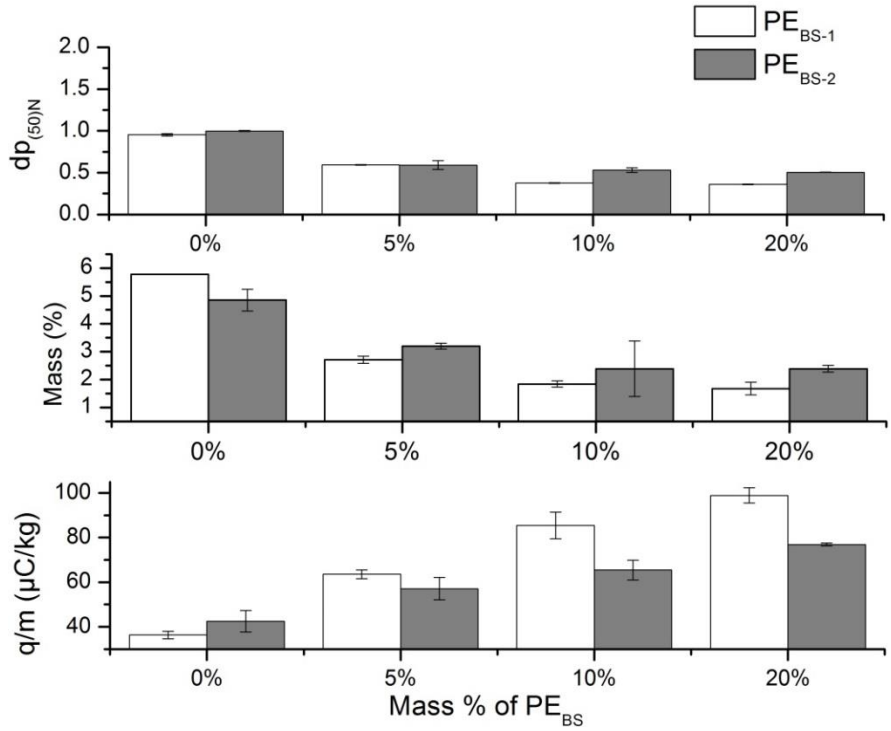

Figure 4.4: Wall particles mass%, net q/m and $dp_{(50)N}$ after fluidization of various binary mixtures of PE_{BS} and PE_{BL} resin in the large fluidization system.

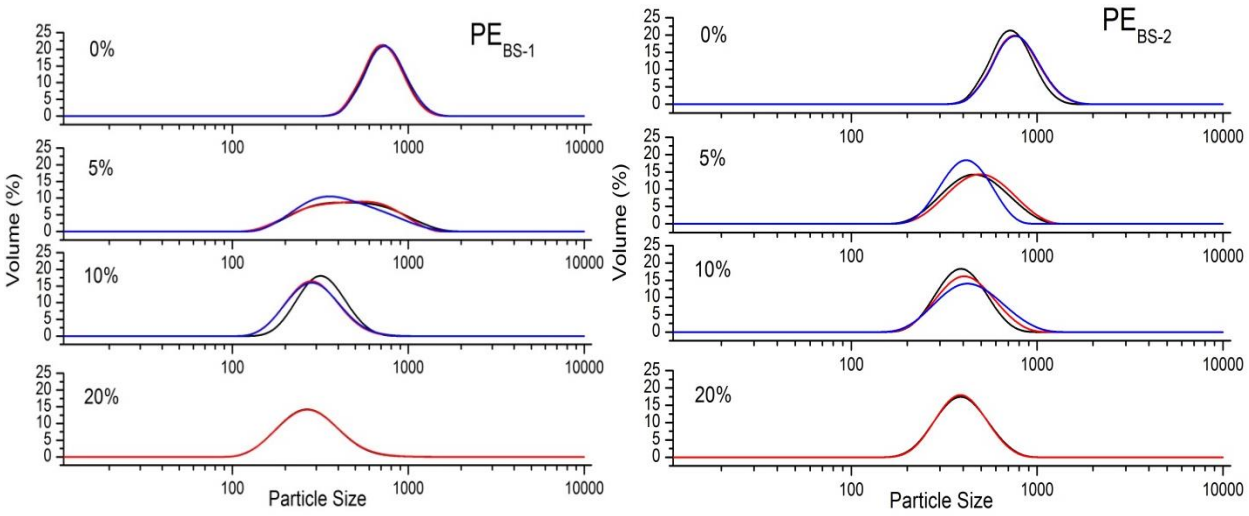

Figure 4.5: Wall particles size distribution for various binary mixtures of PE_{BS} and PE_{BL} particles fluidized in the large system.

The comparison of the wall particles net q/m of PE_{BS-1} cases with that of PE_{BS-2} illustrates that the PE_{BS-1} particles, which were smaller (212-300 μm), obtained a higher charge for all mixtures tested. It is important to note that the magnitude of wall fouling for PE_{BS-1} cases were smaller than that of PE_{BS-2} indicating that the smaller particles gained a higher degree of charge and as previously discussed repelled the similarly charged particles to the bulk, resulting in less amount of wall coating.

On the other hand, the bubble dynamics will also have an influence on the degree of particles mixing and in turn their charging degree. Formisani (1991) found that the addition of small particles up to 50 wt% results in viodage reduction. Similar bubble size reduction results were found by Beetstra et al (2009) .As gas bubbles rise through a fluidized bed, they create pressure fluctuations with amplitudes directly proportional to their diameter (Davidson and Harrison, 1963). In addition, as the bubbles size increases so does their rise velocity reaching the bed surface. These effects in turn affect the extent of particles contacting each other and the column wall and the degree of bed electrification. To examine this effect, the standard deviation of the pressure fluctuations was examined for experiments presented in this chapter. As can be seen from Figure 4.6, the standard deviation of pressure fluctuations decreased by the addition of small particles (0% case in comparison to 5 and 10% cases), indicating that the bubble size decreased. This is simialr to findings of Wu et al (2007) where it was shown that for wider

particle size distributions, it is difficult to form large bubbles under the same rate of superficial gas velocity. This in addition confirms the results found in present work in which the standard deviation of the pressure fluctuations were found to be smaller for the mixture that had smaller particles (Figure 4.6). The larger bubbles which also travel faster to the bed surface allow more particle-particle and particle-column wall contacts. This could explain the highest magnitude of wall coating that was observed for the 0% case where no small particles were present. The larger bubbles provide more chances for particles to contact the column wall contacts and become charged.

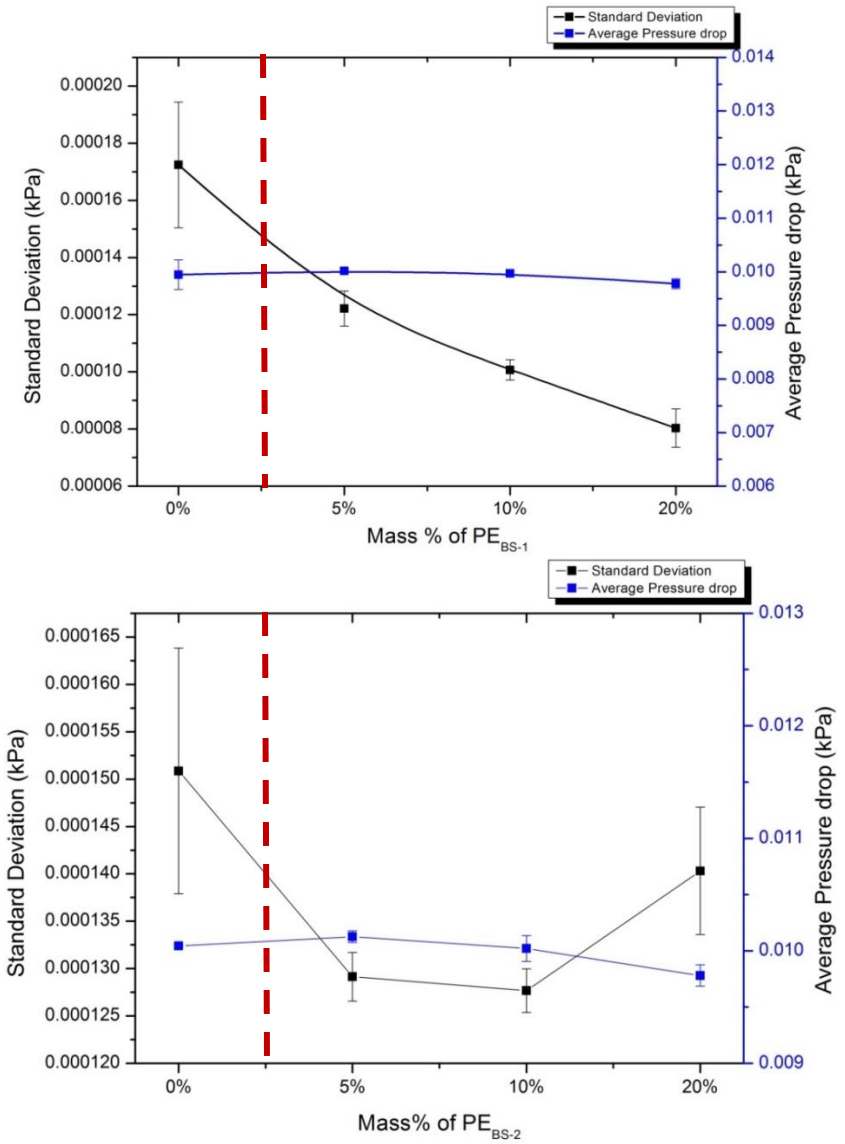

Figure 4.6: Average pressure drop and the standard deviation of pressure fluctuations measured during 1 hour fluidization of various binary mixtures of PE_{BS} and PE_{BL} particles in the large fluidization system.

4.5 Charged Particle Separator

It can be seen from Figure 4.7 that for both type of binary mixtures, the wall particles were bipolarly charged. Mass collected in FC3 dominated the wall particles. Particles collected in FC2, FC3 and FC4 charged positively, confirming that the majority of the wall particles charged positively. The reason that FC2 charged positively was due to the particles being charged less and thus the gravitational force dominating. The particles in FC1 only consisted of small particles for both types of mixtures.

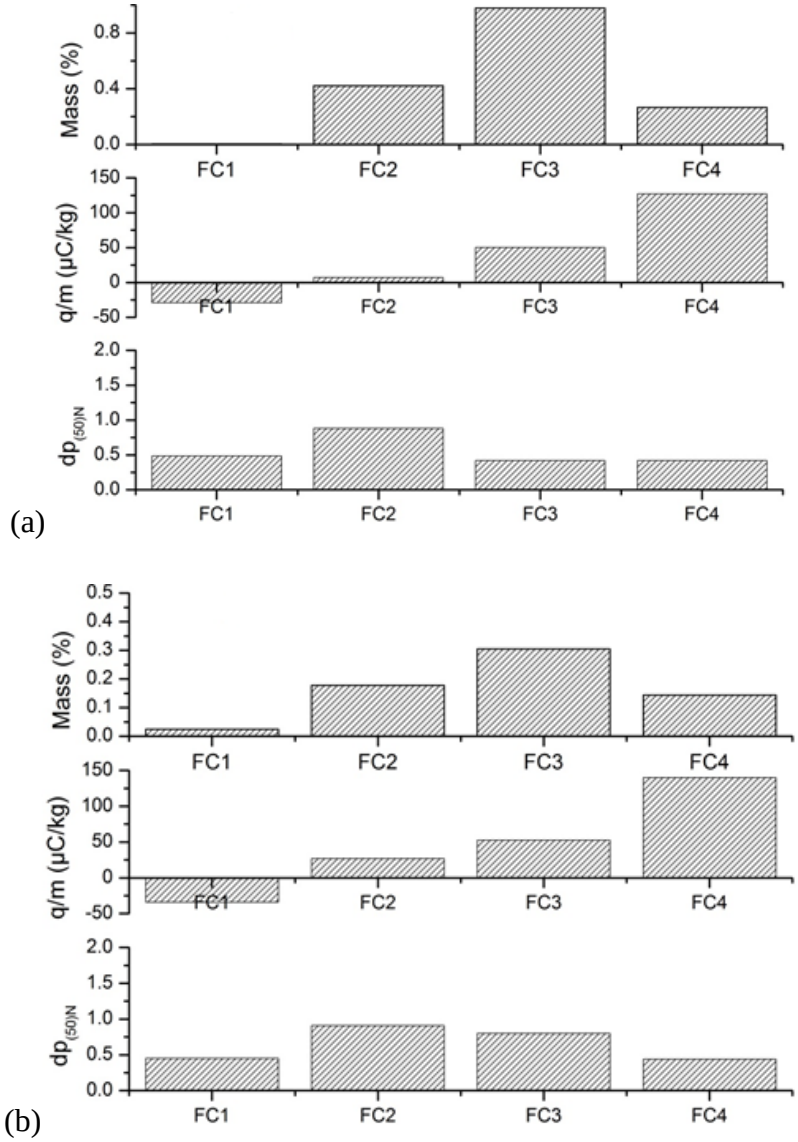

Figure 4.7: Mass%, net q/m and $dp_{(50)N}$ of particles collected in the four Faraday cups of the CPS unit for 5% case: (a) PE_{BS-1}; (b) PE_{BS-2}.

4.6 Bench-Scale Shaking Experiments

The charging behaviour due to particle-wall contacts of small samples of the same particles used in the fluidization were examined in a bench-scale shaking test. Results illustrated in Figure 4.8 indicate that for all size ranges, particles charged positively after contacting with the stainless steel wall. These results are comparable with those found in the fluidization experiments presented earlier in this chapter.

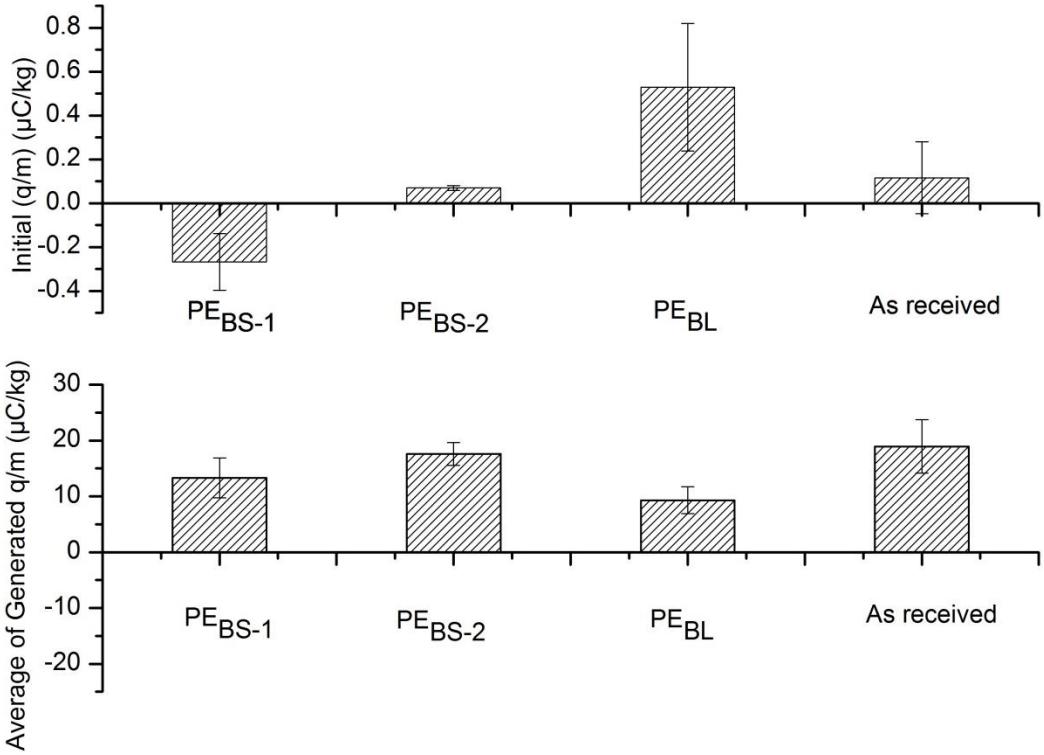

Figure 4.8: net q/m of different PE_B particle size ranges before and after shaking in a stainless steel tube.

4.7 Summary

In large fluidization system, binary mixtures of $PE_{BS-1}$and PE_{BS-2} with the PE_{BL} particles displayed similar impact on the extent of electrostatic charge generation within the bed and the wall fouling formation. For both types of mixtures, small particles replaced large particles in forming the wall coating. This confirmed the previous study that certain size particles of resins as received adhere to the fluidization column wall (Sowinski, et al., 2010). The small particles were

found to be highly charged which would then prevented the wall coating growth after its formation. However, these highly charged small particles had higher tendency to being attracted towards the column wall due to image force generated as a results of induction charging. In other words, although increasing the fraction of small particles would reduce the amount of wall fouling, but it could accelate the unset of fouling formation. Acoording to simiple pressure drop signal anylysis, it is suggested that presence of the small paticles has an impact on the bubble dynamics where bubble size decreased when adding small particles.

For both types of mixtures, it could be seen that the net q/m of wall particles in binary mixture trials was quite larger than that of mono-sized trials consisting of only large particles. This finding translates to small particles having higher tendency to migrate toward the column wall due to induction charring resulting in strong image forces.

Examining the results of PE_B particles in the small and larger fluidization system shows that the polarity of the wall particles is opposite. Although the charge polarities are found to be opposite, this has no impact on the wall fouling formation mechanism. In large fluidization system, the mechanism of wall layer formation is similar as that of small system, previously presented in Figure 3.24. The particles net positive charge induces a negative charge on the inner column wall surface (Figure 4.9). The generated image force would then attract the positively and repel the negatively charged particles. As a result, the first positive layer is formed. Both of particle-particle and particle-wall contacts contribute to the generation of the positively charged particles. When the electric field of the positive layer is strong enough, it will repel the positive particles to the bulk of the bed while attracting the negative particles towards the column wall. This is the reason why the wall coating consists of both positively and negatively charged particles. Therefore, the charge polarity of particles after contacting with the column wall has no effect on wall fouling formation mechanism.

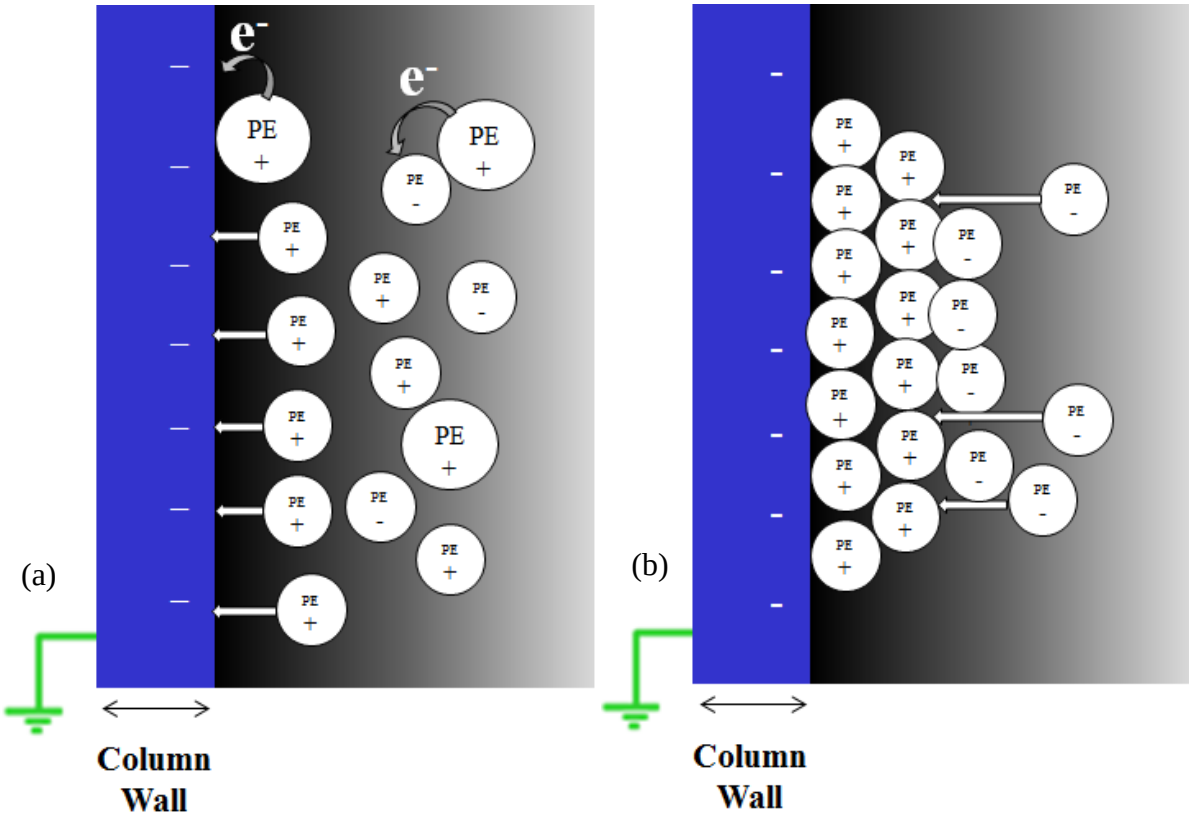

Figure 4.9: Schematic of wall fouling formation mechanism: (a) charge generation due to particle-particle and particle-wall contacts and formation of image force between the column wall and negatively charged particles; (b) Wall coating layer formation and growth.

Chapter 5. Conclusions and Recommendations

The outcome of the continuous particle-particle and particle-wall contacts in gas-solid fluidized beds is the generation of electrostatic charge. As a result, the major problem of reactor wall fouling occurs, which is known as "sheeting" in Polyolefin industry. When fouling/sheeting occurs, the reactor requires shut down for clean-up resulting in significant economic loss. It is thus essential to investigate the factors that influence the degree of charge generation in such reactors to enable the better understanding of the underlying charge generation mechanisms, and ultimately to find means to reduce or eliminate this problem. The objective of this thesis was to investigate the effects of fluidizing particle size; especially particle sizes of 400 μm and smaller on the magnitude of wall fouling and fluidized bed electrification.

5.1 Conclusions

Regardless of the type of polyethylene resin used (PE_A or PE_B), it was found that particles with a certain size (400 μm and smaller) had a tendency to coat the column wall when the resin was fluidized as received (i.e., having a large particle size distribution). Thus binary mixtures of small (212-300 μm and 300-425 μm) and large (600-710 μm) were examined via fluidization and bench-scale shaking tests.

From the results of binary mixture fluidization, small particles, both 212-300 μm and 300-425 μm, obtained a higher charge-to-mass ratio comparing to large particles. The particles net specific charge also increased as the fraction of small particles increased. The high net q/m of the small particles was found to be the reason why the presence of smaller particles prevented the large particles from contacting the column wall and replaced the large particles while forming the wall coating. At concentrations close to 20%, small particles were found to occupy the majority of the wall layer.

Although the magnitude of specific charge of particles in the wall region increased, but the degree of wall fouling declined by increasing the fraction of small particles in the binary mixture. This was found to be due to the degree of particles charging which increased

for the small particles which also formed the first layer on the column wall resulting in forming a repulsive electrostatic force that prevented further migration of the particle towards the column wall and the growth of wall build-up. Although by adding small particles the extent of wall coating declined, it does not mean that addition of small particles of the same material of the fluidizing particles can be used as a method to reduce the magnitude of wall fouling. Since small particle can become highly charged, they would create image forces that result in these particles quick adherence to the column wall, even in the first 15 minutes of fluidization, and thus could accelerate the unset of wall fouling. Such effect in the case of commercial reactors where reaction is present could still result in the growth of the wall coating.

For runs conducted in the larger system where the effects of two sizes of small particles were studied, comparing 212-300 μm cases versus 300-425 μm cases, for all fractions the smaller particles gained a higher net specific charge but generated less wall fouling.

Overall based on the results found in this research it can be concluded that the percentage of small polyethylene particles (400 μm and smaller) should be kept under 5% and for samples as received a narrower size distribution to be considered.

A quick evaluation of the fluidized bed pressure fluctuation signals indicated that the addition of small particles influences the fluidized bed hydrodynamics by reducing the bubble size. This in turn could affect the degree of particle-particle and particle-wall contacts.

It was also concluded that the particles charge polarity within the bed does not impact the wall fouling formation mechanism. When entrainment is not present, particle-particle contacts generate a null net charge while the particles-wall contacts generate opposite charge polarity on the particles and the metallic column wall. The charged particles, regardless of their charge polarity, will then generate induction charging on the column wall which then creates attractive image forces between the particles and the column wall. This is the unset of wall fouling. The coating layer would then grow through the attractive electrostatic forces between the particle layer on the column wall and oppositely charged particles within the bulk of the bed. This growth continues until the electric field of the particles attached to the column begins to repel the similarly charged particles to the bulk of the bed. The coating thickness would thus depend on the net q/m of the wall coating.

Finally, it is important to indicate that results of this research confirmed our earlier findings that the net charge-to-mass ratio is not an indication of the magnitude of the wall fouling.

5.2 Recommendations for Future work

The following recommendations are proposed for future work:

1. In this work all experiments were conducted at atmospheric condition. The large fluidization system is designed to operate at high pressures of 2500 kPa which is close to pressure of commercial polyethylene reactors. The experiments examined in this research can be extended to high pressure conditions to be more industrially relevant.
2. In commercial polyethylene reactors, polyethylene resins are present along with the catalyst particles. Thus, experiments operated under pressure then can be extended to examining ternary mixture of particles where catalyst used in producing the same polyethylene resin could also be added to the mixture. Such case not only adds a third component that has much smaller size (less than 100 μm) but also a different surface chemistry.
3. Commercial polyethylene reactors operate under turbulent flow regime where mounts of particles would be entrained. Similar scenario to be investigated while allowing the entrained particles to be recycled back to the fluidized bed.
4. For future experiments it is recommended to conduct more advanced examination of the bed pressure fluctuation signals to better understand the effects of small particles on fluidized bed hydrodynamics, especially bubble size and rise velocity.

REFERENCE

Adams，C.K, 1986. Nature's Electricity. *McGraw-Hill Companies,* p. 160.

Ahuja, S. K., 1976. A collision model of charge exchange between metal and polymer spheres. *Phys. D: Appl. Phys,* Volume 9, pp. 1305-1314.

Ali, A., Chranowski, S., Foster, J. & Geoghegan, T., 1998. *Static Control with TEOS.* s.l. Patent No. WO/1998/012231.

Ali, F., Ali, M., Ali, R. & Inculet, I., 1998. Minority charge separation in falling particles with bipolar charge. *Journal of Electrostatics,* 45(2), pp. 139-155.

Apodaca, M. M. et al., 2010. Contact electrification between identical materials. *Angewandte Chemie International Edition,* Volume 49, pp. 946-949.

Bafrnec, M. & Beña, J., 1972. Quantitative data on the lowering of electrostatic charge in a fluidized bed. *Chemical Engineering Science,* Volume 27, pp. 1177-1181.

Bartilucci, M. et al., 2003. *Method and apparatus for reducing static charges during polymerization of olefin polymers.* US, Patent No. 09/802,090.

Baytekin, H. et al., 2011. The Mosaic of Surface Charge in Contact Electrification. *Science,* Volume 333, pp. 308-312.

Beetstra, R. .., Nijenhuis, J., Ellis, N. & Van Ommen, J., 2009. The influence of the particle size distribution on fluidized bed hydrodynamics using high-throughput experimentation. *Particle Thechnology and Fluidization,* pp. 2013-2023.

Beret, S., Jenkins, J. M., Jones, T. M. & Jones, R. L., 1986. US, Patent No. 4588790A.

Boland, D. & Geldart, D., 1972. Electrostatic charging in gas fluidised beds. *Powder Technology,* 5(5), pp. 289-297.

Brouwer, G., van Ommen, J. R., Wagner, E. & Mudde, R. F., 2012. Effects of Pressure and Fines Content On Bubble Diameter in a Fluidized Bed Studied Using Fast X-Ray Tomography. *Chemical Engineering Journal,* Volume 207-208, pp. 711-717.

Burgo, T. A. et al., 2012. Triboelectricity: Macroscopic Charge Patterns Formed by Self-Arraying Ions on Polymer Surfaces. *Langmuir,* Volume 28, p. 7407−7416.

Burgo, T. et al., 2011. Electric potential decay on polyethylene: Role of atmospheric water on electric charge build-up and dissipation. *Journal of electrostatics,* 69(4), pp. 401 -409.

Cartwright, P., Singh, S., Bailey, A. G. & Rose, L., 1985. Electrostatic charging characteristics of polyethylene powder during pneumatic conveying. *IEEE Transactions on Industry Applications,* IA-21(2), pp. 541-546.

Chew, J. & Hrenya, C. M., 2011. Link Between Bubbling and Segregation Patterns in Gas-Fluidized Beds with Continuous Size Distributions. *AIChE Journal,* 57(11), pp. 3003-3011.

Chirillo, J., Kimbrough II, K. & McHattie, P., 1989. *Method for reducing sheeting during polymerization of alpha-olefins.* US, Patent No. 4855370.

Ciborowski, J. & Wlodarski, A., 1962. On electrostatic effects in fluidized beds. *Chemical Engineering Science,* 17(1), pp. 23-32.

Cross, J., 1987. *Electrostatics: Principles, Problems and Applications.* Bristol: Adam Hilger.

Davies, D., 1969. Charge generation on dielectric surfaces. *British Journal of Applied Physics:Journal of Physics D2*, pp. 249-259.

Diaz, A., 1993. Contact charging of organic materials: Ion vs. electron transfer. *IBM Journal of Research and Development*, 37(2), pp. 249-260.

Elsdon, R. & Mitchell, F. R. G., 1976. Contact electrification of polymers.. *Phys. D: Appl. Phys.*, Volume 9, pp. 1445-1460.

Fasso, L., Chao, B. & Soo, S., 1982. Measurement of electrostatic charges and concentration of particles in the freeboard of a fluidized bed. *Powder Technology,* 33(2), pp. 211-221.

Formisani, B., 1991. Packing and fluidization properties of binary mixtures of spherical particles. *Powder Technology*, Volume 66, pp. 259-264.

Forward, K., Lacks, D. & Sankaran, R., 2009. Triboelectric charging of granular insulator mixtures due solely to particle - Particle interactions. *Industrial and Engineering Chemistry Research,* 48(5), pp. 2309-2314.

Fulks, B., Sawin, S., Aikman, C. & Jenkins III, J., 1989. *Process for reducing sheeting during polymerization of alpha-olefins.* US, Patent No. 4,876,320.

Fulks, B., Sawin, S., Aikman, C. & Jenkins, J. I., 1985. *Process for reducing sheeting during polymerization of alpha-olefins.* United States, Patent No. 4532311.

Gajewski, A., 1985. Investigation of the Electrification of Polypropylene Particles during the Fluidization Process. *Journal of Electrostatics,* Volume 17, pp. 289-298..

Gao, J. et al., 2009. Hydrodynamics of gas-solid fluidized bed of disparately sized binary particles. *Chemical EngineeringScience,* Volume 64, pp. 4302-4316.

Geldart, D., 1973. Types of gas fluidization. *Powder Technology,* 7(5), pp. 285-292.

Giffin, A. & Mehrani, P., 2013. Effect of gas relative humidity on reactor wall fouling generated due to bed electrification in gas-solid fluidized beds. *Powder Technology,* Volume 235, pp. 368-375.

Goode, M., Hasenberg, D., McNeil, T. & Spriggs, T., 1989. *Method for Reducing Sheeting During Polymerization of Alpha-Olefins.* US, Patent No. 4,803,251.

Goode, M. et al., 2000. *Static control in olefin polymerization.*. US, Patent No. 6,11,034.

Gooding, M. D. & Kaufman, K. G., 2014. Tribocharging and the Triboelectric Series. *Encyclopedia of Inorganic and Bioinorganic Chemistry*, pp. 1-9.

Grzybowski, B. A., Fialkowski, M. & J. A. Wiles, 2005. Kinetics of Contact Electrification between Metals and Polymers. *Phys. Chem. B,* Volume 109(43), pp. 20511-20515.

Guardiola, J., Rojo, V. & Ramos, G., 1996. Influence of particle size, fluidization velocity and relative humidity on fluidized bed electrostatics. *Journal of Electrostatics,* Volume 37, pp. 1-20.

Hagerty, R. O. et al., 2005. *Method for controlling sheeting in gas phase reactors.* US, Patent No. 20050148742 A1.

Ham, R., Galtier, P. & Bergougnou, M., 1992. *Electrostatics in an air/catalyst fluidized bed at ambient temperature and pressure.* Brisbane, Engineering Foundation, pp. 611-620.

Harper, W. R., 1967. *Contact and Frictional Electrification.* Oxford: Oxford University Press.

Harper, W. R., 1998. *Contact and Frictional Electrification.* Morgan Hill: Laplacian Press.

Hendrickson, G., 2006. Electrostatics and gas phase fluidized bed polymerization reactorwall sheeting. *Chemical Engineering Science,* Volume 61, p. 1041 – 1064.

Kiselnikov, V., Vyalkov, V. & Filatov, V., 1967. On the problem of electrostatic phenomena in a fluidized bed. *Int.Chem.Eng* , pp. 428-431.

Komatus, T. S. et al., 2004. Static electrification by asymmetric rubbing. *Applied Surface Science,* Volume 235, pp. 60-64.

Kornfeld, M., 1969. Nature of frictional electrification. *Soviet Physics Solid State,2(6),* pp. 1306-1310..

Kunii, D. & Levenspiel, O., 1991. *Fluidization Engineering.* 2nd ed. Newton(MA): Butterworth-Heinemann.

Lacks, D. & Mohan Sankaran, R., 2011. Contact electrification of insulating materials. *Journal of Physics D: Applied Physics,* 44(45), p. art. no. 453001.

Law, k., Taranawskyj, I., Salamida, D. & Debies, T., 1995. *Chemisty of Materials*, 11, Issue 7, pp. 2090-2095.

Lewis, W. K., Gilliland, E. R. & Bauer, W. C., 1949. Characteristics of Fluidized Particles. *Industrial & Engineering Chemistry*, 41(6), p. 1104–1117.

Liu, C. & Bard, J. A., 2008. Electrostatic electrochemistry at insulators. *Nature Materials*, Volume 7, pp. 505-509.

Liu, C. & Bard, J. A., 2009. Electrons on dielectrics and contact electrification. *Chemical Physics Letters*, 408(4-6), pp. 145-156.

Liu, C. & Bard, J. A., 2010. Electrostatic electrochemistry: Nylon and polyethylene systems. *Chemical Physics Letters*, 485(1-3), pp. 231-234.

Lowell, J., 1977. The role of material transfer in contact electrification. *Journal of Physics D: Applied Physics*, Volume 10, p. L233.

Lu, H. & Gidaspow, D., 2003. Hydrodynamics of binary fluidization in a riser:CFD simulation usingtwogranulartemperatures. *ChemicalEngineeringScience,* Volume 58, pp. 3777-3792.

Lu, H. et al., 2007. Investigation of mixing/segregation of mixture particles in gas–solid fluidized beds. *Chemical Engineering Science,* Volume 62, pp. 301-317.

Masuda, H., Gotoh, K., Higashitani, K. & Matsusaka, S., 2006. *Adhesive Force of a Single Paticle in Powder Technology Handbook.* 3 ed. Florida: CRC Press.

Matsusakaa, S., Maruyamaa, H., Matsuyamab, T. & Ghadiri, M., 2010. Triboelectric charging of powders: A review. *Chemical Engineering Science,* 65(22), p. 5781–5807.

McCarty, L. S. & Whitesides, G. M., 2008. Electrostatic Charging Due to Separation of Ions at Interfaces: Contact Electrification of Ionic Electrets. *Angew. Chem. Int. Ed.,* Volume 47, p. 2188 – 2207.

McCarty, L. S., Winkleman, A. & Whitesides, G. M., 2007. *Angew. Chem. Int. Ed.,* Volume 129, p. 4075.

Mehrani, P., Bi, H. & Grace, J., 2005. Electrostatic charge generation in gas-solid fluidized beds. *Journal of Electrostatics,* 63(2), pp. 165-173.

Mehrani, P., Bi, H. & Grace, J., 2007. Electrostatic behaviour of different fines added to a Faraday cup fluidized bed. *Journal of Electrostatics*, Volume 65, pp. 1-10.

Miller, C. O. & Logwinuk, A., 1951. Fluidization studies of solid particles. *Industrial & Engineering Chemistry*, Volume 43(5), pp. 1220-1226.

Moughrabiah, W., Grace, J. & Bi, X., 2009. Effects of pressure, temperature, and gas velocity on electrostatics in gas-solid fluidized beds. *Industrial and Engineering Chemistry,* Volume 48, pp. 320-325.

Moughrabiah, W., Grace, J. & Bi, X., 2012. Electrostatics in gas-solid fluidized beds for different particle properties. *Chemical Engineering Science,* Volume 75, pp. 198-208.

Mun, T. C., 2005. *Production of Polyethylene Using Gas Fluidized Bed Reactor.* [Online] Available at: http://www.klmtechgroup.com/PDF/Articles/Fluidized-Bed-Reactor.pdf [Accessed 30 07 2013].

Murata, Y. & Kittaka,S, 1979. Evidence of electron transfer as the mechanism of static charge generation by contact of polymers with metals. *Japanese Journal of Applied Physics,* Volume 18, p. 421.

Osberg, G. & Charlesworth, D., 1951. *Chem. Eng. Prog,* Volume 47, p. 566.

Park, A.-H., Bi, H. & Grace, J., 2002. Reduction of electrostatic charges in gas–solid fluidized beds. *Chemical Engineering Science,* Volume 57, pp. 153-162.

Piperno, S., Cohen, H., Bendokov, T. & M. Lahav, I. L., 2011. Absorption vs. redox reduction of Pd2+ and Cu2+ on triboelectrically and naturally charged dielectric polymers. *Physical Chemistry Chemical Physics,* 14(16), pp. 5551-5557.

Rojo, V., Guardiola, J. & Vian, A., 1986. A capacitor model to interpret the electric behaviour of fluidized beds. Influence of apparatus geometry. *Chemical Engineering Science,* 41(8), pp. 2171-2181.

Salama, F., 2013. Electrostatic Charge Generation and Wall Fouling in a High-Pressure Gas-Solid Fluidized Bed: Implementation and Preliminary Testing of a Measurement Technique. *Master Degree Thesis.*

Salama, F., Di, S. & Poupack, M., 2013. *Characterizing Electrostatic Charges in High-Pressure Gas- Solid Fluidized Beds: Experimental Design and Preliminary Results.* s.l., ECI Symposium Series.

Servais, T. & Bernot, C., 2000. *Measurement of electrostatic effects in a fluidized bed reactor.* s.l., s.n.

Song, G.-H., Rhee, A. & Lowder, G., 1995. *Method for Reducing Sheeting and Static Charges during Polymerization of Ethylene Polymers.* US, Patent No. 5,391,657.

Sowinski, A., Mayne, A. & Mehrani, P., 2012. Effect of fluidizing particle size on electrostatic charge generation and reactor wall fouling in gas-solid fluidized beds. *Chemical Engineering Science,* Volume 71, pp. 552-563.

Sowinski, A., Miller, L. & Mehrani, P., 2010. Investigation of electrostatic charge distribution in gas-solid fluidized beds. *Chemical Engineering Science,* 65(9), pp. 2771-2781.

Sowinski, A., Salama, F. & Mehrani, P., 2009. New technique for electrostatic charge measurement in gas-solid fluidized beds. *Journal of Electrostatics,* 67(4), pp. 568-573.

Tagami, N., Mujumdar, A. & Horio, M., 2009. DEM simulation of polydisperse systems of particles in a fluidized bed. *Particuology,* Volume 7, pp. 9-18.

Tanoue, K. & Masuda, H., 2006. Electrostatic separation. In: *Powder Technology Handbook.* Florida: Taylor & Francis Group, LLC, p. 656.

van Willigen, F. K., van Ommen, J. R., van Turnhout, J. & van den Bleek, C., 2003. Bubble Size Reduction in a Fluidized Bed. *International Journal of Chemical Reactor Engineering,* 1(1), pp. 1542-6580.

Wiles, A. J., Grzybowski, A. B., Winkleman, A. & Whitesides, M. G., 2003. A Tool for Studying Contact Electrification in Systems Comprising Metals and Insulating Polymers. *Anal. Chem,* Volume 75(18), pp. 4859-4867.

Williams, M. W., 2012. Triboelectric charging of insulating polymers–some new perspectives. *AIP Advances,* 2(1), p. art. no. 010701.

Wolny, A. & Opalinski, I., 1983. Electric charge neutralization by addition of fines to a fluidized bed composed of coarse dielectric particles. *Eletrostatics,* 14(3), pp. 279-289.

Wu, B., Shepperson, J. & Lee, L. v. d., 2007. *HYDRODYNAMICS OF GAS-SOLIDS BUBBLING FLUIDIZED.* s.l., International Conference on Fluidization.

Yu, X. et al., 2010. Wang, H. Effect of polymer granules on the electrostatic behavior in gas-solid fluidized beds. *Industrial and Engineering Chemistry Research,* 49(1), pp. 132-139.

Zhao, H., Castle, G., Inculet, I. & Bailey, A., 2003. Bipolar charging of poly-disperse polymer powders in fluidized beds. *IEEE Transactions on Industry Applications,* 39(3), pp. 612-618.

Appendix

Appendix 1. The Pressure Signal Analysis for PE_B particles in Small System

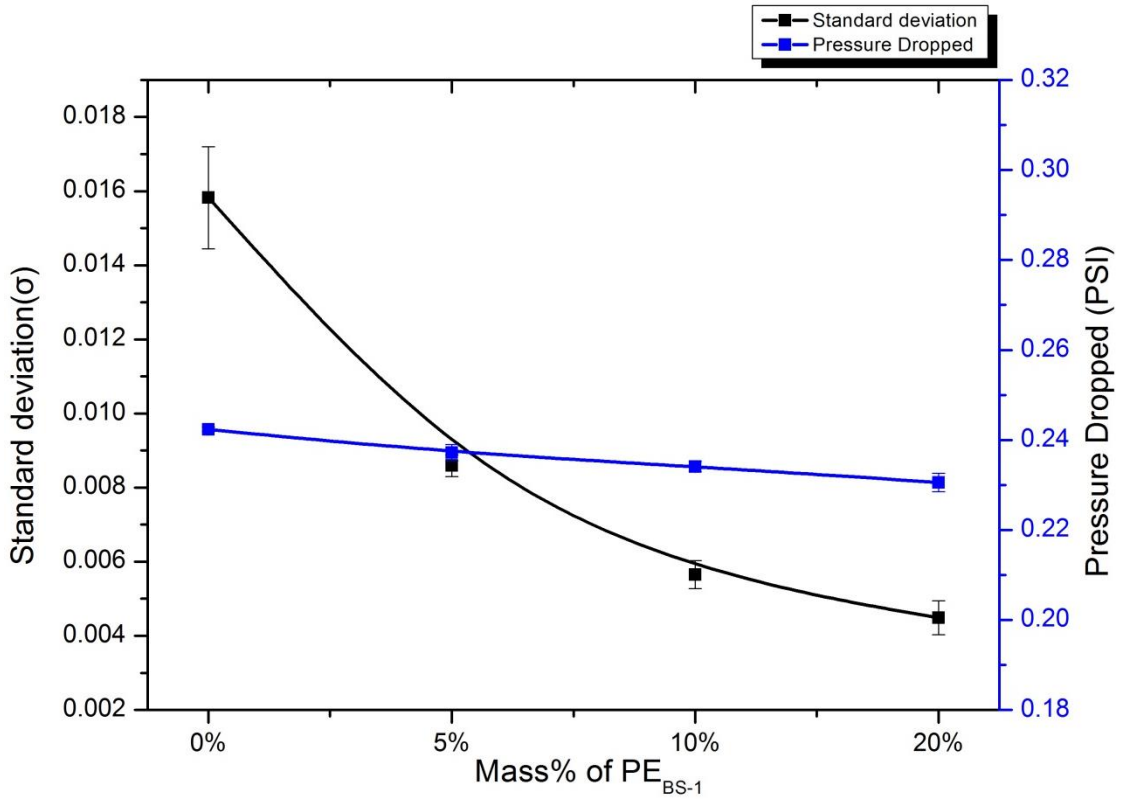

Figure A.1: Standard deviation of pressure fluctuations measured during 1hour fluidization of various mixtures of PE_{BS-1} and PE_{BL} particles in the small fluidization system.